Doctoral Dissertation

Mohammad Fahad

Széchenyi István University

2024

Mohammad Fahad

Modelling the Impacts of Autonomous Trucks on Pavements

Doctoral Dissertation

Supervisor: Prof. Csaba Koren

Széchenyi István University

Multidisciplinary Doctoral School of Engineering

Table of Contents

1 Research scope and questions

Impacts of heavy vehicles on pavements is a well-researched topic. However, the movement characteristics of autonomous heavy vehicles has some differences compared to the human driven vehicles.

Identification of unaddressed research problems is important in order for the autonomous trucks Hereinafter: ATs to be smoothly integrated into current environment. Current literature only deals with a generic asphalt pavement and a single load for impact assessment of autonomous trucks. Currently there is a lack of research available on assessing the effects on different types of pavements, whether it is an asphalt pavement or a PCC pavement with varying cross-sections such as a full depth asphalt pavement, or a conventional flexible pavement. Therefore, there is a need to analyze how certain pavement types and with varying cross-sections would perform once subjected to the autonomous truck traffic. Another issue in the current literature is the exclusive of dependence of traffic speed on pavement performance, the speed of moving load is recommended to be modelled during simulation runs.

Moreover, the effect of autonomous trucks based on different climatic conditions has not been addressed either based on previous research. As it has been proven that the channelized loading of AVs would accelerate the rutting progression in pavements. It is expected that the severity of rutting would increase during summer climatic conditions. However, the findings from current literature is based on evaluating a generic asphalt pavement without having to deal with any effect of climatic conditions. Therefore, it is essential to identify and analyze the impacts of varying climatic conditions on the pavement structure as a result of using autonomous trucks.

Autonomous trucks are deemed to follow one another in a group of greater than ten trucks, termed as a Platoon. However, there is no detailed research available on the recommended platoon size. Since asphalt pavement is a viscoelastic material, after repeated cyclic loading a rest period is needed for the material to come back to its original state. In order for the asphalt pavement to recover and maintain its functionality throughout its design life, determination of maximum number of trucks in a platoon, the spacing of trucks, maximum cumulative load of trucks inside the platoon as well as the spacing of different platoons is quite essential.

Furthermore, the recommendations in terms of cost savings and budget control with the development of optimum lane width have not been given in the available research since with inclusion of autonomous trucks in the current traffic environment, recommendations in terms of optimum lane width are essentially required for minimizing construction costs.

The following are the research questions:

- How the pavement performance is affected by employing different lateral wander modes?
- (Assuming that autonomous trucks can be produced in all kinds of axle configurations) which type of axle configuration is more detrimental to pavement performance under different lateral wander modes?
- Does truck platooning number (number of trucks in a platoon) and the headway has any effect on the pavement performance in terms of fatigue?
- How the pavement performance may vary based on different pavement cross sections and construction material's properties under different lateral wander modes?
- What should be the optimum lane width for the usage of 100% autonomous trucks?

2 Research Objectives

The main aim of performing this research is to present a complete sourceful scientific framework that would help vehicle manufacturers, researchers, students and transport authorities in understanding various prospects related to effect of autonomous trucks in a transport infrastructure system. In this matter, the goal is to fully understand all the aspects of autonomous technology and their effects on the existing transport sector which is in this research is related to the performance of pavement structure.

The objective of this research is to study and identify different forms of impacts of the usage of autonomous trucks on pavement performance and to finally develop a framework for the integration of autonomous trucks in current transport infrastructure system without disruption. For this purpose, determining and analyzing the effects of parameters related to traffic (platoon size and axle loading) and pavement structure (full depth, conventional, lane width) is highly essential. In order to develop the fully performing framework it is important to determine the following subobjectives in this research:

1. Obtaining in depth knowledge of various lateral wandering modes (Normal Distribution, Zero Wander and Uniform Distribution) of autonomous trucks on pavement performance. Focus shall be implemented on the use of uniform distribution of autonomous trucks which has proven to be quite beneficial for pavement performance.
2. Understanding of how a platoon works, the main objective here is to keep the effect of repetitive loading of different axles in check so as to allow the pavement to recover significantly, once the platoon has passed over one section of the pavement. This objective shall be accomplished by identifying the platoon size, maximum cumulative axle loads of trucks within a platoon, number of allowable trucks in a platoon, the spacing of trucks in a platoon and the spacing of different platoons.
3. Performing analysis of microstrains due to moving loads on the pavement structure. The magnitude of horizontal tensile strain and vertical compressive strain generated on the pavement under the moving load leads to calculation of fatigue cracking and rutting distress mechanisms respectively.
4. The final objective aiding this research is to help compel the transport authorities and highway agencies to bring modifications in geometric alignment of highways especially in terms of variable lane width for the autonomous truck lane in case there is a dedicated lane. The design thickness of asphalt pavement can be decreased if the unform lateral distribution is utilized, if the width of pavement lane is further increased the design thickness can be further decreased as well. This will highly decrease the construction costs for pavements especially by decreasing the demand of high-quality materials with the help of reduced thickness.

3 Research Methodology

The methodology of this research is based on simulating different lateral wandering modes on different forms of autonomous trucks. The development of autonomous trucks' framework deals in the beginning with the comparison of lateral wander modes in regard to rutting using the 2D model, comparisons of 2D and 3D models for rutting progression, fatigue damage analysis under different lateral wander modes, determining optimum platooning pattern and determination of optimum lane width on each of the lateral wandering mode using Life Cycle

Cost Analysis. This section provides a brief overview of the methodology used in each part of this research. Since, each methodology is identical to each of the framework steps mentioned above. The detailed methodology for each step is mentioned separately.

3.1 Selection of Each Lateral Wander Mode

The first lateral wandering mode is a Zero Wander mode, in this case the truck would follow a dedicated path within the lane without any lateral wander just like a train moving on the tracks, the second mode is Normal Distribution mode, this mode represents the lateral wandering behavior of human driven trucks and the third mode is Uniform Distribution mode, in which the trucks would follow a uniform lateral movement inside the traffic lane, thus uniformly distributing itself laterally throughout the length of the traffic lane.

3.2 FEM (ABAQUS) Working Protocol

ABAQUS determines the critical stress and strain values on each element when the load is applied. Load application will be sequential step load having a speed of 1 mm/sec. Modelling of pavement in ABAQUS will be in two forms. The first form is a full depth asphalt pavement and the second form is a conventional HMA pavement.

Furthermore, input parameters for the ABAQUS program are used specifically for the material model establishment. Both the Creep Power Law and Prony Series parameters are employed for thorough modeling of viscoelastic properties of the modelled pavement structure. 2D and 3D modelling techniques are also compared for time and accuracy analysis. The material model parameters sued for modelling are validated using wheel rutting tests and indirect tensile strength tests on asphalt specimen.

3.3 2D and 3D finite element modeling of rutting and fatigue cracking

Rutting and fatigue cracking are the two major forms of pavement distress mechanisms analyzed in this research. The use of 2D modelling in ABAQUS is employed for time efficient analysis of rutting in the asphalt pavement layer by using zero and uniform wander modes under various speed patterns. Traffic speeds of 50 km/h, 60 km/h, 90 km/h are used for detailed analysis. Furthermore, super slows speed of 5 km/h is also analyzed for modelling the structural impact on pavement by autonomous trucks during traffic congestion due to accidents and work zones. Creep power law parameters are employed for the development of material model. Therefore, a detailed analysis using various speeds, two lateral wander modes and two different tire configurations is performed.

3.4 Tire footprint determination and loading analysis

Since excessive repetitions of truck loading lead to the fatigue damage in the pavement. Both the lateral wander modes are analyzed for progression of premature fatigue damage. A material model for asphalt layer is employed using basic parameters and Miner's fatigue law is used to perform detailed fatigue analysis. The concept of time step loading is used for speed variations, and tire footprint contact pressure is applied using a super single wide tire and a conventional dual tire assembly. Addition of different tire footprints analysis enhances the research with the use of a zero wander mode and uniform wander mode. Furthermore, detailed analysis of horizontal tensile strain and vertical compressive strain is performed.

3.5 Comparison of results from 2D and 3D finite element models

2D and 3D models in ABAQUS are compared as a part of this research. Inclusion of comparative analysis highlights the advantages and disadvantages of using different modelling techniques. Both 2D and 3D models are compared using same material and cross section parameters. Major differences between the two options are related to time efficiency during computations and modelling and accuracy in the modelling results. Comparisons of both models is combined with the use of a zero wander mode and uniform wander mode. Furthermore, rutting analysis is performed and results from both different models are analyzed and compared.

3.6 Role of class A40 truck as an autonomous truck

Since the majority of the trucks in the traffic mix are semitrailers and with higher axle loads are compared to the rigid body trucks, it is useful to analyze in detail the impact of the semitrailer as an autonomous truck. Furthermore, the autonomous truck trials are only being conducted using the semi trailers. Therefore, a class A40 type European semitrailer consisting of five axles is used for rutting and fatigue damage analysis along with the use of zero wander mode and uniform wander mode. In this research, the tire contact pressure and axle loading is sued to determine the contact patch length of the tires in each axle of the semitrailer. This approach provides in depth analysis of progression of horizontal tensile strains and vertical compressive strain in the pavement structure. Moreover, a strain profile along the longitudinal and transverse cross section is generated.

3.7 Optimum Platoon Pattern

In order to determine optimum platooning pattern, the simulations in ABAQUS are run by introducing different categories of axle load configurations along with the trial headway starting from 10 meters to 20 meters between each truck in a platoon with 2 meters increment for each simulation run. Three different platoon mixes are proposed in this research. It is certain that with the further development of autonomous vehicles technology, autonomous trucks would be manufactures in all axle configurations possible which are identical to human driven trucks. The first platoon to be simulated only consists of semi-trailers in its traffic mix. The second platoon to be simulated only consists of rigid body trucks. The third platoon consist of a random mix of semi trailers and rigid body trucks. The complete simulation package is used for each lateral wandering mode until it is completed.

3.8 Optimum Lane Width

The selection of optimum lane width is highly dependent on the best performing lateral wander mode. In case of selection of a uniform lateral wander mode, testing on both forms of asphalt pavements with the best scenario of optimum platooning pattern are employed to start with trial increments of existing lane width of 3.75 m with 0.15 m increments until a total lane width of 4.35 m is reached. Each increased step of lane width will the be compared against the corresponding loss of design thickness by employing the American Association of State Highway and Transportation Officials (Hereinafter: AASHTO) MP-1 Pavement structural design guide. The following step will be the inclusion of Life Cycle Cost Analysis (Hereinafter: LCCA) as per pavement management protocol in order to determine the most cost-effective solution that results in maximum design thickness reduction with the minimum increment in lane width by introducing the effective pavement maintenance interventions Hence, the

optimum lane width can finally be selected based on the performance of traffic stream in the platoon.

The detailed methodology flowchart is shown in **Fig. 3-1**

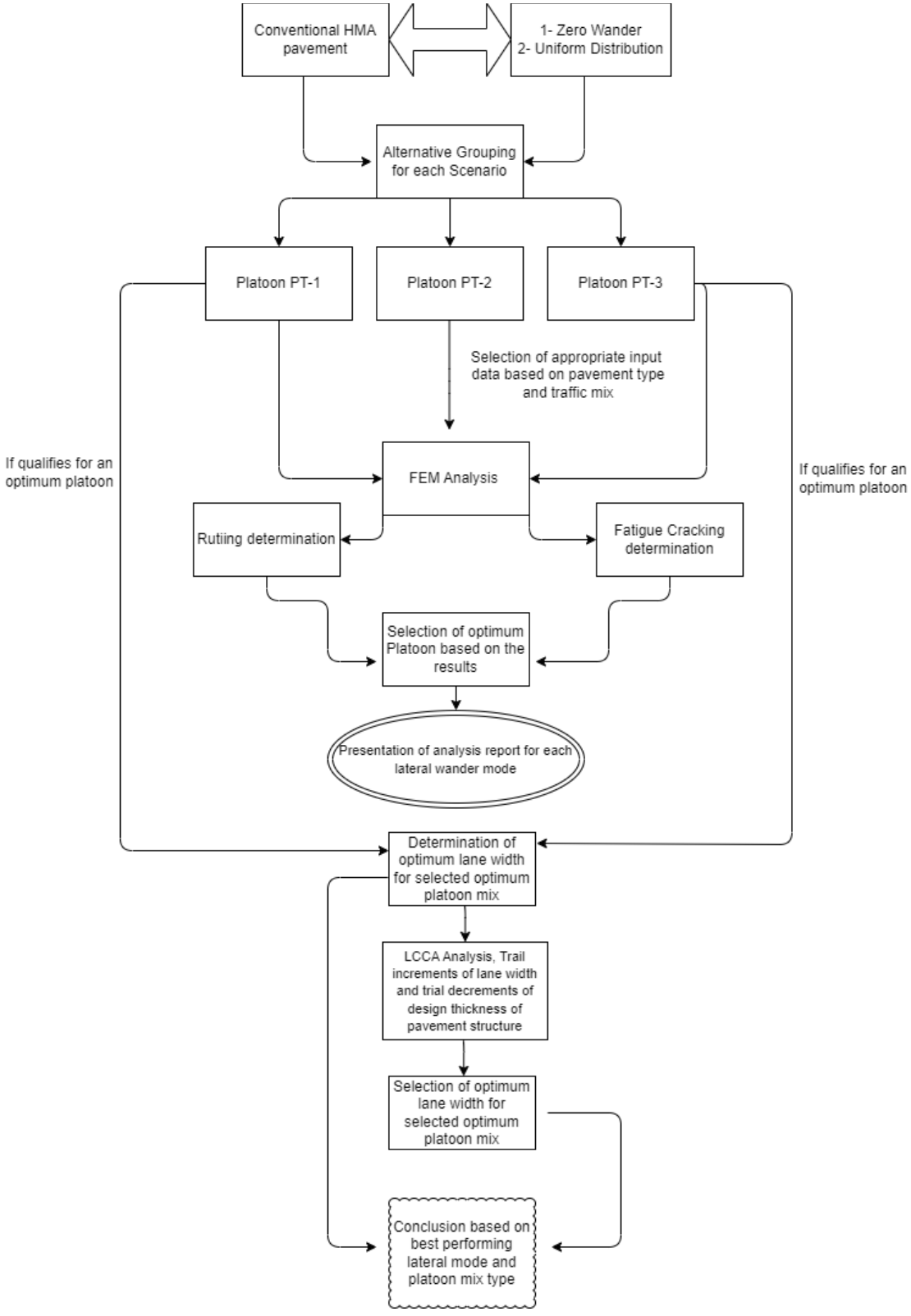

Fig. 3-1: Comprehensive breakdown of research methodology.

As observed from figure above, a conventional hot mix asphalt HMA pavement is subjected to loading in the forms of different tire configurations using different footprint data from Michelin and Goodyear. Therefore, the super single wide and the conventional dual tire are compared using the zero wander modes and uniform wander modes. Moreover, various speed scenarios are also incorporated with the use of time step loading. Tire footprint contact pressure is employed for the loading progression on the pavement. The rutting and fatigue damage analysis is carried out in this first phase using the 3D model in ABAQUS and conclusions are generated.

Furthermore, the use of class A40 autonomous truck is incorporated for independent analysis of pavement distress mechanisms under both lateral wander modes. The loading configuration optimization methodology developed in this study is then used for platoon analysis. During the platoon analysis, two different rigid body trucks are included. The comparison is performed based on the tire footprint and loading magnitude calculated under each axle of each truck used. Therefore, three different platoon types are compared and pavement distress analysis in terms of fatigue cracking and rutting is conducted. Best performing platoon is selected based on the least damage related to rutting, fatigue cracking. Headway distance between each truck in a platoon and interplatoon distance are the two significant variables analyzed during optimum platoon analysis.

Effective methodology development is essential to incorporate significant parameters consisting of speed variations, axle loading, loading configurations, material model parameters, pavement layer properties, pavement cross section, lane width variations, loading and boundary condition details in ABAQUS, maintenance interventions used for LCCA, headway distance variations, interplatoon distance variations and platoon size determination. These aforementioned parameters are utilized in various stages to perform a complete analysis related to the impacts of autonomous trucks on the pavement.

Optimum lane width determination is significant in terms of added extra potential for the uniform wander mode that can yield further improvement in pavements life in terms of rutting and fatigue cracking. Therefore, there is a possibility of further reduction in pavement structural layer thickness on the expense of increased lane width if a uniform lateral wander mode is sued. However, layer thickness variations are only limited to the asphalt layer, since it contributes to the majority of construction and maintenance costs among the other underlying layers. Furthermore, cost analysis is conducted and LCCA is performed using effective alternative intervention techniques in terms of increased salvage value and pavement's life. Lane width increment is only viable to a certain extent, and further increment makes the scenario uneconomical. Furthermore, the asphalt layer thickness can be deceased to a certain limit in order to keep the pavement in well performing structural condition. The use of zero wander mode is also included to assess its impact on pavement's life cycle.

The methodology concludes by selecting the effective lateral wander mode combined with the effective platoon mix and optimum lane width determination. Furthermore, a side by side comparison exists with the recommended tire type used in autonomous trucks and the super single wide tire provides significant improvements in terms of vertical and horizontal strains induced in the pavement when compared to the dual tire assembly. Further improvement options related to enhancing the properties of pavement layers by adding cement rated base course for subgrade and using polymer modified asphalt layer exists, however these options are independent of the autonomous truck impact analysis performed in this research. The

conclusions mentioned in each section of this framework contribute the final step of this research methodology.

4 Autonomous truck's framework components

The entire framework of this research consists of various components and variable parameters that are analyzed based on their impacts on pavement structure as a result of usage of autonomous trucks, as shown in **Fig. 4-1**. Major components consist of modeling orientations, material modelling techniques, types of lateral wander modes used, loading modes sued for simulations in FEM, Tire types used for loading and distress analysis, types of pavement distress modes considered, platoon optimization variables, individual methodologies developed for tire pressure, speed and loading magnitudes' determination, further improvement of uniform wander mode with increased lane width and economic analysis for the corresponding, reduced asphalt layer thickness along with maintenance intervention scheduling for the pavement's life cycle.

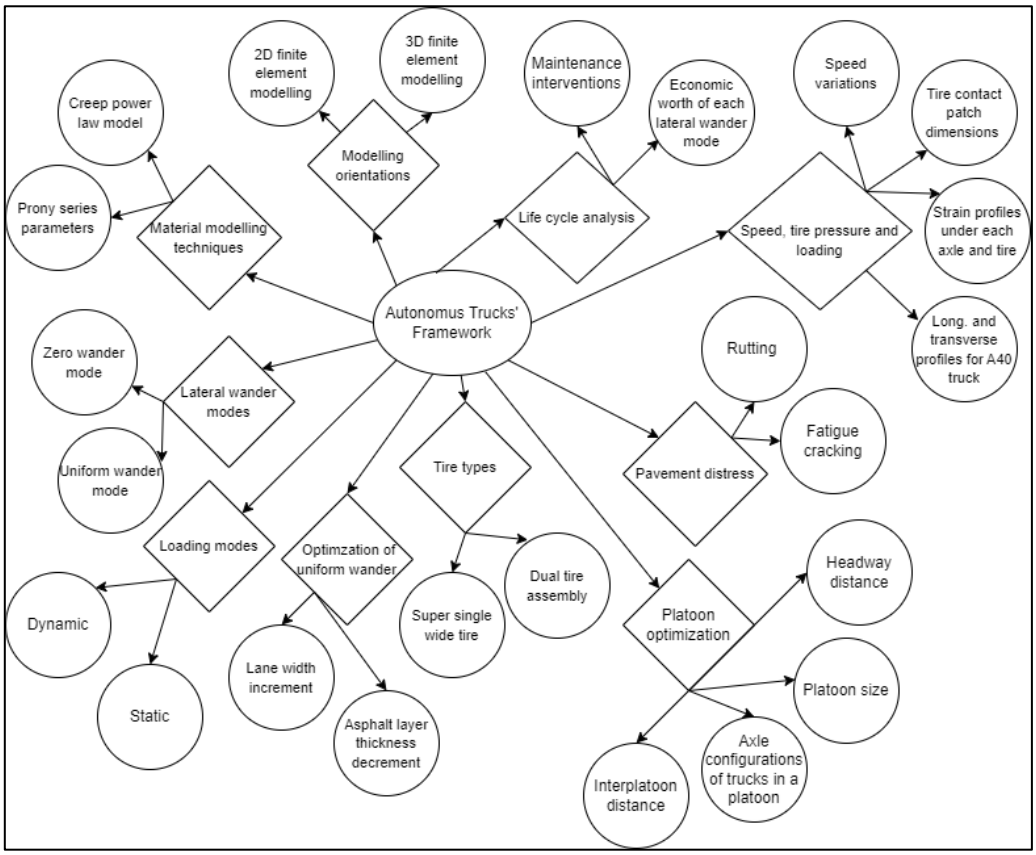

Fig. 4-1: Detailed framework components.

Creep power law model and Prony series parameters are analyzed based on their applications in 2D and 3D FE models for a thorough analysis of viscoelastic behavior of asphalt. Lateral wander modes are also included, in terms of a uniform wander mode and zero wander mode, along with dynamic and static loading modes employed during simulations. Furthermore, tire types consisting of a super single wide tire and a dual tire are also incorporated into these components. Moreover, speed variations have been included based on time step loading techniques.

Methodologies for tire pressure calculation based on tire contact pressure, axle loading and tire loading have been introduced for trucks with variable axle and loading configurations. Longitudinal and transverse strain profiles have been extracted and analyzed for autonomous trucks with varying axle configurations. Platoon analysis has been performed with variations in headway distance scenarios, number of trucks in a platoon based on their axle and loading configurations.

Distress analysis leads to performance analysis of pavement structure in terms of rutting and fatigue cracking as per the aforementioned variables considered. Rutting is observed in terms of number of tire passes, loading cycles and time required to reach a certain rut depth value. Fatigue damage is analyzed based on number of repetitions and resulting remaining fatigue life depending on combinations of tire types, later wander modes and vehicular speeds. Both distress types have been measured in terms of number of cycles and tire passes and the corresponding value of time.

Uniform wander mode has been further optimized by providing the increased allowable lane width for autonomous trucks and cost reduction analysis has been performed for decreased layer thickness for the asphalt layer for compensating with additional costs generated by increasing the lane width. Life cycle cost analysis has been conducted along the provision of maintenance interventions required for each of the two lateral wander modes. Economic, impact of each lateral wander mode is analyzed. Therefore, these framework components interconnect with one another and the effect of each variable parameter on the structural and economical performance of the pavement is analyzed.

5 General introduction and literature

5.1 Introduction

Autonomous trucks are bound to bring new challenges into the current transport by significantly impacting the current transport infrastructure in fields of traffic safety, highway design and pavement structural design. These trucks drive are kept in the lane with the use of Light Detection and Ranging sensors (Hereinafter: LiDARs), ultrasonic sensors, vision cameras and Global Navigation Satellite System (Hereinafter: GNSS) sensors [1]. These aforementioned sensors help steer the vehicle in a controlled path. Typically, the original path is primarily a fixed movement of the truck within the lane without any lateral wander.

Since, the use of no lateral wander option for the trucks can create channelized loading on the pavement structure with very little relief time provided for the pavement, rutting and fatigue cracking may occur much sooner. Usage of autonomous trucks with no lateral wander can accelerate the damage to the pavement structure in terms of fatigue cracking and rutting [2]–[5]. Therefore, the trucks should be programmed to distribute laterally in an uniform fashion with minimized occurrence of channelized loading on the pavement. Less repetition of loading on the same section of pavement would help in prolonging the service life of pavement.

Platoon size, distribution and configuration for the trucks also affects the pavement response to repetitive loading. It is observed that rest time give to the pavement can affect the long term performance of the asphalt mixture since asphalt behaves in a viscoelastic manner under the influence of loading [6]. Therefore, the use of uniform wander option for trucks is beneficial when combined with the use of autonomous truck platoons.

Autonomous trucks are programmed to follow a certain predetermined path along the highway lane. Given with an assumption of 100% autonomous trucks using the lane, with current selection of a zero wander mode in which the truck will follow a straight line path without any lateral wander, a group of trucks would pass through the same path all the time resulting in channelized loading. As the channelized loading frequency increases, the pavement would prematurely fail, either due to rutting or fatigue cracking. If the predetermined path is programmed in such a sway that the vehicle can maneuver laterally inside the lane to minimize the loading on the same specific point on the pavement, the risk of channelized loading can be reduced.

Impacts of autonomous trucks on the pavement structure can vary based on the loading magnitude, tire pressure, axle configuration, speed, platoon formation, existing condition of the pavement structure and lateral wander parameters. With the oncoming integration of autonomous trucks in the current transport infrastructure, a framework for the integration of autonomous trucks provides adequate analysis, leading to a smoother process of integration of autonomous trucks. Since the major impact by autonomous trucks on pavement structure is related to the lateral wander mode being used, further parameters consisting of speed, lane width, platoon size, interplatoon spacing, headway distance of trucks, pavement layer properties, tire footprint, tire pressure and life cycle analysis are combined with zero and uniform lateral wander modes for the framework development.

5.2 Current progress of autonmous trucks development

There are currently several companies including Daimler, Otto, Tesla and Volvo working on manufacturing vehicles with different levels of autonomous modes starting from assisting the driver in terms of increased safety to fully autonomous trucks [7]. Global autonomous trucking firm TuSimple has been performing its trials on public roads with autonomous trucks in the US since 2021. These trucks will be able to observe forward over a thousand meters and with the help of sensors, these trucks can be operated in night time and rainy weather.

Volvo has reportedly been working with automated vehicle software provider Perceptive Automata to use truck based Artificial Intelligence to analyze the behavior of other road users as shown in **Fig. 5-1**.They are currently working with 360 degrees of monitoring of road users near the truck with embedded cameras and sensors in the trucks. This allows the automated system in trucks to avoid collisions with motorized and non motorized traffic [8].

Fig. 5-1: Demonstration of Perceptive Automata's tracking and signaling. Source: Volvo Trucks.

Daimler and its autonomy partner Torc Robotics based in Virginia, US are working on operating the level 4 automonous trucks as per Society of Automotive Engineers (Hereinafter: SAE) as shown i. As per this level of autonomy, field trials are in progress with the help of licensed safety driver and an engineer for monitoring the progress along the operation of the truck [9].

Fig. 5-2: Self driving truck test run in Virginia, US. Source: Daimler.

5.3 Components of autonmous vehicle system

Self driving cars have been developed by Google and Defence Advanced Research Projects Agency (Hereinafter: DARPA) since 2010, the technology consists of cameras that have afield

view of 360 degrees around the vehicle and can collect thousands of data points in seconds as shown in **Fig. 5-3** [10].

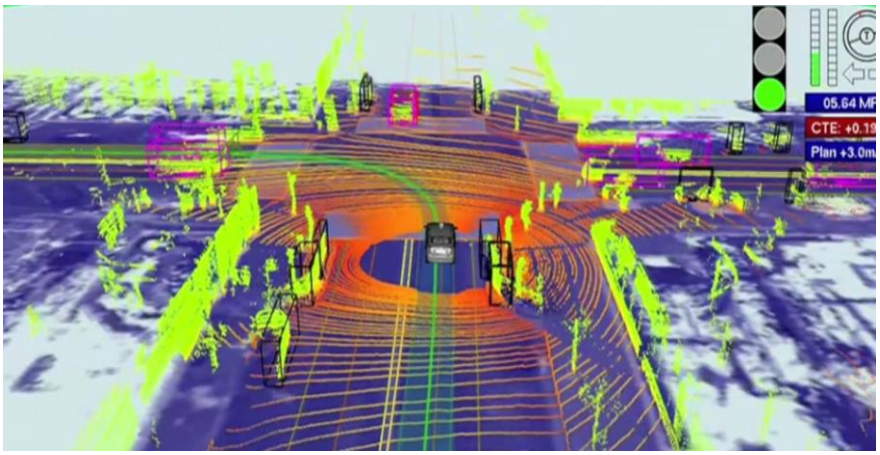

Fig. 5-3: Sensors inputs into a Google self driving car. Source: Ted.com Google inc.

There are five automation levels defiend by National Highway Traffic Safety Administration (Hereinafter: NHTSA) [11].

1. Level 0 – No Automation : The human is in complete and sole control of safety-critical functions (brake, throttle, steering) at all times
2. Level 1 – Function Specific Automation: The human has complete authority, but cedes limited control of certain functions to the vehicle in certain normal driving or crash imminent situations. Examples: adaptive cruise control, ESC, automatic braking (but not in combination so as to enable hands-off-steering wheel/foot-off-pedal operation
3. Level 2: Combined function Automation: Automation of at least two control functions designed to work in harmony (e.g., adaptive cruise control and lane centering) in certain driving situations. Enables hands-off-wheel and foot-off-pedal operation. Driver still responsible for monitoring and safe operation and expected to be available at all times to resume control of the vehicle.
4. Level 3: Limited Self Driving: Vehicle controls all safety functions under certain traffic and environmental conditions. Human can cede monitoring authority to vehicle, which must alert driver if conditions require transition to driver control. Driver expected to be available for occasional control.
5. Level 4 – (Full Self Driving Automation) Vehicle controls all safety functions and monitors conditions for the entire trip. The human provides destination or navigation input but is not expected to be available for control during the trip.

AV technology can be divided into four basic components: sensors, mapping, perception, and communication. Sensor technology includes a variety of hardware such as forward looking infrared sensors for night conditions, multiple video cameras for daylight conditions, , radar for measuring range and velocity, Global Positioning Systems (hereinafter referred to as GPS) to determine location, and detection of humans and animals, accelerometers and gyroscopes to detect changes in speed and direction, and Light Detection and Ranging (hereinafter referred

to as LIDAR) that employs spinning lasers and photoreceptors to create a three dimensional model of the immediate environment.

Coordinate files of points and line segments are used in Mapping that represent streets, origin and destination addresses, and other features, including digital aerial photography, ground level imagery of roadway features, traffic control devices and obstacles. Mapping also may include stored terrain models created with LIDAR as shown in **Fig. 5-4**.

Perception includes the set of software processes that fuse data from the various sensors, compare it with stored mapping and determine how the vehicle will react to the various inputs. Perception includes determining and maintaining the vehicle's position within the traffic lane and with respect to other moving vehicles, monitoring and reacting to traffic control devices, detecting and reacting to pedestrians and other obstructions in the vehicle's path, keeping track of the vehicle's location with respect to the map, and monitoring and reacting to the forces acting on the vehicle. Other functions include monitoring the health of the vehicle and its automated systems.

Communication technology can be either Vehicle to Vehicle (Hereinafter: V2V) or Vehicle to Infrastructure (Hereinafter: V2I).V2V communication can allow vehicles to exchange information about their position and movement intentions, allowing other vehicles to anticipate and respond to maneuvers. V2I communications can allow vehicles to communicate with traffic control devices and allow the exchange of mapping data between stationary sources and vehicles [12].

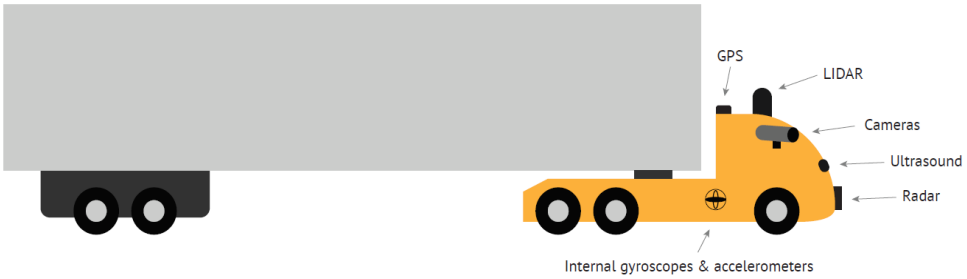

Fig. 5-4: Key technology used in self driving trucks. Source: Bishop et al. [13]

Shokoufeh et al. [14], has identified two groups of autonomous vehicle systems The first group is termed as intermittent autonomy. This system consist of features such as Advanced Driver Assistance Systems (Hereinafter: ADAS), which consist of lane departure assist and fully automated driverless experience, however it all happens in the presence of a human driver. The second group is termed as True Autonomy, in which there is no human presence and all the system whether it is a hardware or software works independently throughout the trip.

Chottani et al. [15] stated that 65% of consumable goods in the US are transported by trucks. With the provision of fully automonous trucks the operating costs would decline by 45% which means the truck industry will save between 85 billion to 125 billion. Mckinsey Center for Future Mobility have developed a proposed evelution plan of automonous trucks with an increasing level of autonomy with time. It is expected that int he US market, the automonous trucks will roll out in four waves as shown in **Fig. 5-5**.

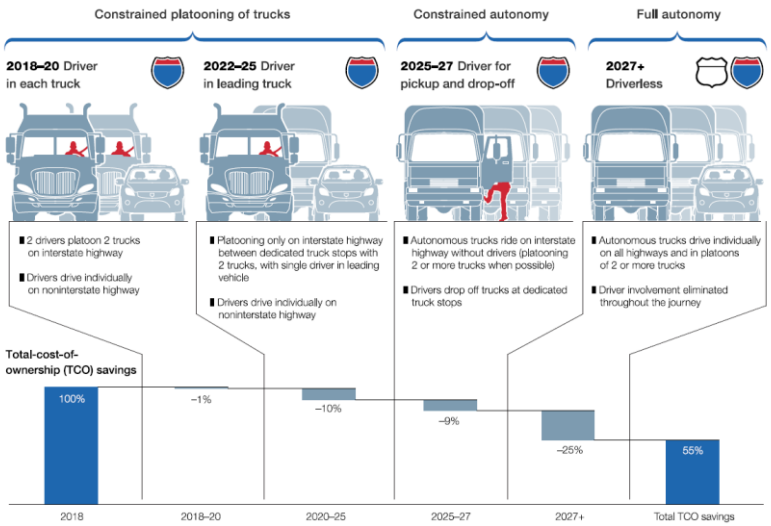

Fig. 5-5: The fast track to the future of commercial vehicle industry. Source: Chottani et al. [15].

The first two waves mentioned herein correspond to the level 3 automony of SAE. Which will require driver as in Conditional Automation. It includes Platooning of trucks in which a group of trucks are connected wirelessly and they are followng a lead truck in the platoon. Th next wave is going to be driverless platooning in which only the driver in the lead vehicle is incharge and the vehicles following the lead truck are unmanned. As they leave the highway, drivers will resume control of each truck. The fourth wave corresponds to level 4 autonomy of SAE. In which unmanned trcuks are expected to use the interstae highway system without platoons, the drivers will be picked up at the nearest stop at the inetrsate exit and they will drive the trucks to destination. The fully autonomous trucks will be the last wave as it correspons to level 5 automony of SAE, in which everything from loading to delivery will be performed by unmammned automonous trucks.

5.4 Impact on transport costs

Andersson et al. [16] performed a cost benefit analysis on the incorporation of autonomous trucks and vehicles in the existing market. The parameters calculated were generalized costs, external effects and social marginal costs. A summary related to saved driver costs for trucks and decreased travel time costs were converted into monetary terms to help visualize the benefits of AVs. It has been stated in this study that there are lower generalized costs generated in terms of vehicle kilometers (Hereinafter: vkm) when the AVs are used. Three vehicle categories based on axle type and weight magnitude were used in this study. Long distance vehicles having 6-7 axles and capacity of 40 tonnes, distribution vehicles with 2 axles and capacity of 16 tonnes, construction material transport vehicles having 3 axles and capacity of 16-24 tonnes. The market share of these vehicles in vkm as of 2015 is 70%, 13% and 17% respectively. Similarly, the average speed for calculations was 38 km/h, 22,5 km/h and 22,5 km/h. Authors stated that with the platooning of long distance autonomous trucks there will be less wind resistance and smooth driving conditions, in this way there will be 10% less fuel cost. With the use of autonomous trucks, as mentioned earlier there will be no driver costs. It has been estimated in this study that the saved long distance driver costs would be 31,4 million euros in 2025 and 706,8 million euros by 2040. With increased traffic safety, the costs are reduced by 1,7 million euros by 2025 and 44 million euros by 2040.

5.5 Impact on traffic safety, fuel and time efficiency

Reduction in congestion, increment in mobility and increased in traffic safety has been identified in various studies. The costs incurring are lost jobs for autonomous trucks [17], increase in fuel efficiency decrease in traffic congestion has been identified by Fagnant and Kockelman [18]. A study performed by Litman [19], summarized the benefits as increased fuel efficiency, mobility, parking capacity and support for shared vehicles. The costs identified in this study were capital costs for vehicles and infrastructure, reduced employment, increased travelling and increased risks. In a study conducted by Milakis et. al [20] on autonomous vehicles, positive review in regards to fuel efficiency, traffic safety, reduced emissions, increased road capacity and reduced accidents has been observed. However with AVs the travel demand also increases and their effect on public safety, economy and land use should be clarified. Gruel and Stanford [21], identified long-term potential impacts of AVs and conclude that there are positive and negative outcomes, and that it is unclear whether they will be a societal net benefit or harm. In all scenarios safety and mobility will increase, better use of travel time and lower fuel consumption are among the benefits but more travelling increases costs. Wadud [22] concluded that the owners of commercial vehicles are most likely to be early adopters because they can save on driver costs and their ratio of benefits to costs is high. For regular cars, the largest gains are among people with the highest income, because they travel more and place a high value on time.

Bao and Mundy [23] examined how driverless trucks and platooning combined could decrease relative costs for road transport compared to rail and thereby result in modal shifts from rail to road. Their findings suggest that road transport costs can be cut by approximately 40% which greatly increase the transport distance at which road transport is cost-competitive against rail transport. The resulting decrease in rail demand is estimated by using two methods, an elasticity-based method suggesting an effect of 45% and a cost-curve-based method which suggests an effect of around 20%. Huang and Kockelman [24] studied the impacts of driverless trucks on freight transport patterns in the U.S. by using a multiregional input-output model with a random-utility-based mode-choice model including rail and road transport (the "RUMBRIO" model). For the assumed reduction in road freight transport costs per Tonne-Kilometre (Hereinafter: TKM) by 25%, it is estimated that road-TKM increase by 11%, partly explained by a modal shift from rail and partly by changes in origin choice. The use of trucks increases for all but one commodity type and all distances except for the longest distances.

5.6 Impact of Pavement Structure

Autonomous trucks will have major effects on the cost component of highway maintenance and repairs. Since the autonomous trucks are preprogrammed to control their lateral trajectory within the lane, if the autonomous trucks continuously follow a straight-line path without any lateral movement in lateral wander mode termed as Zero Wander mode, accumulation of channelized loading can prematurely damage the pavement. However, the term Uniform wander of loading is proposed by various researchers, where the truck would uniformly distribute itself in the lane to minimize the repetition of loading thereby increase the pavement life and reduced maintenance costs. Noorvand et al. [4] conducted a study on different lateral wander modes of autonomous trucks and it was found that with proper use of uniform lateral wander mode, the maintenance costs would decrease by 35% if 100% autonomous trucks are used. Cheng et al. [25] also analyzed the impact of autonomous trucks on pavement damage. Various lateral wander modes were analyzed from zero wander to uniform wander mode. The

zero-wander mode indicted the highest damage to pavement, while the uniform wander mode indicated increase in pavement life as compared to human driven trucks. It was found that maintenance year is prolonged by 2.3 years if autonomous trucks are used with uniform wander mode. Wu et al. [26] have used the Heavy Vehicle Simulator (Hereinafter: HVS) for evaluating rutting performance of asphalt mixtures along with lateral distribution impact of loads on rutting progression. The temperature was elevated for increased rutting progression and simulations were conducted on a finite element model. Results showed good capability of the developed finite element model to predict the rutting progression when compared to that of the HVS. Fahad et al. [27] also conducted creep loading analysis by autonomous trucks on pavement damage using realistic tire footprints from a dual axle. Damage effects among human driven truck and various modes of lateral wander were compared against each other, and it was found that pavement life would increase by 3 years in terms of rutting accumulation if proper positioning of uniform wander mode is sued. Hence, if proper positioning of lateral wander of autonomous trucks is sued, the highway maintenance costs can be reduced as compared to using human driven trucks. Pais et al. [28] have also performed the study for the autonomous trucks by in the MPEDG software with different allowable widths for the lateral wander of autonomous rucks from 0.2 m to 0.6 m. results showed favorable increment in fatigue and rut life of the pavement when the 0.6 m lateral wander is employed.

The summary of effected parameters as a result of autonomous trucks based on the combination of analysis done by various researchers is shown in **Table 5-1** below.

Table 5-1 Summary of parameters under usage of autonomous trucks.

Parameters	**Predicted Values**	**Researchers**
Increased Traffic Safety	10% reduction in accidents in 2025 and 30% reduction in 2040	[12], [16], [17], [29], [30]
Decrease in transport costs	15% in 2025 and 50% in 2040	[23], [24], [29], [31]
Decrease in environmental impacts	15% reduction in emissions	[32], [29], [33], [34], [35]
Improved infrastructure utilization	30% more utilization	[31], [33], [36], [37]
Decrease in fuel consumption	10% in 2025 and 50% in 2040	[15], [29], [31], [33]
Decrease in road repair and related costs	30% reduction in maintenance costs, 40% reduction in fatigue cracking and rutting with the use of uniform wander mode	[4], [27], [38], [39], [28]

5.7 3D and 2D finite element modeling for rutting analysis

Rutting is considered as one of the major forms of distresses in the flexible pavements [40]. It usually happens along the wheel path used by heavy moving traffic [41]. Damage in terms of rutting usually happens in the pavement when accumulated loading in the pavement leads to permanent deformation and the pavement can no longer stay in operational condition [42].

Typically the permanent deformation on the surface of the asphalt layer contributes to the majority of rut depth compared to other layers in the pavement structure [40].

3D and 2D finite element models have been used to predict rutting in asphalt pavements. Huurman et. al have used 3D FEM for predicting rutting in case of steel decks [43]. Ali.et al have used a viscoplastic constitutive model in 2D plain Strain FEM to evaluate the nonlinear behaviour of pavements under complex traffic conditions [44]. It was identified that the rutting phenomenon is highly affected by traffic speed and lateral wander of vehicles. Sadeghnejad used the 2D FEM by incorporating the creep model developed to predict the rutting behaviour of Glasphalt mixtures and the effect of temperature and stress on these mixtures. It was identified that the presented creep model in the studies successfully evaluate the rutting prediction of Glasphalt mixtures [41]. 3D and 2D FE modelling can be used to predict rutting of asphalt layers. 3D FEM, however, is expensive in terms of computational time [40]. Comparison of results for 2D and 3D FE was done by [44]. The rut depth profiles were predicted using both methods for 5000 load passes and it was found that the difference in maximum rut depth in two methods was 2% which is not significant in terms of rutting prediction of asphalt pavements.

Since asphalt is a rheological material, hence creep models can be used to determine deflection in asphalt layers. Wong et al. utilized the dynamic creep test to study permanent deformation if foamed asphalt mixtures and reported that resulting creep strains accumulations are good indicators of permanent deformations in pavements [45]. Al Qadi et al. [46] evaluated the creep behaviour of asphalt mix at intermediate and high-temperature ranges using a time hardening version of creep power law in 3D FEM simulation and found a through validation of results when compared with field measurements at Virginia Smart Road [47].

Creep power law model in a finite element modelling software ABAQUS has been successfully employed to investigate the permanent deformation in forms of rutting for various asphalt mixtures in Finite element analysis. [48][41] and [49] Power law model is simple yet suitable for determining the rutting behaviour of asphalt mixtures. [41] and [50]. ABAQUS utilizes two different types of creep models namely power law model and hyperbolic sine model. In power law model, the time hardening version is used.

5.8 Fatigue damage evaluation using finite element modelling

Fatigue damage is a major form of distress in flexible and rigid pavements [51]. Fatigue cracking occurs in the pavement as a result of cumulative traffic loading on the pavements [52], [53], [54]. Fatigue damage in asphalt pavements is highly dependent on variation in temperatures and corresponding stress strain levels [55], [56], [57]. Since the human driven trucks never utilize the complete width of the lane hence the repetition of concentrated loading along the narrow region of wheel path is increased. Hence, higher accumulation of loads along the same point can result in development of fatigue cracks hence prematurely failing the pavement structure. Moreover, fatigue cracking prevails at much faster rate in regions with lower pavement temperature in winter climatic conditions [58].

Development of fatigue cracking differs by pavement type in case of rigid and flexible pavements. For conventional Hot Mix Asphalt (Hereinafter: HMA) pavements, fatigue damage is highly dependent on temperature variations since asphalt is a viscoelastic material [58]. In case of rigid pavements, fatigue resistance can be increased by providing a jointed reinforced concrete pavement with the help of dowel bars for load transfer and reinforcement to resist

cracking due to presence of tensile stresses at the bottom of the concrete slab [59]. In case of HMA pavements speed of loading can highly affect the occurrence of permanent deformation [60]. Since permanent deformation in pavements is also a function of speed which indicates loading time at a certain point in the pavement, using this concept the frequency of loading as well as the loading time can affect the fatigue life of pavement also. Since fatigue damage is a common distress in pavements, it is important to address the impact of autonomous trucks on fatigue life of pavements.

Gungor et al. [61] developed a flexible pavement design framework termed as Wander 2D for optimizing the lateral coverage by autonomous trucks within the lane. The recommended framework was applied on Mechanistic-Empirical Pavement Design Guideline (Hereinafter: MEPDG). Research concluded with possibility of MEPDG to be used for determining lateral wander impacts of autonomous trucks. Noorvand et al. [4], studied the impacts of various lateral wander modes and traffic composition of human driven and autonomous trucks by performing the analysis on MEPDG software with conclusions based on minimum recommended percentage of Autonomous Trucks to be 50% in the traffic mix under a uniform lateral wander mode. Zhou et al. also performed comprehensive analysis on the use of different lateral wander modes of ATs on rutting and fatigue cracking. Two lateral wander modes namely, zero wander and uniform wander mode were analyzed. Results showed that if the lateral wander was limited then, the pavement fatigue life would shorten by 22%. Authors recommended the use of wider lateral coverage by ATs to improve fatigue life [62].

3D and 2D Finite Element models have been successfully used to investigate fatigue cracking in rigid and flexible pavements. Sotelino et al. [59] performed the damage analysis of jointed plain concrete pavements using the 3D FE model. The effect of soil conditions, slab thickness and slab stiffness on developed stresses on rigid pavement sections were investigated. Moreover, the developed FE model was further improved by optimizing load simulation, mesh refinement, interaction between pavement layers and model geometry. FE model was used to develop simulation tests on pavements and results were then compared with modelling of actual skewed pavements. The developed FE model could successfully determine the cause and orientation of failure. It was also found that non-linear accumulated damage reduces the fatigue life by a greater magnitude than that caused by non-linear fatigue damage.

Wang et al. [63] performed dynamic loading analysis using 3D FE model to simulate loading under non-uniform tire contact pressures. Dynamic load coefficient was sued to understand the severity of damage by vehicle's load classification. Results showed that pavement with rough surface would show more damage accumulation in terms of fatigue damage and permanent damage with increased vehicle loading class.

Hadian et al. [64] used 3D FE model for investigation of fatigue cracking progression in synthetic asphalt pavements. Tensile strain was measured at the bottom most part of the pavement. Moreover, the friction in between successive pavement layers was adjusted to measure its effect on deformation and fatigue cracking. It was found that increasing the elastic modulus of material layers could reduce the tensile strain by a small margin and fatigue cracking was prevalent in stiffer AC mixtures.

Song et al. [65] employed the use of 2D FE model to determine fatigue life of pavement under the influence of autonomous trucks by using Palmgren-Miner linear damage hypothesis. Moreover, the parameters of truck platoon such as number of vehicles, lateral offset of trucks

within the lane and headway was determined to account for fuel savings. Different lateral offset options were tested for improved fuel savings and reduced fatigue damage, the study concluded with the recommended lateral offset of 100 mm to 150 mm which improved the fuel saving by 8% and fatigue damage reduction by 30%.

Tóth et al. [66] evaluated the effects of pavement temperature variations by dividing the asphalt layers into 19 sublayers using 3D finite element model develops in finite element modelling software ANSYS. Resulting horizontal tensile strains and vertical compressive strains were evaluated, and fatigue analysis was performed to validate the predictions made by the model. Results showed that equivalent temperature method could provide good prediction for pavement's structural performance.

Chen et al. [38] used the 2D FE model to assess the impacts of various lateral wander modes of autonomous trucks on rutting and fatigue cracking. For fatigue cracking determination, Palmgren-Miner linear damage hypothesis was used. Types of lateral wander modes tested were zero-wander mode, uniform mode, double peak Gaussian mode and a two-section uniform mode. These modes were then combined with different ratios of human driven and autonomous trucks in the traffic mix. Results concluded with favor of use of 100% autonomous trucks when their lateral trajectory is controlled using a two-section uniform wander mode in which the reduction in fatigue damage to upto 30% can be achieved. Palmgren-Miner linear damage hypothesis also termed as Miner's rule has been used in calculating fatigue damage and remaining number of tire passes for a specific period of time [65], [38].

5.9 Pavement modelling using modified subroutines

Pavement distress in terms of rutting induced by autonomous truck traffic can be measured using static and part dynamic loading scenarios as provided in ABAQUS, however these methods are only limited to application where no lateral wander is considered in by traffic. Moreover, in another concept the moving load can be simulated by shifting the load and its amplitude over a loading path step by step until one wheel pass is completed [67], [68] and [69]. A dload subroutine written in FORTRAN, on the other hand can be used to define position, time, element number and load integration point number being a function of distributed load magnitude. A Vdload subroutine can be used to define position, time and speed of applied load [6]. Such allowance would result in field like simulation conditions where lateral wander of autonomous trucks can be tested.

For the zero wander mode, a series of nodes and elements along a single coordinate axis are defined for an entire length of the model, making the simulation procedure rather simple, however in case of a uniform wander mode, an amount of time is allocated on each element throughout the whole traversable section of pavement model. With the passage of time and movement of a truck tire, a suitable path is created and an unevenly distributed load of a constant magnitude is induced on nodes and elements.

Application of programmed scripts and dload subroutine integrated into ABAQUS has been done in previous research. [70] performed simulations of dynamic loading load on a pavement surface in a 3D model developed in ABAQUS by incorporating the dload subroutine written in FORTRAN. The research dealt with setting up of self powered surface sensing sensors and their capability to detect bottom-up cracks in the pavement, results concluded with good capability of suggested framework for indicating the progression of bottom-up cracking in pavement by self sensing surface sensors. [71] performed dynamic analysis on a 3D FE model

developed with the help of user subroutine to assess the performance of asphalt overlays over rigid pavements. Moreover, axle weights and lateral displacements were included in ABAQUS with help of customized subroutine and results showed good coherence with data obtained from the Falling Weight Deflectometer.

Pi et al. [72] investigated the effect of using PolyLevel foams under rigid pavement for improving smoothness by performing simulations in 3D FE model ABAQUS using a dload subroutine written in FORTRAN. Simulations were conducted under various cyclic loading scenarios and load magnitudes. Research concluded with good capability of polyurehtane foam to improve smoothness in rigid pavements. [73] performed 3D FE simulations using a dload subroutine developed in FORTRAN to investigate the use of geotextiles in reducing reflective cracking in pavements. Load was assumed to be uniformly distributed, and direct cyclic loading using a half-sine function was employed. Results showed that with the use of geotextiles were able to absorb 15% of the stress. Summary of researchwork for the subroutines used in shown in Error! Reference source not found..

Table 5-2 Summary of previous research using Dload and vDload

Authors	**Model Geometry**	**Programming language/subroutine**	**Remarks**
Lajnef et al. [70]	3D	FORTRAN/Dload	Application of dynamic moving loads
Cho et al. [71]	3D	FORTRAN/Dload	Temperature and loading
Si et al. [74]	3D	NA/Dload	Application of dynamic moving loads
Dong et al. [75]	3D	FORTRAN/Dload	Application of dynamic moving loads under constant speed and tire pressure
Chen et al. [6]	3D	NA/VDload	Application of dynamic moving loads under direct load magnitude and constant speed
Cao et al. [76]	3D	NA/Dload	Rutting progression analysis

Authors	Model Geometry	Programming language/subroutine	Remarks
Pi et al. [72]	3D	FORTRAN/Dload	Application of dynamic loading under cyclic loading with constant load magnitude
Sun et al. [73]	3D	FORTRAN/Dload	Application of dynamic uniformly distributed loading under constant speed and load magnitude
Yoo et al. [77]	3D	NA/Dload	Application of transient dynamic loading through a developed model

5.10 Platoon analysis of autonomous trucks

Human driven trucks follow a normal distribution of lateral position in the lanes [62]. A conventional truck platoon with consists of 3 to 8 trucks in a group can have detrimental effects on the pavement structure. In case of human driven trucks, around 80% of loading is channelized along the usual wheel path, which corresponds to acceleration in pavements fatigue damage [61]. However, in case of autonomous trucks, the pavement damage can be reduced inside the truck platoon by using a certain lateral wander mode so that the channelized loading is minimized.

A truck platoon affects the pavement structure based on factors such as speed of the trucks inside the platoon, headway of trucks inside the platoon, loading class and axle configurations of trucks inside the platoon. However, the most contributing factors related to truck platoons damage to pavement is the concentration of loading on the same point of the pavement. Higher speeds result in reduced accumulation of strains under the asphalt layer as well as on top of subgrade layer [78]. Occurrence of creep related distresses is minimized at higher speeds. Headway of the trucks is selected to reduce fuel consumption and adequate reaction time for stopping distance. Current headway times used for trucks may favor fuel efficiency and safety, but its effect on pavement damage is compromised.

Loading class and axle configurations can affect the damage difference between different platoons. Modular truck types with loads exceeding 50 Tons can be damaging if used in platoons. Hence, a platoon size can affect the pavement response during its pass. Platoon size should be carefully controlled and limited based on total number of trucks and total accumulated load on the pavement. Distance in consecutive platoons can be increased to give a relief time to pavement when the next platoon arrives. With the use of preprogrammed lateral wander mode, the damage to the pavement from each platoon can be minimized.

In truck platoon, multiple trucks drive at fixed distances between them with the use of LIDARS and wireless communication networks at a constant speed efficiently [79]. Most efficient type of typical platoon matchmaking is a Real time platooning where the trucks find their match

with other tracks based on similarly in routes moments before any departure interval, usually in case of stop breaks or starting the journey in the beginning [80]. The most common concept of truck platoons consists of the leading vehicle that is followed by one or more following vehicles and the following vehicles brake, steer and accelerate according to the leading vehicle [81]. Increased efficiency and decreased fuel consumption of up to 4.7% with the use of truck platoons as a result of increased aerodynamics occurs. The concept of truck platooning is very much in conjcution with progression of autonomous trucks in case of phase 3, in which trucks will have 100% autonomy with no human involvement [13].

5.10.1 Loading Intervals

Truck platooning is considered to be beneficial for traffic safety and fuel consumption however, repeated loading with minimum loading intervals can accelerate pavement fatigue. Song et al. [65] analyzed the effect of number of variables, lateral wander and loading interval in a truck platoon using finite element modelling. Simulations were run based on various lateral offset modes for the following trucks in a platoon, along with corresponding fuel savings for each scenario. Results showed that a lower number of trucks is preferred in case of fuel savings with optimum number of trucks reduced to two using lateral offset which decreases the fatigue damage by 30% and fuel consumption by 8%. Al Qadi et al. [82] performed detailed analysis on impacts of truck platoons on pavements by proposing an optimization method for reducing pavement life cycle costs without compromising the fuel savings by a truck platoon. Finite element modelling was used to analyze the loading intervals, lateral wander scenarios to optimize the use of platoons. Results showed that an optimized truck platoon pattern would decrease pavement life cycle costs by 48% compared to conventional channelized loading of human driven truck platoons.

5.10.2 Effect on Pavement Response

Melson [83] performed traffic congestion and mechanical impact analysis of truck platoons on transport infrastructure. In the field of mechanical impact analysis using the pavement design software, it was suggested that lateral wander had a significant impact on fatigue propagation and permanent deformation in the pavement structure. Results showed that without considering lateral wander, up to 35% of decrease in fatigue life can occur for a 20 year design period with maximum increase in maintenance costs of 46%. Bouchihati [84] investigated the effect of truck platooning on surface wear related to raveling, fatigue damage and permanent deformation using Dutch pavement design strategies. Results showed that with conventional use of traffic lane in the pavement, truck platoons would negatively affect the fatigue life and permanent deformation in the pavement and further optimization strategies are required to mitigate the extensive pavement damage. Marsac et al. [85] conducted optimization analysis by incorporating the lateral wander option for the trucks inside the platoon using pavement design software Viscoroute [85].

5.10.3 Truck Spacing

Spacing of trucks inside the platoon and space between each platoon is a function of rest period given to the pavement to properly recover in terms of permanent deformation and fatigue damage. Nejad et al. [86] has identified the effect of prolonged rest period on decreased deformation in pavements. Kim and Kim [87] have identified minimum amount of rest period beyond which the permanent deformation may occur. Al Qadi et al. [82] found that with a 10 ft spacing between trucks, around 99.5% of vertical elastic strain is recovered and the recovered strain amount reduces as the spacing gets smaller than 5ft. Jimenez et al. [88] stated that

provision of rest periods can allow for applications of loads until failure caused by fatigue. Al Mansoori et al. [89] suggested the use of extended rest period for asphalt mixtures to minimize permanent deformation. Zeiada et al. [90] investigated the effects of rest period and loading waveform patterns on laboratory prepared asphalt specimens on fatigue damage. Results showed that the strains occurring from rest type loading were four times less than that of continuously loading conditions. **Table 5-3** shows the suumary of research concuted on truck platoons.

Table 5-3 Summary of previous research for platoon analysis.

Researchers	**FE Model Type**	**Nuber of Trucks in Platoon**	**Measured Distress Parameter**	**Remarks**
Song et al. [65]	3D FE	2,3,4,5,6	Fatigue Damage	Use of various lateral offset options for trucks in a platoon
Al Qadi et al. [82]	3D FE	NA	Fatigue Damage and Rutting	Use of different truck spacing and lateral position scenarios
Melson et al. [83]	3D FE	2,3,4,5	Fatigue damage and permanent deofrmation	Use of offset options and platoon size for assesing pavement damage
Marsac et al. [85]	Viscoroute 2	3	Induced strain	Use of lateral wander for trucks in platoon and measurement of induced vertical strains under loading

5.11 Increased lane width and Life cycle cost analysis for pavements

Since the use of uniform wander mode requires the complete use of width of the lane, therefore, a larger width of lane can provide a larger area thereby decreasing the risk of repetitive loading on the pavement. With the conventional lane width in highways available to the trucks, a certain amount of overlapping in wheel paths exists even in case of uniform wander mode [4]. Service life of the pavement be further prolonged by increasing the truck's lane width. Similarly, the pavement cross section can be adjusted with decreased pavement layer thickness in case of asphalt layer by increasing the pavement width, thereby reducing the initial construction costs.

With reduced construction costs and increased pavement lifetime, pavement rehabilitation strategies can be designed in life cycle costs analysis to maximize the benefits obtained from the use of uniform wander mode. With increased lifetime, using better materials and controlled mode of loading, less number of maintenance interventions are required, since the occurrence of fatigue cracking and rutting happens at a much later stage in pavement's lifetime [91].

Therefore, the decrease in asphalt layer thickness is compensated with increase in the lane width while maintaining the increasing trend of pavement lifetime.

Life cycle cost analysis gives information about the economic viability of construction and maintenance procedures by providing different alternatives for types of interventions used [92]. Due to huge amount of expenditures arising from highway infrastructure maintenance costs, LCCA helps in reducing the cost required for maintenance interventions by providing the most economically feasible alternative [93]. LCCA has been performed by various researches using deterministic and probabilistic models in finding the best alternative for pavement maintenance [94]–[96].

Riekstins et al. [95] used the deterministic and probabilistic approach using Monte Carlo method for LCCA by comparing five different maintenance and rehabilitation strategies and evaluated their impacts on CO_2 emissions and rehabilitation costs. Two different alternative strategies are Full Depth Removal and Placement and Full Depth Reclamation. The total costs related to maintenance strategies included workforce, materials, periodic maintenance and fuel. Highest amount of costs were exhibited by materials followed by fuel and workforce. Both approach strategies encouraged the use of Full depth reclamation intervention due to lower CO_2 emissions of upto 60% and rehabilitation costs upto 50%.

Braham [94] compared the effect of conventional maintenance strategies and full depth reclamation using LCCA procedures provided by FHWA. LCCA was conducted for the total pavement design life of 50 years. Analysis showed that the costs generated by using conventional rehabilitation strategies by each 4 year maintenance interval surpassed the total cost generated by using the full depth reclamation technique. Results showed that full depth reclamation would also increase the loading capacity of pavement structure during the span of pavement lifetime, being the best alternative for pavement rehabilitation procedures.

Akbarian et al. [97] have compared the costs generated using asphalt rubber with the conventional bitumen based asphalt mix. LCCA was performed by using thin structural overlay and milling as rehabilitation alternatives. Maintenance strategies were categorized by traffic volume on specific regions, with pavement having lower traffic volume getting less thickness of asphalt overlay during rehabilitation. Deterministic and probability approach was sued using the Net Present Value (NPV) with a discount rate of 4%. Results showed that use of rubber asphalt is a cost-effective alternative with lower cost of rehabilitation strategies required, thus improving the longevity of pavement lifetime.

6 Impacts of autonomous trucks on rutting under various speed, tire footprint and lateral wander mode variations

Impacts of autonomous truck passes on pavement have been analyzed in this research with speed variations of 90 km/h, 50 km/h, 40 km/h, 30 km/h, 5 km/h and 2.5 km/h along with the inclusion of two different tire footprints modelled in the finite element modelling software ABAQUS. Two tire type footprints used are Michelin super wide tire 455/55R22.5 and Goodyear dual tire G159A-11R22.5. Two types of lateral positioning namely zero wander and uniform wander along with both tires and variable speeds in a 2D model in ABAQUS. Further details can be found in [27].

6.1 Thesis 1

I have determined the impacts of autonomous trucks on RUTTING under various speed, tire footprint and lateral wander mode variations and came to the following results for Thesis 1:

1. Channelized loading caused by zero wander mode leads to 25% more damage by rutting.
2. Usage of wide tire leads to 20 % less rutting when compared to conventional dual tire.
3. An abrupt increase in rut depth occurs with a magnitude of 38 % below the speeds of 30 km/h.

6.2 Related publications

1. M. Fahad, R. Nagy, and P. Fuleki, “Creep model to determine rut development by autonomous truck axles on pavement,” Pollack Period., pp. 1–6, 2021, doi: 10.1556/606.2021.00328.
2. R. Nagy, and M. Fahad, “A comparison between rut depth values obtained from 2D and 3D Finite Element modelling”, In: IEEE International Conference on Cognitive Infocommunications (eds.) 12th IEEE International Conference on Cognitive Infocommunications (CogInfoCom2021) : Proceedings Online kiadás, International : IEEE (2021) 1,098 p. pp.735-746. , 12 p.
3. A. Borsos, C. Koren, E. Mako, D. Miletics, R. Nagy, M. Fahad, and Z. Magyari, “Road environment for autonomous vehicles In: Horváth, Balázs; Horváth, Gábor (eds.) XI. Nemzetközi Közlekedéstudományi Konferencia: „Közlekedés a Járvány után: folytatás vagy újrakezdés” Győr, Hungary : Szechenyi Istvan University (2021) 567 p. pp. 140-147. , 8 p.

6.3 Material model and vehicle speed

Creep power law model in ABAQUS, in Eq. 6-1, has been successfully employed to investigate the permanent deformation in forms of rutting for various asphalt mixtures in finite element analysis [41], [48] and [49]. Power law model is simple yet suitable for determining the rutting behavior of asphalt mixtures [41]. In power law model, the time hardening version is used.

$$\varepsilon = A\sigma^n t^m \qquad 6\text{-}1$$

where, ε is the creep strain rate; σ is the deviatoric stress (MPa); t is the total time (sec); A, n, m are creep parameters, where $A > 0, n > 0, -1 < m < 0$.

Integral expression of Eq. 6-1 is obtained and shown in Eq. 6-2.

$$\varepsilon = \frac{A}{m+1}\sigma^n t^{m+1} \quad 6\text{-}2$$

Parameters m of creep, power law can be related to parameters β with the followjng Eq. 6-3 [98].

$$m = \beta - 1 \quad 6\text{-}3$$

Viscoplastic strains can be rearranged and shown in Eq. 6-4.

$$\varepsilon_{vp}(\sigma, t, N) = (b_1\sigma + b_2\sigma^2)t^{\beta} \quad 6\text{-}4$$

Where b_1 and b_2 are coefficients, t^{β} (sec) is the time value for a relevant average slope of tangent β at specified temperature. However, the mode of loading is cyclic or continuous, it is going have a same effect on predicted strain rate since the whole loading time is same if time hardening version is used to describe material's behavior [44], [41].

Method introduced by Uzarowski 2006 [99], in which the number of wheel passes are converted into step loading time fits perfectly with application of creep power law model [100] and [101]. As shown in Eq. 6-5, using the equation given in MEPDG code [12], the time of loading can be calculated as follows:

$$t = \frac{L_{eff}}{17.6V_s} \quad 6\text{-}5$$

where t is the time of loading (sec) ; L_{eff} is the effective length (in) ; V_s is the vehicle speed (mph)

6.4 Tire loading and footprint details

Since the majority of rut depth occurs in the surface layer of pavements and the effect of wheel wander is significant in thinner asphalt pavements [102], [40]. Hence in this study an asphalt layer of 63 mm resting on a rigid surface (Portland Cement Concrete (PCC) foundation) is considered for modeling purposes. Lane width for the truck axle is kept at 3.5 m. **Fig. 6-1** and **Fig. 6-2** depict the illustrations of a dual tire and a super single wide tire assembly respectively.

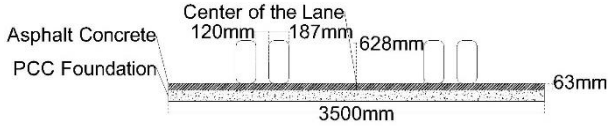

Fig. 6-1: Illustration of a dual tire assembly on the pavement.

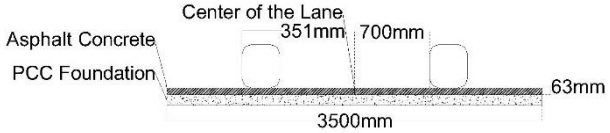

Fig. 6-2: Illustration of a super single wide tire assembly.

An axle load of 75.6 kN with a nominal tire pressure of 720 kPa has been considered in this study. Two different tire types, a super single wide base tire 455/55R22.5 developed by Michelin and a conventional dual tire G159A-11R22.5 developed by Goodyear are presented in **Fig. 6-3** and **Error! Reference source not found.** respectively.

Fig. 6-3: Digital tire footprint of a super single wide tire.

Fig. 6-4: Digital tire footprint of a dual tire.

Since the tire contact pressure is not uniformly distributed [99], [46], [103], therefore the effects of varying tire pressure is included to help understand the process of permanent deformation. As it can be observed from **Fig. 6-5** and **Fig. 6-6**, the magnitude of contact pressure in a wide base tire is less and is distributed in a wider area as compared to that of a dual tire. High concentration of contact stresses would occur as a result of usage of dual tire assembly.

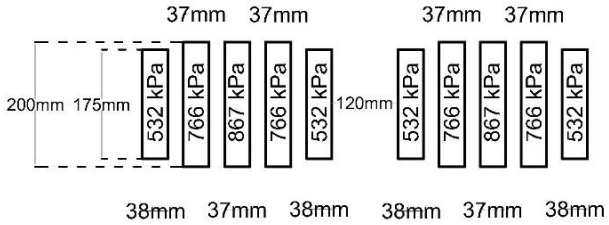

Fig. 6-5: Footprint details of a Goodyear G159A-11R22.5 dual tire used in simulations.

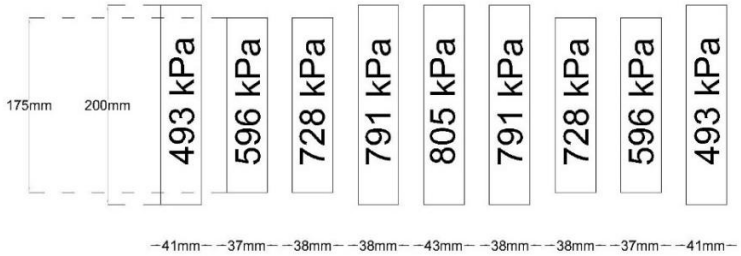

Fig. 6-6: Footprint details of a Michelin455/55r22.5 super single wide tire used in simulations.

6.5 Incorporation of Uniform and Zero Wander modes

Effect of ATs on pavement performance can be studied based on various lateral wander modes. In this study, two lateral wander modes have been considered, (a) Zero Wander, and (b) Uniform Wander. In the zero wander mode, the ATs are programmed to strictly follow a predetermined path within the lane with no allowance of lateral wander. Although utilization of this mode would be beneficial in terms of decreased lane width and traffic safety however analysis have shown that this mode results in higher concentration of stresses along the fixed

wheel path, which in result accelerates the rutting as shown in the results. In case of an uniform wander mode, the ATs are programmed to uniformly distribute themselves along the available width within the lane so as to limit the concentration of stresses along the wheel path. Figures below show detailed illustration of position of truck tires within one side of the lane. Moreover, the possible positioning of truck tires in a uniform wander mode has also been shown in **Fig. 6-7** and **Fig. 6-8**.

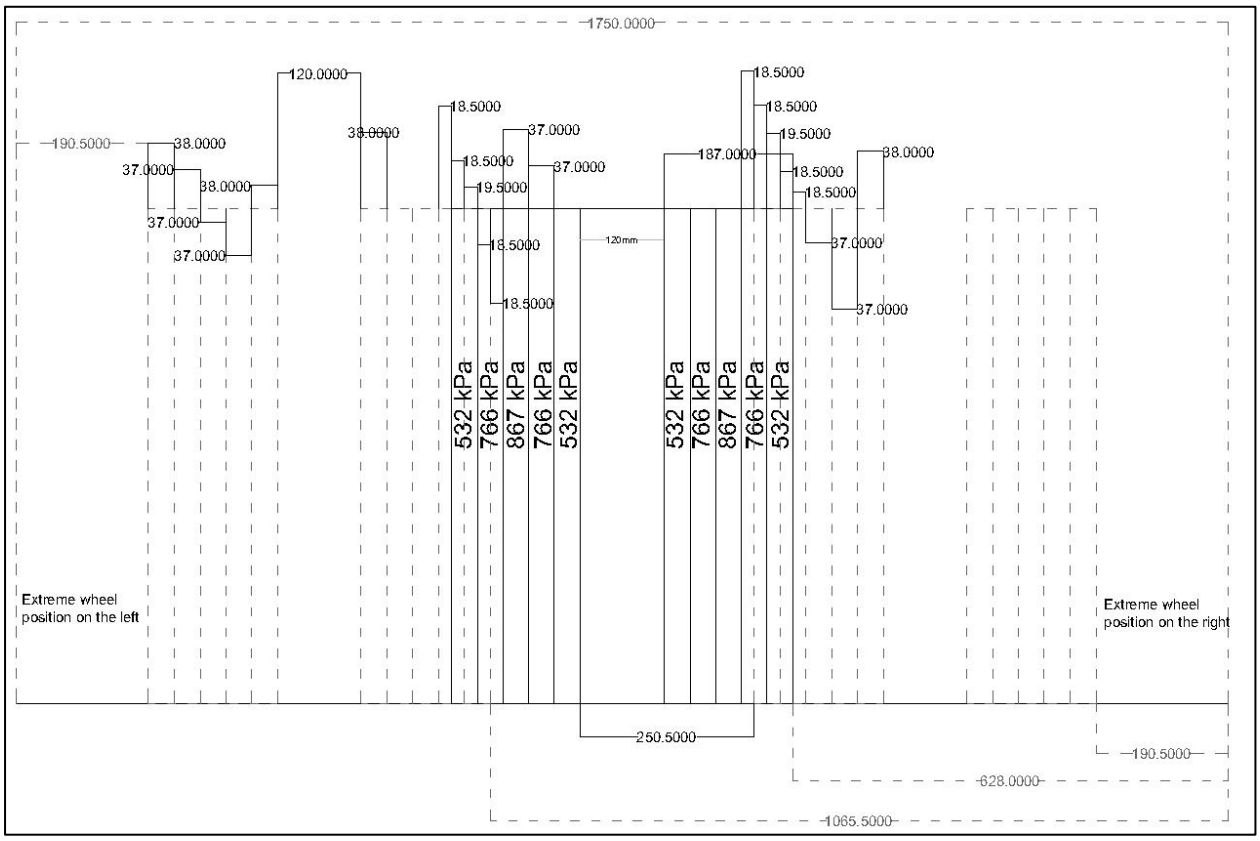

Fig. 6-7: Lateral positioning options of a Goodyear G159A-11R22.5 dual tire. Units in mm.

Since either sides of a truck axles are symmetrical so only one side is considered for simulation purposes. Since a total lane width considered in this study is 3.5 m, in a symmetrical case only half of the lane width is used which is 1.75 m. In this case, three different lateral positions of a truck tire are assumed to be used for zero and uniform wander modes. The total lateral width covered by a dual tire assembly on either of one sides is around 50 cm. A safety distance of 20 cm is provided along the edge of the lane so all the possible lateral distribution positions would lie within the highway lane. In case of a zero wander mode, the inside edge of a right most wheel is 63 cm away from the center of the lane. In case of a uniform wander mode, the first positioning of truck tires strat at 20 cm from the inner edge of truck tire to the center of the lane, in second positioning, the distance is 63 cm and in the third positioning, the distance is 1.06 m. Hence the total number of truck passes shall be distributed equally in three different lateral positions while evaluating the effects of uniform wander mode. As it is observed in **Fig. 6-8**, due to the increased width of a dual tire assembly where the additional distance is resulting from the spacing of 12 cm between dual tires, there is an overlap on number of passes starting at a distance of 1.06 m and 63 cm from the center of the lane.

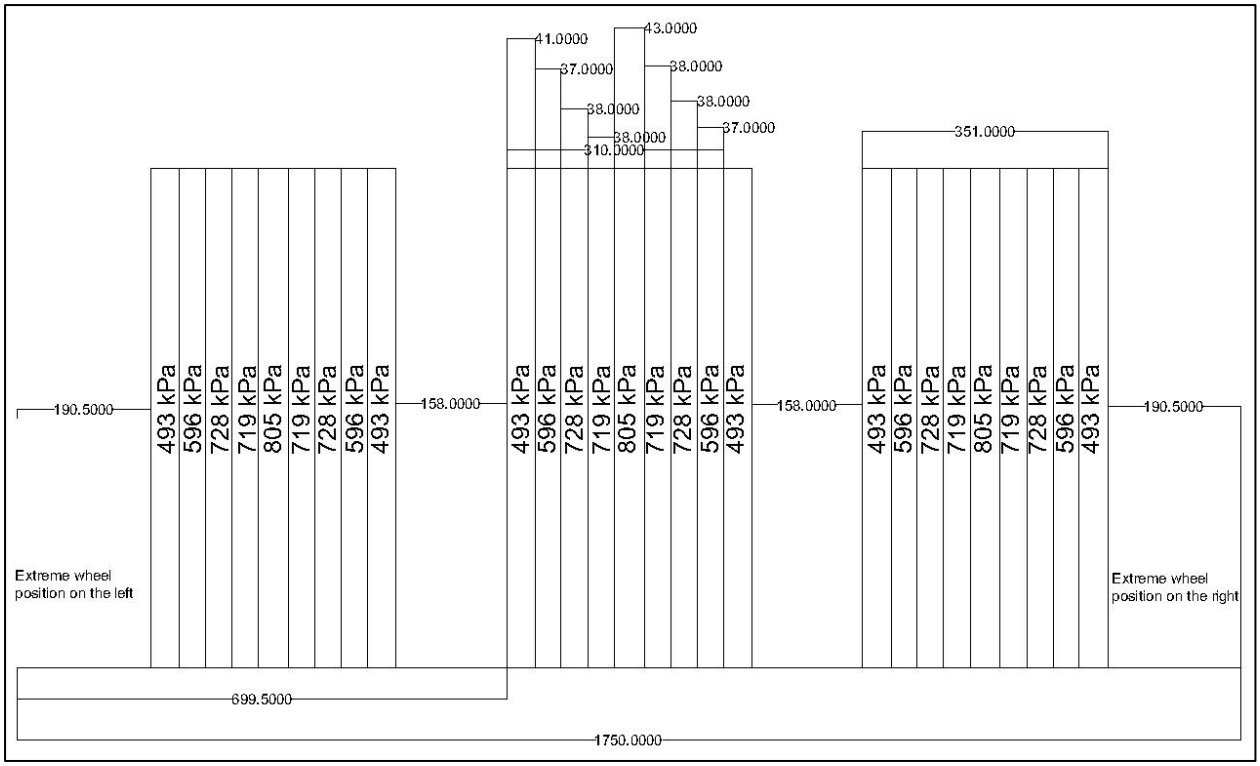

Fig. 6-8: Lateral positioning options of a Michelin 455/55R22.5l tire. Units in mm.

The same principal as in case of a dual tire assembly is employed for the wide base tire. Since it is only a single wheel system hence the width is less as compared to the dual wheel system. This results in no overlapping of truck passes. A safety distance of 20 cm has been taken from the edge of the lane. In case of a zero wander mode, the distance from the center of the lane to the inner edge if tire is 70 cm. In case of a uniform wander mode, the first positioning of truck tire starts at 20 cm from the center of the lane, the second positioning, the tire is spaced at 160 cm from the first positioning and another 160 cm distance is given for the third positioning of the truck tire.

6.6 Data preparation for ABAQUS

Following parameters are needed in ABAQUS to perform creep analysis using the power law model as it is presented in **Table 6-1** [41]. Wheel rutting tests have been performed with tests run for 400 passes and corresponding data for viscoelastic strains in secondary and tertiary zones with time is recorded and corresponding power law parameters are obtained. Parameters (m) and (A) are adjusted after running trial simulations corresponding to the rut depth obtained from 400 wheel passes in a wheel rutting tester. The simulated environmental parameters correspond to the normal temperature conditions of the pavement structure with no rain or extreme weather conditions considered.

Table 6-1. Elastic and creep parameters

Material	**Material Parameters**	
	Elastic Parameters	**Creep Parameters (Constant)**

HMA Layer	Elastic Modulus (kPa)	Poisson's Ratio	A ($\mathbf{x10^{-8}}$)	n	m
	950000	0.41	41	1.48	-0.63

Total traffic volume is assumed to be 30 million tire passes for a period of 20 years. Vehicle speed used in this study is the nominal speed of heavy goods vehicles, weighing greater than 12 tons can be 90 km/h, 80 km/h, 60 km/h and 50 km/h.

While considering the zero-wander mode, for an outside tread's footprint length of 175 mm, the time of loading for the first step is 118,000 seconds as calculated from Eq. 6-5. The other areas in footprint are longer by 15 percent; hence for step 2, the extra loading time is 18,000 seconds. The total loading time for zero wander mode and uniform wander mode has been shown in **Table 6-2**.

Table 6-2. Loading time for zero wander mode for a 30 million tire passes

Speed (km/h)	Loading Time (sec)	
	Step 1	Step 2
90	105000	16000
50	189000	29000
40	236000	36000
30	315000	47000

The total cumulative time calculated from Eq. 6-5, has been distributed in six steps as mentioned in **Table 6-3**. Steps 1 and 2 are for the first positioning of tire and further steps indicate second and third positioning.

Table 6-3. Loading time for uniform wander mode for 30 million passes

Speed (km/h)	Loading time (sec)					
	Step 1	Step 2	Step 3	Step 4	Step 5	Step 6
90	35000	5300	35000	5300	35000	5300
50	63000	10000	63000	10000	63000	10000
40	79000	12000	79000	12000	79000	12000
30	105000	15000	105000	15000	105000	15000
5	630000	94500	630000	94500	630000	94500
2.5	1260000	189000	1260000	189000	1260000	189000

6.7 2D FE model

Since the tire assembly is symmetric, hence only one portion of dual and single wheel assembly is considered in FE analysis. This approach would reduce the computational time and will have no effect on results obtained by performing the analysis on uniform wander and zero wander modes. **Fig. 6-9** and **Fig. 6-10** present the 2D model for a dual and super single tire assembly respectively.

Fig. 6-9: 2D Model for dual tire assembly.

Fig. 6-10: 2D Model for a super single wide tire assembly.

The mesh density including the element type and size is same for both models created for dual wheel and wide base tire assembly. The mesh size is kept at 50. The model used is a quadrilateral plain strain hourglass with reduced integration CPE4R consisting of 4550 linear quadrilateral elements with 4914 nodes. Reduced integration as been used for faster computation and due to the size of the model, reduced integration doesn't affect the accuracy in simulation results. A screenshot of developed mesh is presented in **Fig. 6-11**.

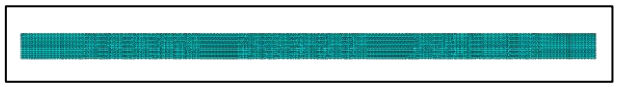

Fig. 6-11: Mesh formation used in FE analysis.

Fig. 6-12 and ***Error! Reference source not found.*** represent the boundary conditions for dual tire and super single wide tire respectively.

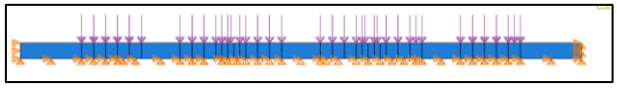

Fig. 6-12: Loading and boundary conditions for a dual tire assembly.

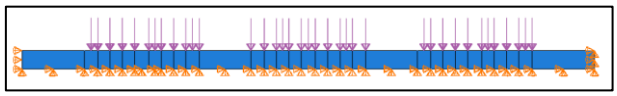

Fig. 6-13: Loading and boundary conditions for a super single wide tire assembly.

6.8 Simulation results and discussion

Simulation results for a dual tire assembly under zero and uniform wander mode at 90 km/h are shown, respectively. The simulation environment deals with average pavement temperature condition for an unaged pavement structure. Simulations were performed for a total traffic of 30 million tire passes over a period of 20 years as shown in **Fig. 6-14** and **Fig. 6-15**, respectively. The microstrains are obtained after 35 increments with final step time of 16000 seconds and after 38 increments with final step time of 5300 seconds respectively. In **Fig. 6-16,** for the uniform wander mode, the passes are accumulated to show the simulated effect if the passes are merged. As observed, rutting progression has been decreased. However, this figure only depicts the accumulated passes scenario. In the analysis part, the upheaval increment is not included in rutting depth in this study.

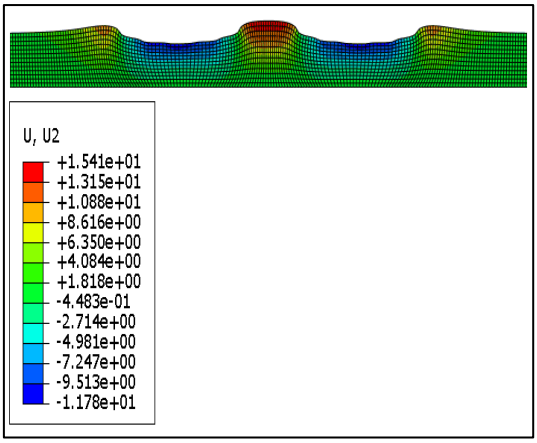

Fig. 6-14: Simulation result for dual wheel zero wander at 90 km/h.

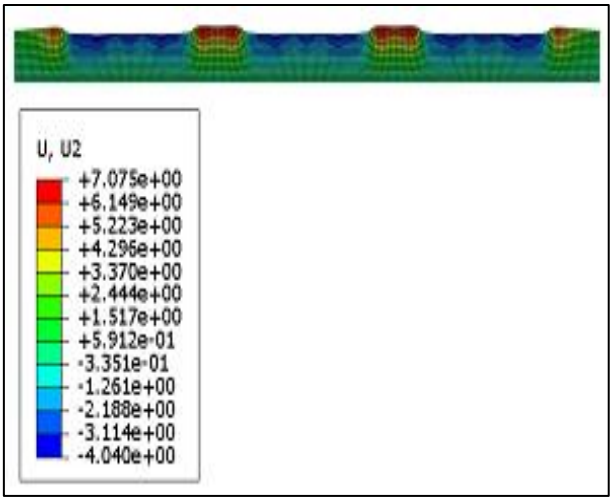

Fig. 6-15: Simulation result for wide wheel uniform wander at 90 km/h.

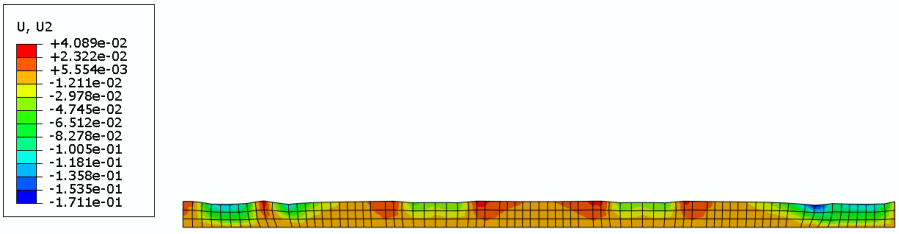

Fig. 6-16: Accumulated passes simulation for wide base tire at 90 km/h.

Since validated model parameters have been used to simulate the effect of lateral wander modes for autonomous trucks along with the boundary conditions and material properties used as mentioned before, therefore the simulation results were verified based on element size, element type and mode of loading used. Variation of stress and strain values along the "Nodes" showed close resemblance to the parallel research as mentioned in Section 6.6 and shown in **Table 6-4**.

Table 6-4 Validated simulation results.

Layers	Depth	Measured strains using simulations	Actual strains using reference research	Difference	Overall strain propagations towards depth	
					Simulated	Research
Asphalt	25 mm	251 microns	265 microns	3.8 %	77.1 %	77.4%
	50 mm	147 microns	152 microns	3.3 %	55.1 %	54.9 %
Foundation	63 mm	120 microns	123 microns	2.4 %	34.1 %	33.2 %

Due to low contact pressures and wider distribution of contact stresses for a wide tire, the deformation at 90 km/h for the wide tire is 6 mm, which is almost half the deformation of dual tire at 11.8 mm using a zero-wander mode as presented in **Fig. 6-17** and **Fig. 6-18**, respectively.

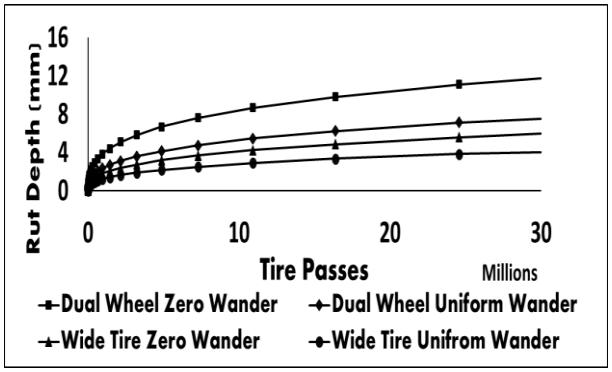

Fig. 6-17: Rut depth for various lateral modes and tire types at 90 km/h.

A significant increase in rut depth happens as the speed is reduced to 30 km/h, the increment is highly significant in case of using a dual tire in a uniform wander mode. When measured at super slow speeds of 5 km/h and 2.5 km/h, an abrupt increase in rut development can be observed as presented in ***Error! Reference source not found.*** Permanent deformation of 9.6 mm and 11.8 mm has been accumulated at speeds of 5 km/h and 2.5 km/h respectively.

Condition of the flexible pavement starts to deteriorate once the rut depth reaches 6 mm, [102], [104], therefore it is of high concern that the number of passes for each of the tire type along with a lateral mode used should be analyzed until the rut depth reaches 6 mm. **Fig. 6-19**, shows abrupt increase in rutting depth at super slow speeds.

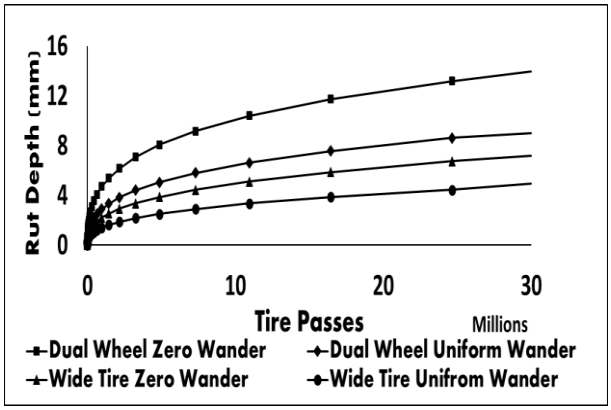

Fig. 6-18: Rut depth for various lateral modes and tire types at 30 km/h.

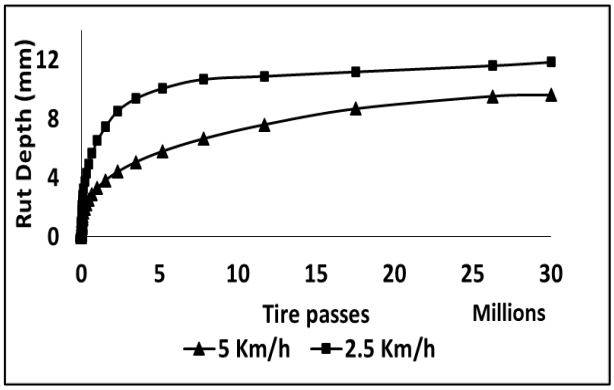

Fig. 6-19: Rut depth for uniform wander mode at super slow speeds.

The rate of increase in rut development is much prominent at lower speeds. As it is presented in **Fig. 6-20**, the rut development rate is linear from 90 km/h to 30 km/h.

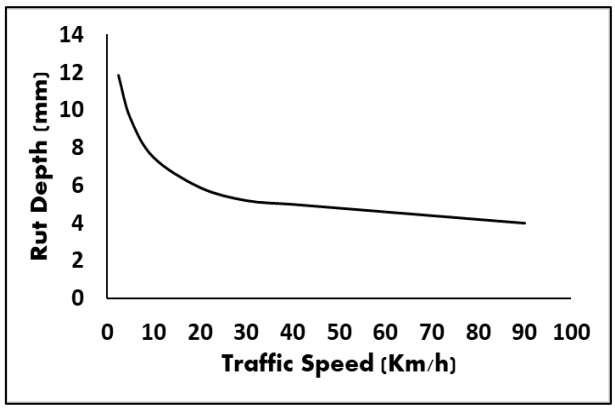

Fig. 6-20: Effect of traffic speed on rut depth for super single tire at uniform wander mode.

6.9 Findings and conclusions

The key findings in this study are mentioned below:

1. Rut depth increases by a factor of 2 from wide tire to dual tire, the factor slightly increases as the speed gets down to 50 km/h.
2. Effects of uniform wander and zero wander are highly significant when dual tire assembly is used;

3. In case of super single tire, the rut depth decreases by an average of 2 mm if uniform wander is used instead of zero wander mode.
4. The decrease in rut depth from zero wander to uniform wander increases significantly at lower speeds.
5. In case of super single tire, the rut depth increases by 0.2 mm for every 10 km/h decrease in the speed.
6. Wider lane width can facilitate in even more uniform distribution of lateral wander by introducing more paths at fixed distances from center line of the lane, thereby reducing the rutting potential.
7. Dual tires at zero wander only require 3.23 million passes to reach a rut depth of 6 mm, on the other hand, super single tire require 30 million passes to reach a rut depth of 6 mm using zero wander mode.
8. An abrupt increase in rut development start as the vehicle speed gets lower than 30 km/h and the curve tends to go vertical until the speed approaches zero.
9. For a super single wide tire at uniform wander mode, rut develops at a factor of 2 mm at super speed lower than 50 km/h.

7 Impact of autonomous trucks on fatigue under various speed, tire footprint and lateral wander mode variations

Two different tire configurations consisting of a dual tire and a super single wide tire having different range and distribution of contact pressures have been analyzed along with the effect of speed on development of pavement damage at speeds of 5 km/h, 50 km/h and 80 km/h under zero and uniform wander modes. A 3D model has been developed in the finite element software ABAQUS. The model represents a four layered pavement structure consisting of asphalt layer, base course layer, subbase course layer and subgrade. Time step loading method has been sued for different speed variations. Miner's rule has been used to determine the fatigue damage induced as a result of strain values obtained from modelling. Further details can be found in [105].

7.1 Thesis 2

I have determined the impacts of autonomous trucks on FATIGUE under various speed, tire footprint and lateral wander mode variations and came to the following results:

1. Decrease in speed by 10 km/h increases the accumulation of fatigue damage by a factor of 0.5.
2. Wide tire is 18 % more efficient in terms of fatigue damage than the conventional dual tire.
3. Uniform wander mode leads to 25% increase in fatigue life of the pavement.

7.2 Related publications

1. M. Fahad and R. Nagy, "Fatigue damage analysis of pavements under autonomous truck tire passes," Pollack Period., vol. 17, no. 3, pp. 59–64, 2022, doi: 10.1556/606.2022.00588.
2. M. Fahad and R. Nagy, "A burkolatok fáradásos károsodásának elemzése autonóm tehergépkocsik esetén" AZ ASZFALT: A MAGYAR ASZFALTIPARI EGYESÜLÉS (HAPA) HIVATALOS SZAKMAILAPJA 29 : 2 pp. 53-57. , 5 p. (2022).
3. R. Nagy, and M. Fahad, "Autonóm járművek sávtartásának hatása a pályaszerkezet méretezésre – irodalomkutatás": Effect of lane keeping of autonomous vehicles on road pavement design – literature review In:XXIV. Nemzetközi Építéstudományi Online Konferencia – ÉPKO Hungarian Technical Scientific Society from Transilvania (2020) pp. 117-121.

7.3 Methodology

A pavement with a lane width of 3.5 m is considered for this study. Since the pavement and tire assemblies are symmetric, only half the lane width of 1.75 m is considered for analysis. Two tire types are used for exerting the load pressure on pavement since the distribution of loading under a tire is non-uniform [106]. Environmental conditions for the pavement are kept at average without any extremes to reduce the bias related to temperature variations for fatigue damage. Although in [107], reduced pavement temperature is used to accelerate fatigue damage. A typical four layered asphalt concrete pavement consisting of asphalt concrete surface layer, aggregate base course, aggregate sub-base course and subgrade is considered for fatigue analysis. **Fig. 7-1** and **Fig. 7-2** show the illustrations of a dual tire and a super single wide tire assembly respectively.

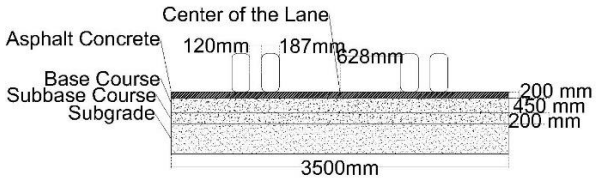

Fig. 7-1: Illustration of dual tire assembly on the pavement.

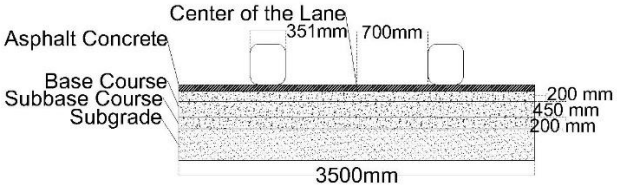

Fig. 7-2: Illustration of single wide tire on the pavement.

7.4 Wheel loading and configurations

A nominal tire pressure of 720 kPa generated by an axle load of 75.6 kN has been used. Tire types used are a super single wide base tire 455/55R22.5 developed by Michelin and a conventional dual tire G159A-11R22.5 developed by Goodyear. Using two tire types having different contact pressures and lateral dimensions would be beneficial in analyzing the contact stresses at various wander modes and speeds as it is shown in **Fig. 7-3** and ***Error! Reference source not found.***

Fig. 7-3: Wide (left) and dual (right) tire footprint.

Since it has been proved that distribution of tire pressure under the tire is non-uniform [14-16]. Hence the data has been taken from [106] and incorporated in this study and footprints for each tire configuration are it is presented in **Fig. 7-4** and***Error! Reference source not found.***.

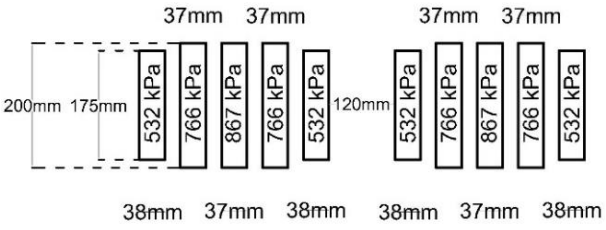

Fig. 7-4: Footprint details of a Goodyear G159A-11R22.5 dual tire used in simulations.

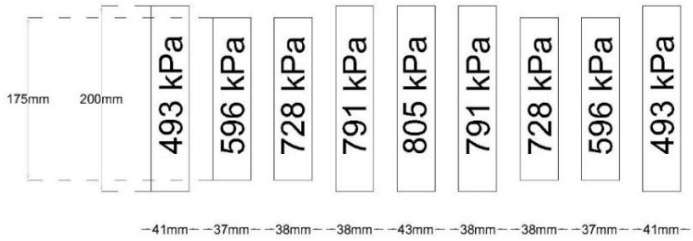

Fig. 7-5: Footprint details of a Michelin455/55r22.5 super single wide tire used in simulations.

7.5 Data preparation for ABAQUS code

Validated pavement material parameters have been taken from Cheng et al. [25] and are shown in **Table 7-1**.

Table 7-1 Material properties used in ABAQUS.

Layer type	**Thickness (cm)**	**Elastic modulus (kPa)**	**Poisson's ratio**
Asphalt	20	950000	0.41
Base course	40	500000	0.35
Sub-base course	20	350000	0.35
Subgrade	-	60000	0.4

The modelling environment is kept at average for pavement with material parameters and the modelled developed as unaged structure. For vehicles weighing greater than 12 tons, three different speeds of 5 km/h, 50 km/h and 80 km/h have been assumed and details of which are mentioned in **Table 7-2**.

Table 7-2. Speed selection criteria

Speed	**Scenario**
5 km/h	Simulation of approaching bus stops, traffic congestion/accident on highways
50 km/h	Speed limit for heavy goods vehicles on urban roads/passing through road works zones
80 km/h	Nominal speed of heavy goods vehicles in rural highways

Loading time used in ABAQUS code has been calculated by the method mentioned in [27], where based on the tire footprint size and the speed of simulated autonomous trucks of 5 km/h, 50 km/h and 80 km/h, loading time was determined. Loading times for both zero wander and uniform wander modes were calculated for each step of loading. Zero wander modes consist two loading steps while the uniform wander mode consisted of six total steps.

7.6 3D FE model

A 3D model has been developed with longitudinal and lateral dimensions of 1.75 m by 1.75 m. Since dual and single tire assemblies are symmetric, hence half of the pavement width is considered for finite element analysis. The total depth of the model is 4.8 meters, which includes all the pavement layers considered. Both the models have the same mesh density as well as element size to keep the results in maximum accuracy for the sake of comparison. Model element type is an 8 - node plain strain linear brick element with reduced integration, CPE8R. The model consists a total of 25584 elements with an element size of 120 for increased accuracy as well as adequate calculation time. **Fig. 7-6** shows mesh formation of both models.

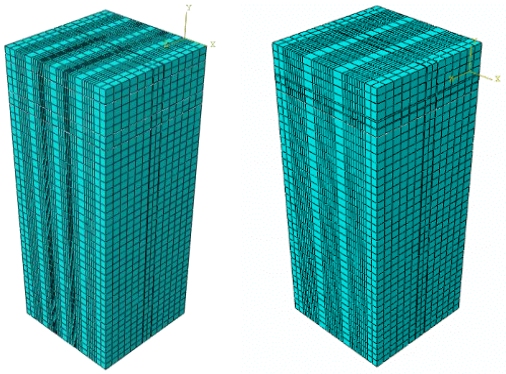

Fig. 7-6: Mesh details for dual tire (left) and single wide tire (right).

The interaction of layers in the pavement was kept as a normal surface-to-surface contact with hard and frictionless characteristics. For the boundary conditions, nodes were free to move along the normal directions but were restricted in perpendicular horizontal directions. The movement at the bottom of the model was restricted in all three directions. **Fig. 7-7** shows the loading and the boundary conditions for dual wheel and wide tire respectively.

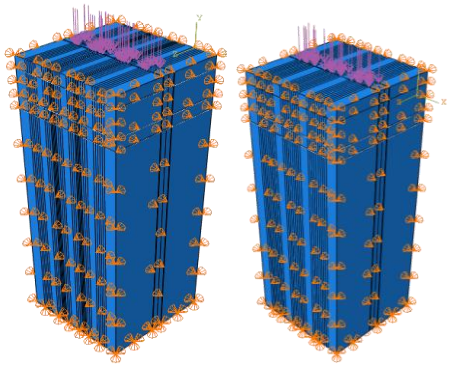

Fig. 7-7: Loading and boundary conditions for dual wheel model (left) and wide tire model (right).

7.7 Results and discussions

Simulation results from ABAQUS code have been presented for speeds of 50 km/h under zero wander and uniform wander mode for dual and wide tires combined. Simulations are conducted for a total of 30 million tire passes over a pavement design life of 15 years.

A noticeable contrast can be observed in the simulated strain values obtained for dual tire as compared to wide tire assembly as it is presented in **Fig. 7-8** and **Fig. 7-9**, that clearly depict

even distribution of load concentrations along the wheel path for a wide tire. Maximum strain values under the asphalt layer decrease by 45% when a uniform wander is used.

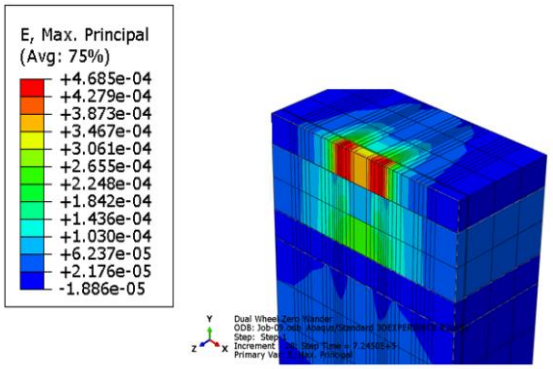

Fig. 7-8: Simulation results for 50 Km/h, dual tire under zero wander mode.

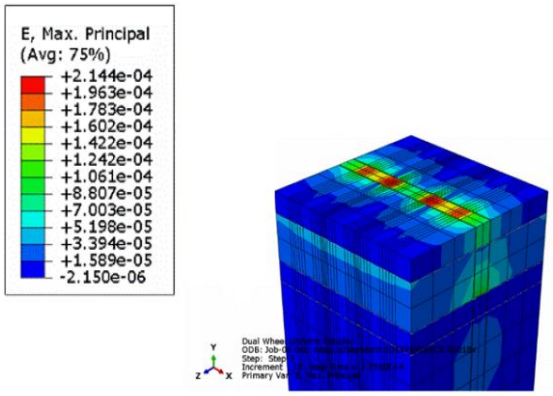

Fig. 7-9: Simulation results for 50 Km/h, dual tire under uniform wander mode.

Validated model parameters for finite element simulations have been used for analysis of stress and strain projections along different "Node" points in ABAQUS. Moreover, element type, element size and boundary conditions are kept the same for accuracy of simulated results as compared with the research mentioned in Section 7.5 and shown in **Table 7-3**.

Table 7-3 Validated simulation results

Layer	**Depth**	**Measured strains using simulations**	**Actual strains using reference research**	**Difference**	**Overall strain propagations towards depth**	
					Simulated	**Research**
Asphalt	50 mm	138 microns	131 microns	5.2 %	77.1 %	77.4%
	100 mm	122 microns	116 microns	5.0 %	66.1 %	66.4 %
	200 mm	114 microns	105 microns	5.2 %	58.3 %	57.5 %
Base Course	350 mm	108 microns	103 microns	4.7 %	46.2 %	46.8 %
Subbase	410 mm	96 microns	91 microns	5.3 %	34.4 %	35.6 %

Subgrade	800 mm	84 microns	84 microns	4.8 %	20.5 %	21.1 %

The highest strain value of 115 microns at speed of 5 km/h is obtained under the asphalt layer as it is presented in **Fig. 7-10**. The magnitude of strain values decrease mas the vehicles accelerated. However, it is noticed that the majority of peak strain values are concentrated in the center of the wheel path directly under each tire of a dual wheel assembly. Magnitude of accumulated micro-strains however decrease at a speed of 80 km/h with a value of 52 microns and however, in case of a dual wheel moving at uniform wander mode, as it can be observed from **Fig. 7-11**, the strain distribution is much even along the entire width of the lane and the magnitude is decreased by a factor of 25% at higher speeds.

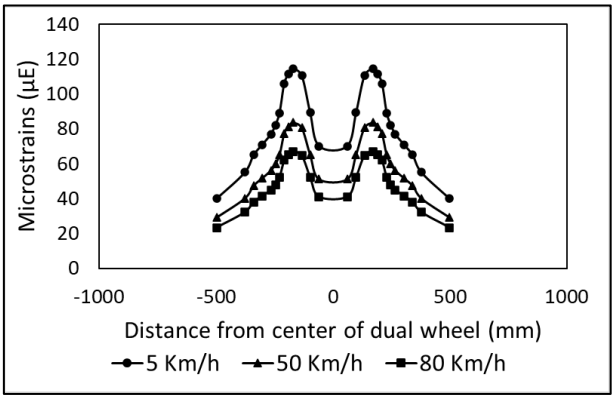

Fig. 7-10: Microstrains calculated at different speeds for dual wheel at zero wander mode.

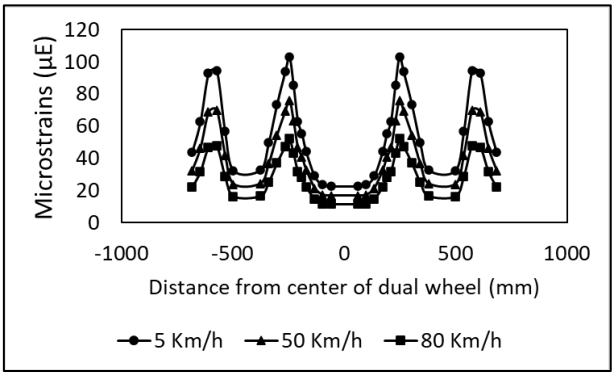

Fig. 7-11: Microstrains calculated at different speeds for dual wheel at uniform wander mode.

Fig. 7-12 shows only the resulting strains directly under the tire while **Fig. 7-13** shows the resulting strains throughout the entire lane width. It can be observed that under a uniform wander mode, magnitude of strain values decreases by 30% when uniform distribution of loading is employed on the pavement. Uniform distribution of loading results in maximum micro-stain magnitude of only 41 microns as compared to 56 microns yielded by a tire moving under a zero-wander mode at a speed of 80 km/h. The difference in micro-strains between zero wander and uniform wander is more pronounced at lower speeds as compared to dual tire assembly.

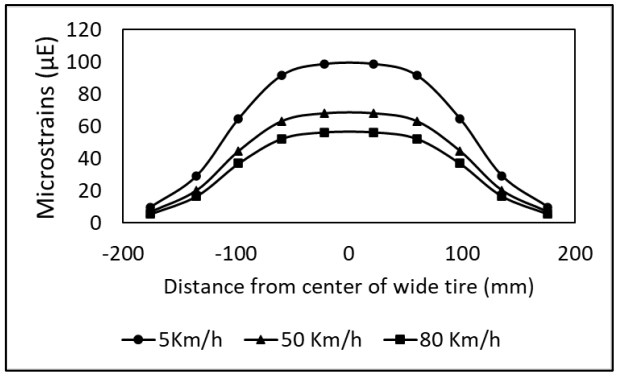

Fig. 7-12: Microstrains measured at different speeds for wide tire at zero wander mode.

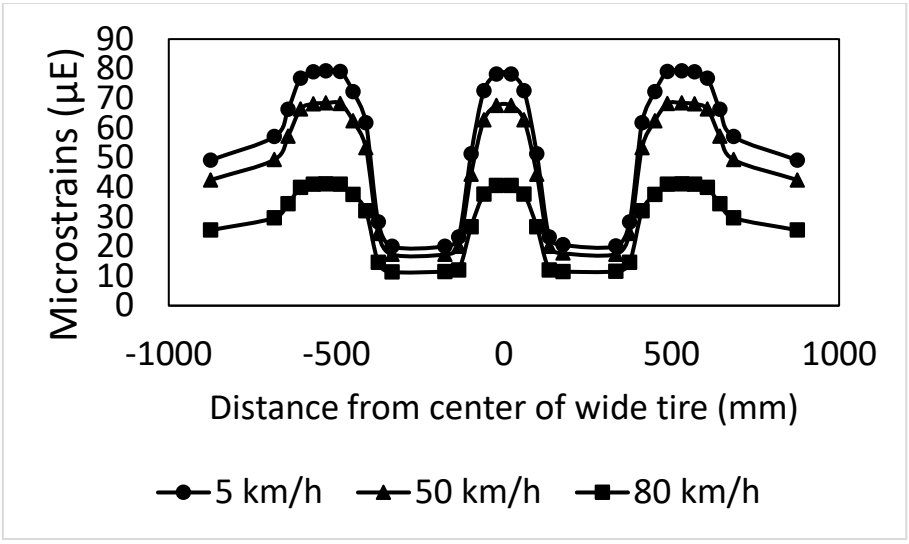

Fig. 7-13: Microstrains measured at different speeds for wide tire at uniform wander mode.

Palmgren-Miner linear damage hypothesis also termed as Miner's rule has been used in calculating fatigue damage and remaining number of tire passes for a specific period of time [13, 18]. Furthermore, it has been observed that bearing capacity and stiffness of asphalt layer changes with change in temperature and resulting cumulative fatigue increases at extreme temperature conditions combined with high volume of traffic loads [108]. Usually, fatigue characteristics are more prevalent during low temperature conditions [109], hence the tensile strain obtained under a specific location of the wheel path, the resulting fatigue damage can be calculated using the derived form of Eq. 7-1[38].

$$D = \sum_{1}^{k} \frac{p_I n_I}{N_f(\varepsilon_i)} \qquad 7\text{-}1$$

Where p_I is frequency of loading (Hz), n_I is the accumulated axial loads, $N_f(\varepsilon_i)$ is the number of loads to reach fatigue life under strain ε_i and k is the number of lateral wander paths.

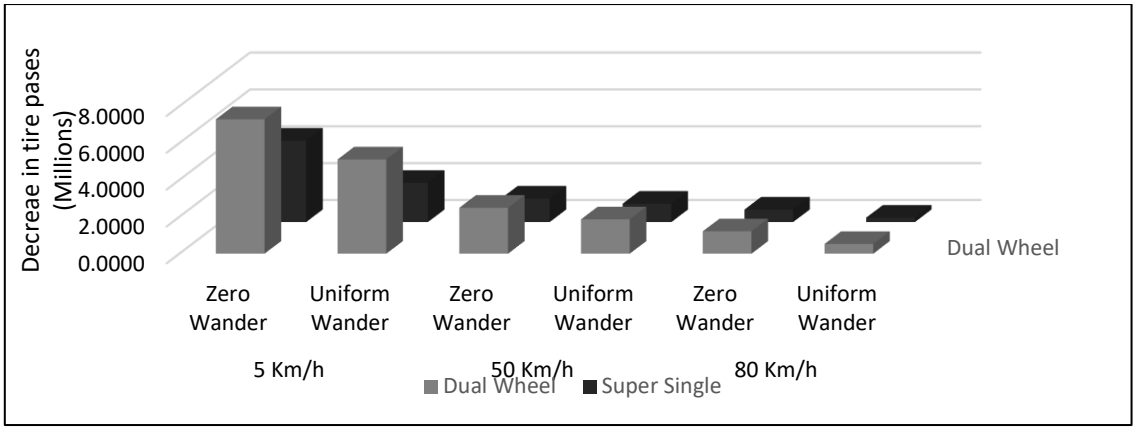

Fig. 7-14: Graphical representation of reduced number of tire passes.

As observed from **Fig. 7-14**, the maximum reduction in tire passes is caused by a dual tire moving at uniform wander mode under super slow speeds of 5 Km/h. A total reduction of 7.2 million tire passes can be observed for dual tire moving at a uniform wander mode. Furthermore, at normal operating speeds of 80 km/h 40% decrease in total number of tire passes happens when a dual wheel is switched from uniform wander to zero wander mode. For a wide tire, the difference is around 47% for the same scenario. Hence, both the tire types exhibit the same amount of damage increment while switching to zero wander mode. The recommended scenario here is using a wide tire under uniform wander mode where the maximum reduction in tire passes is only limited to 239,000 tires passes. Similarly, at higher speeds, the increase in fatigue damage is more prominent for both dual tire and wide tire assemblies. **Fig. 7-15** below shows the reduction in fatigue life calculated for variable conditions of speeds, lateral wander and tire configurations.

Thereby using Eq. 7-1, fatigue damage in number of reduced pavement lifetime was calculated and presented in **Fig. 7-15**.

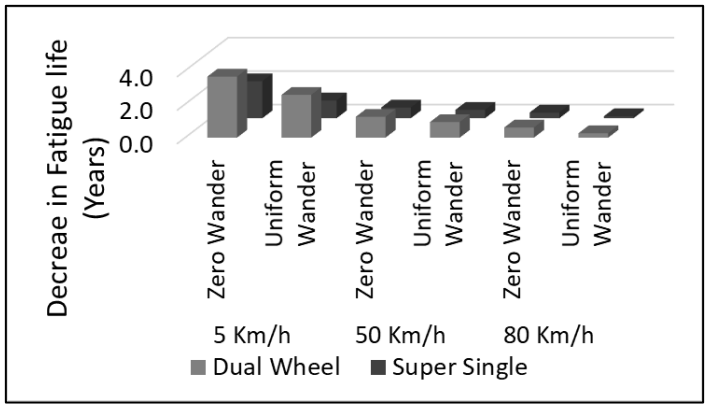

Fig. 7-15: Graphical representation of decrease in fatigue life under different speeds, tire configuration and lateral wander modes.

Since the zero-wander mode for both tire configurations cause concentrated loading cycles, therefor at normal operating speeds of 80 km/h, fatigue life decreases by a factor of 1.5 when a zero-wander mode is used. The decrease in fatigue life is more pronounced at high speeds, specifically for a dual tire configuration. At super slow speeds of 5 km/h, fatigue life of a

pavement can decrease by 3.5 years if zero wander modes is used. If a uniform wander mode is use at super slow speeds, still the minimum reduction in fatigue life stays at 2.6 years.

7.8 Findings and conclusions

The key results in this study are mentioned below:

1. Vertical strains decrease by a factor of 2.5 along the lateral distance away from the tire in case of dual wheel;
2. Vertical strains decrease by a factor of 10 from the center of the wide tire to its edge.
3. Increase in micro-strains is more prominent at lower speeds, since, micro-strains decrease by a factor of 0.5 while moving from 5 km/h to 50 km/h, furthermore, micro-strains increase by factor of 0.3 while going from 50 km/h to 80 km/h;
4. In case of a dual wheel zero wander mode, decrease in micro-strains is more prominent at higher speeds since at lower speeds the load is still exposed to a specific point on pavement for a longer period of time;
5. Decrease in damage for dual wheel uniform wander mode is much less than that of a wide tire uniform wander mode because of wide lateral size of a dual tire assembly, due to which 60% of the wheel passes would always be concentrated in the center of the lane;
6. At super slow speeds, dual wheel moving at zero wander mode, decrease in fatigue life of the pavement is 3.5 years which is 1.45 times more than the dual wheel moving at uniform wander and 3.4 times more than wide tire moving at uniform wander mode;
7. When dual wheel uniform wander and wide tire zero wander is compared, the increase in fatigue damage for a wide tire zero wander is just 1.2 times more than that of dual wheel at uniform wander mode, hence even if high concentration of tire pressure is exerted, the uniform wander saves the pavement from increased fatigue damage.

8 Impact of a class A40 autonomous truck on pavement under lateral wander mode variations

Effects of autonomous trucks' different lateral wander modes under each individual axle of a semitrailer have been analyzed. Two lateral wander modes, a zero-wander mode in which a truck is programmed to follow a predetermined wheel path without any lateral movement and a uniform wander mode, where the truck uniformly distributes itself along the lateral width of the lane, are used. European class A40 truck has been modelled in ABAQUS. The effect of all the axles with varying loading and tire pressures has been analyzed while observing the microstrains from bottom up of the asphalt layer and on the top of subgrade layer at speeds of 90 Km/h. Furthermore, Prony series parameters have been employed for analyzing the viscoelastic behavior of asphalt for a four layered pavement structure. Moreover, method used for determination of tire contact patch and length dimensions from tire contact pressure and tire inflation pressure has been introduced. Rutting and fatigue damage analysis has been performed along with a methodology developed for calculating Load Equivalency Factor (Hereinafter: LEF) for each axle of the class A40 truck. Further details can be found in [110].

8.1 Thesis 3

I have determined the impact of a class A40 autonomous truck on pavement under lateral wander mode variations and came to the following results:

1. Channelized loading in case of zero wander mode leads to premature damage in terms of fatigue cracking and rutting by 25%.
2. Acceleration in rut depth evolution in case of zero wander mode is 2 times more than that of uniform wander mode.
3. Acceleration in fatigue cracking in case of a uniform wander mode is 1.75 less than that of zero wander mode.
4. Drive axle of the class A40 truck contributes to 40% of the damage when compared to all other axles.

8.2 Related publications

M. Fahad and R. Nagy, "Influence of class A40 autonomous truck on rutting and fatigue cracking," Pollack Period., pp. 3–8, 2023, doi: 10.1556/606.2023.00760.

8.3 Pavement details

A typical four layered pavement structure has been selected consisting of an asphalt layer, aggregate base course, aggregate subbase course and a subgrade layer with presumed thickness of 2 meters. Average pavement environmental conditions are assumed for modelling without any excess of extreme cold and hot climatic conditions. The length of the pavement section to be analyzed is kept at 20 meters and the width of the pavement section is kept at 3.5 meters, simulating the width of truck traffic lane.Validated pavement layer properties to be used in ABAQUS have been taken from Cheng et al. [25] as shown in **Table 8-1**.

Table 8-1 Pavement layer properties.

Layer type	Thickness (mm)	Elastic modulus (kPa)	Possions ratio
Asphalt	200	950000	0.41
Base course	400	500000	0.35
Subbase course	200	350000	0.35
Subgrade	-	60000	0.4

Furthermore, to include the viscoelastic behavior of asphalt mixture for permanent deformation calculation, Prony series parameters are used. For determining the linear viscoelastic behavior of asphalt in finite element modelling, Prony series parameters have been used. Values of complex shear modulus obtained from tensile strength tests of asphalt specimen are converted into Prony series coefficients for time dependent viscoelastic behavior of asphalt in finite element modeling. Hence, a generalized Maxwell model is used to establish the Prony series against several Maxwell elements as shown in **Fig. 8-1**.

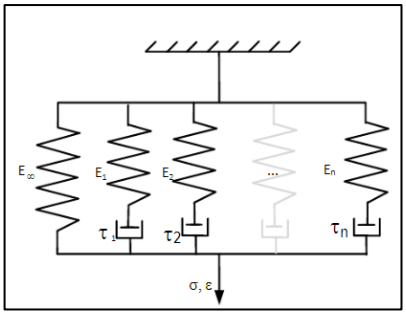

Fig. 8-1: Illustration of a generalized Maxwell

Prony series parameters have previously been used to characterize the viscoelastic behavior of asphalt mixtures [75], [111], [112]. Stress and strain relationship of a viscoelastic material can be described by prony series that is a component of power law series. Time dependency of viscoelastic material in ABAQUS is described by the following prony series expansion in Eq. 8-1 and Eq. 8-2.

$$g(t) = 1 - \sum_{t=1}^{N} g_i(1 - e^{\left(\frac{t}{\tau_i}\right)}) \quad 8\text{-}1$$

$$g(t) = \frac{G(t)}{G(t=0)} \quad 8\text{-}2$$

Where $g(t)$ is the ratio of shear modulus (MPa) at time t (sec), $G(t)$ is the shear modulus (Mpa) at t = 0 (sec), $G(t=0)$, τ_i is the retardation time (sec), and g_i is a prony series coefficient. N is the number of terms in the Prony series. The value $g(t)$ can also be computed

by normalizing $G(T)$ by G_0 which is the instantaneous shear modulus and the $G(T)$ is obtained from relaxation modulus $E(t)$ from the following Eq. 8-3.

$$G(T) = \frac{E(t)}{2(1+\mu)} \quad 8\text{-}3$$

Where μ is the Poisson's ratio and for the asphalt layer, a value of 0.35 is assumed. Finally the series of retardation time is assumed and plugged into Eq. 8-1 and coefficients of Prony series are determined.

Furthermore, the long term shear moulus G_∞ (Mpa) and long term shear modulus G_0 (Mpa) at time t=0 (sec) can be covetered into each other by prony series coeffiecients g_i. In the following equation g_i is the weighted modulus of relaxation time t_i as shown in Eq. *8-4* and Eq. 8-5.

$$G_\infty = G_0\left(1 - \sum_{i=1}^{N} g_i\right) \quad 8\text{-}4$$

$$G_0 = \frac{G_\infty}{1 - \sum_{i=1}^{N} g_i} \quad 8\text{-}5$$

However, the value of complex shear modulus G_∞ is calculated using the elastic modulus E_∞ (Mpa) and Possion's ratio v as shown in Eq. 8-6.

$$G_\infty = \frac{E_\infty}{2(1+v)} \quad 8\text{-}6$$

Dynamic modulus test is used to assess the viscoelastic properties of the asphalt mixture. Furthermore, dynamic modulus test master curves have previosly been employed for evaluating and describing the visoc elastic behvaiour of asphalt mixtures [113]. Deformation long the axis of the specimens is measured using the extensometers. Testing is performed at temperatures of 54.4 ℃, 37.8 ℃, 21.1 ℃, 4.4 ℃ and -10 ℃. Data is collected as per the stated temperature intervals with the use of loading time the load is subjected to. Using the values obtained at different temperature ranges and loading times, a master curve for relaxation modulus is constructed, which is a function of reduced time. Following data in **Fig. 8-2**, **Fig. 8-3** and **Fig. 8-4** has been taken from Dong et al. [75]. The loading time master curve for a temperature of 21.1 ℃ is presented in **Fig. 8-2**.

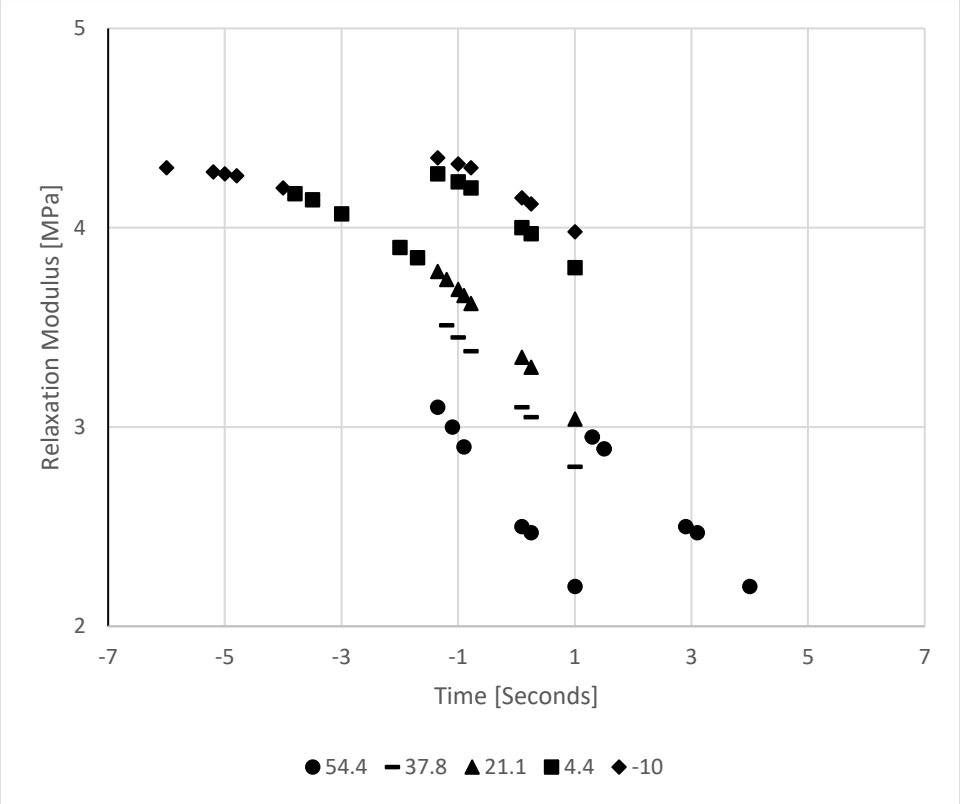

Fig. 8-2: Relaxation Modulus Master Curve Log-Log Scale. (Dong et al.)

The data is fitted with a 6 term Prony series representation. The coefficient of Prony coefficients is more than 0.99. Illustration of Prony series fitting to experimental values is shown in **Fig. 8-3**.

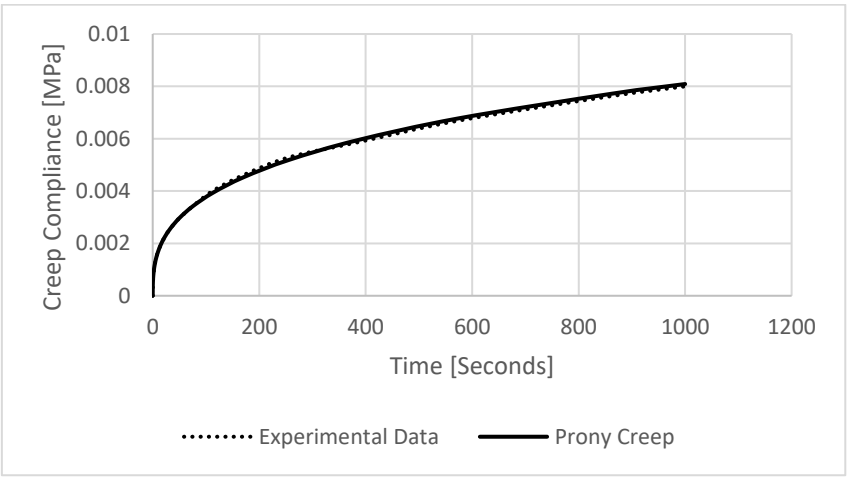

Fig. 8-3: Prony series to experimental data fit. (Dong et al.)

Components of the Prony series are then plotted and fitted to the curve as presented in **Fig. 8-4**. It can be observed that measured and calculated values are almost the same. Due to the substantial decrease in time, the fitting values are further apart a that time instance. Series of retardation times are selected and coefficients of Prony series are calculated by fitting the curve using least square curve fit method. Therefore, six Prony series terms are calculated for evaluation of viscoelastic properties of the asphalt layer.

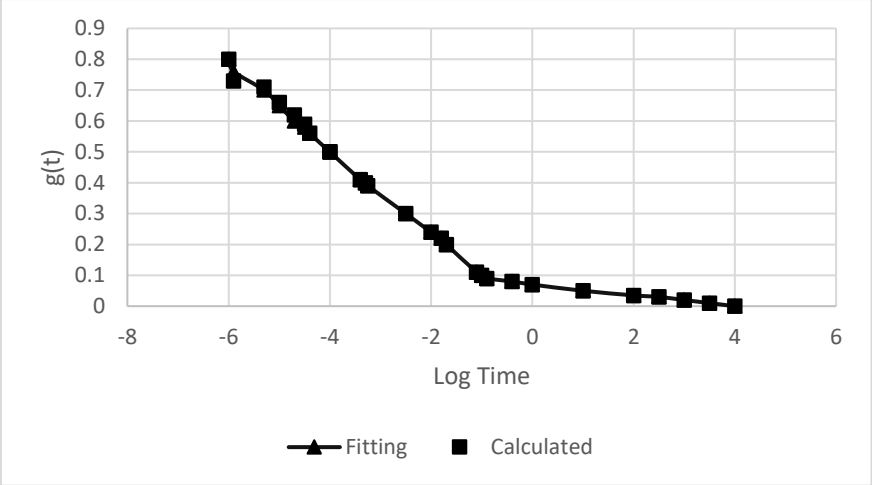

Fig. 8-4: Calculated g_i values fitted to the curve. (Dong et al.)

The validated Prony series coefficients are obtained from the field samples of asphalt layer, where Relaxation modulus values are calculated against reduced frequency [114]. Poisson's ratio used in this case is 0.35 and the calculated instantaneous modulus for the elastic modulus of asphalt layer is 6674 MPa as shown in **Table 8-2.**

Table 8-2 Prony series parameters.

Elastic properties	
Poisson's ratio	**Instantaneous modulus (MPa)**
0.35	6674
Prony constants	
Prony series coeffiecient g_i	**Retardation time τ_i (sec)**
0.611947	0.000063
0.251542	0.012589
0.068537	1.258925
0.03008	12.589254
0.019373	39.810717
0.014803	79.432823

8.4 Loading

For the simulation of pavement loading, a typical Eurpean A40 type semi truck with maximum allowable gross weight of 40 tonnes has been selected. Data from each axle has been obtained from John Aurell et al. [8] with axle configrations and axle loads shown in **Fig. 8-5**.

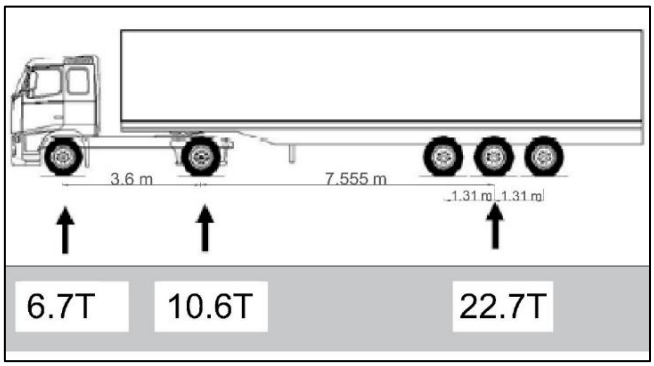

Fig. 8-5: Axle configuration, spacing and dimensions.

Tire contact pressure depends on a number of factors such as tire inflation pressure, tire load and its dimensions [115]. Since, the tire contact area varies with tire inflation pressure. Therefore, a term Tire deflection introduced by Saarilahti [116] signifies the size of contact area and its dependence on tire inflation pressure. Significantly, at lower inflation pressures, tire deflection effects the increase in contact area size. The theoretical expression for tire deflection is shown in Eq. 8-7 below.

$$\Delta = 0.008 + 0.001 * \left(0.365 + \frac{170}{p_i}\right) * G_k \quad \text{8-7}$$

Where, Δ is tire deflection (m), p_i – tire inflation pressure (kPa), G_k – wheel load (kN). Numerical expression below as shown in Eq. 8-8 is used to calculate tire contact area.

$$A = b^{0.8} * d^{0.8} * \Delta^{0.4} \quad \text{8-8}$$

And Eq. 8-9 is used for calculating nominal tire contact pressure.

$$p = \frac{G}{b^{0.8} * d^{0.8} * \Delta^{0.4}} \quad \text{8-9}$$

Where, A – contact area (m^2), G – vehicle mass (kN), b – width of unloaded wheel tire (m), d – diameter of unloaded wheel tire (m). Furthermore, values of contact area and vertical tire contact pressure were further verified with results obtained from Douglas [117] for each tire load type and corresponding tire inflation pressure. Previous studies have shown that the contact footprint of the tire is rectangular [118]. A use of rather circular contact area can underestimate compressive strains on top of subgrade and overestimate the tensile strains at the bottom of asphalt layers [103]. Once the area is calculated, the following Eq. 8-10 taken from [70], is used to calculate longitudinal and lateral dimensions of the tire contact patch.

$$L = \sqrt{\frac{A_c}{0.5227}} \quad \text{8-10}$$

Where L is the constant that is used to measure longitudinal and lateral dimensions of contact patch using the values of 0.6 L and 0.8712 L respectively and A_c is the area of tire conact patch calculated from Eq. 8-8. Used tire type, inflation pressure and wheel load, tire contact pressure and contact patch length are shown in **Table 8-3**. Tire inflation pressure values were obtained from [119].

Table 8-3. Tire load, pressure and dimensions.

Tire type	**295/80R22.5**	**295/80R22.5**	**385/65R22.5**	**385/65R22.5**	**385/65R22.5**
Twin vs Single	**Single**	**Twin**	**Single**	**Single**	**Single**
Axle load (Tons)	6.7	10.6	7.57	7.57	7.57
Load per wheel (kN)	32.85	25.98	37	37	37
Tire inflation pressure (kPa)	690	690	690	690	690
Tire contact pressure (kPa)	430	350	550	550	550
Contact patch Length/Width (mm)	250/330	250/310	275/310	275/310	275/310

8.5 Incorporation of Unifrom Wander Mode

For the zero wander mode, a layout of tire contact patches was organized based on standard dimensions of an European truck with a maximum allowable body width of 2.5 m. **Fig. 8-6** shows detailed setting out plan of contact patches used during simulations.

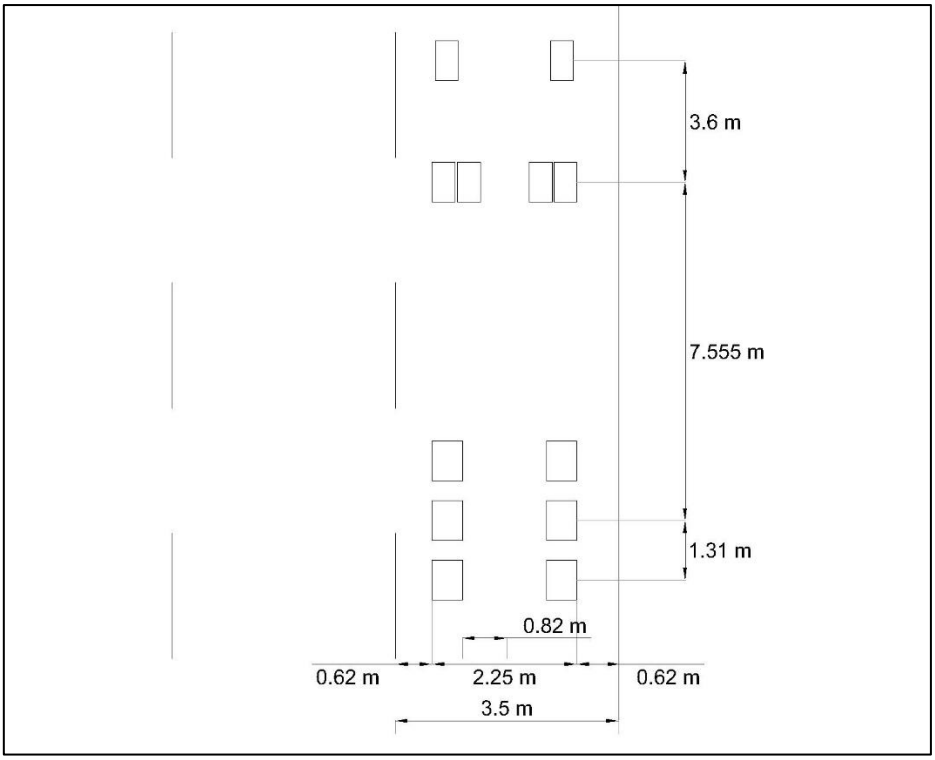

Fig. 8-6: Positioning of the truck under zero wander mode.

For the uniform wander mode, the remaining space of 62 cm is available to be utilized from the outer edge of rear tires to the lane edge, however 20 cm of safety space on each side of lane edge has been provided thus reducing the total allowable lateral wander space of 42 cm from the outer edge of trailer tires. Hence, the lateral path scheme for uniform wander mode consisted of three positioning scenarios, as shown in **Fig. 8-7**. In part (a), the truck's positioning is at the center of the lane, where the distance from the middle of the lane to the inner edge of the rear trailer tire is 82 cm. When the positioning is moved to part (b) where the truck is at its final lateral position along the left side of the lane at this location the distance from the middle of the lane to the inner edge of trailer tires becomes 1.24 m and finally at the third positioning at (c), the distance from the middle of lane to inner edge of rear tires is at 40 cm.

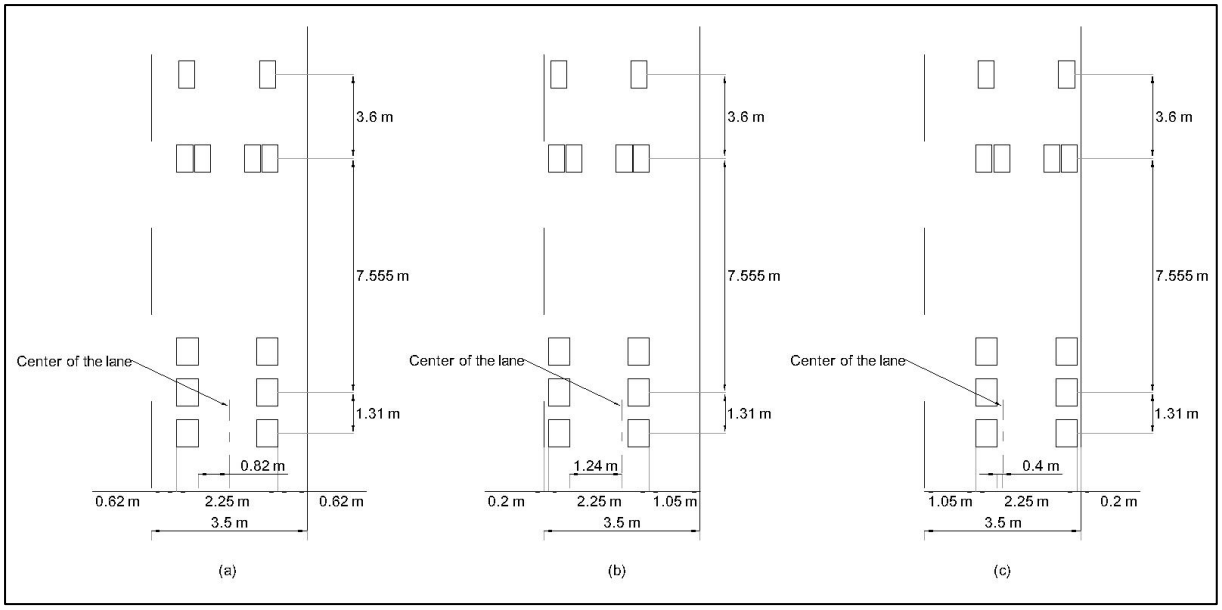

Fig. 8-7: Positioning of the truck under uniform wander mode.

8.6 Finite Element Model

A 3D model has been developed with length of 20 m and width of 3.5 m. The total depth of the model is kept at 2.8 m and the bottom of the model has an interface of elastic foundation to simulate infinite thickness of natural soil foundation. Figure below shows the assembly of the model. Model type used is an 8-node linear brick, reduced integration with hourglass control CPE8R. The model consisted of a total of 25584 elements with an element size of 50 for increased accuracy as well as adequate calculation time. **Fig. 8-8** below shows the mesh formation in the model.

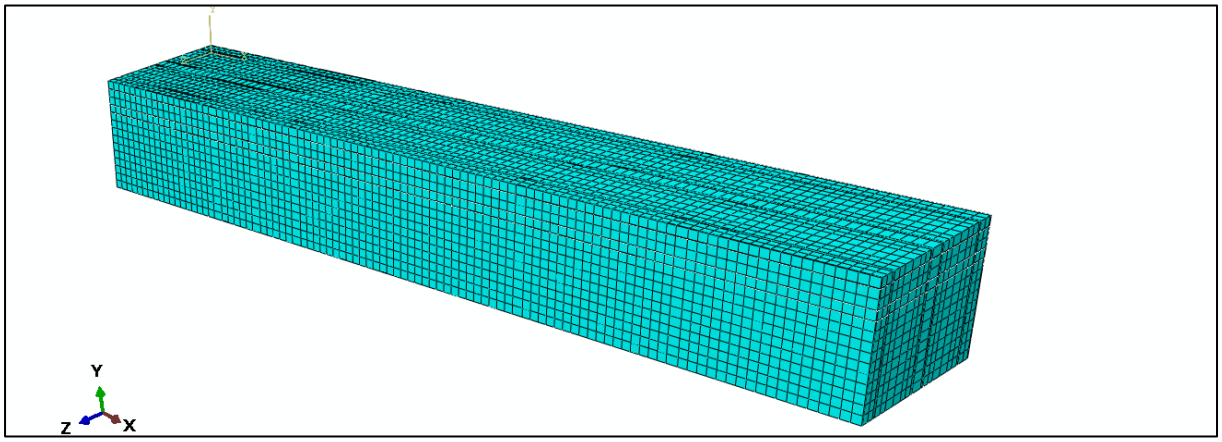

Fig. 8-8: 3D FE mesh details.

The interaction of layers in the pavement was kept as a normal surface-to-surface contact with hard and frictionless characteristics. For the boundary conditions, nodes were free to move along the normal directions but were restricted in perpendicular horizontal directions as presented in **Fig. 8-9**. The bottom of the model was assigned elastic foundation characteristics.

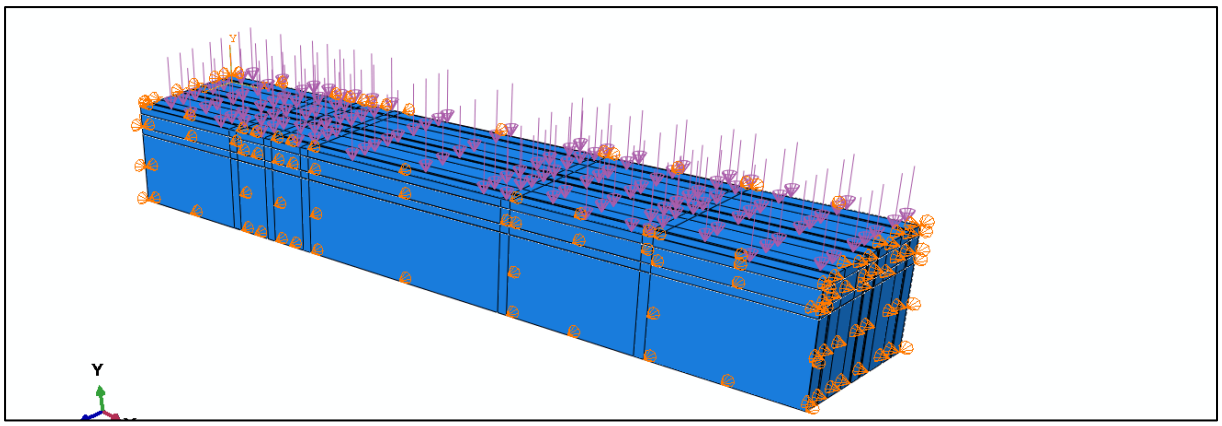

Fig. 8-9: Loading and boundary condition details.

8.7 Results and Discussion

Simulations have been conducted on ABAQUS on a 20 meters long pavement section. Simulations correspond to 5000 average annual truck passes for a design life of 15 years. Screenshots are taken from the simulations for the positioning of tire foootprints at different locations.

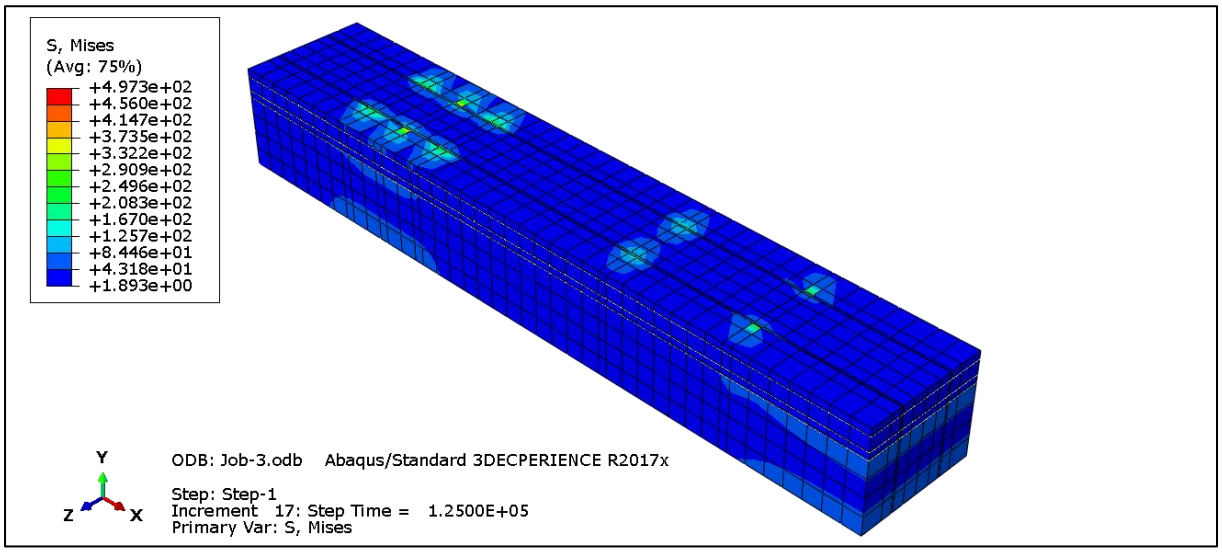

Fig. 8-10: Movement of truck as per a zero-wander mode.

Fig. 8-10 shows the stress values exerted under each tire foootprint while a truck is moving along the middle of the lane corresponding to the zero-wander mode at a moving speed of 90 Km/h. Highest stress accumulation within the truck axles ia observed under the driving axle and along the middle axle of the trailer.

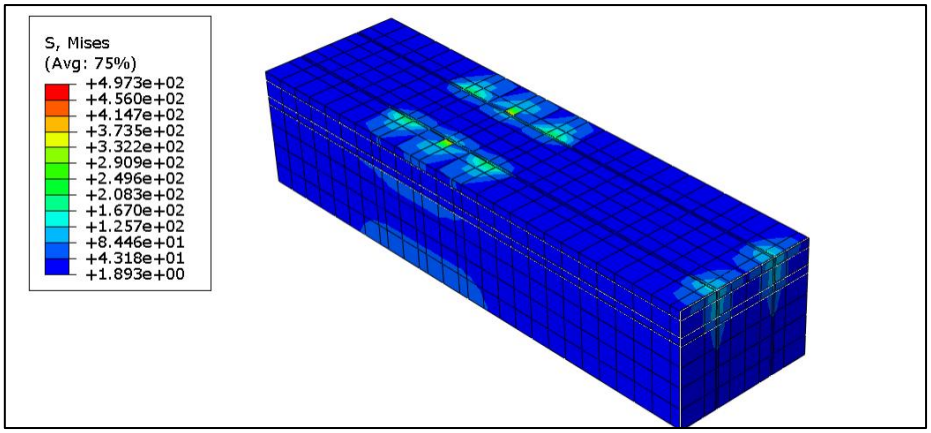

Fig. 8-11: Cross section for stresses under the driving axle.

Cut section manage was used in ABAQUS to yield the stress and strain values under each axle and tires for calculation of fatigue cracking and rutting deformation along with remaining pavement life. The highest portion of exerted stresses were recorded against the driving axle and progression of the stresses along the vertical plane directly under the driving axle can be observed in **Fig. 8-11**.

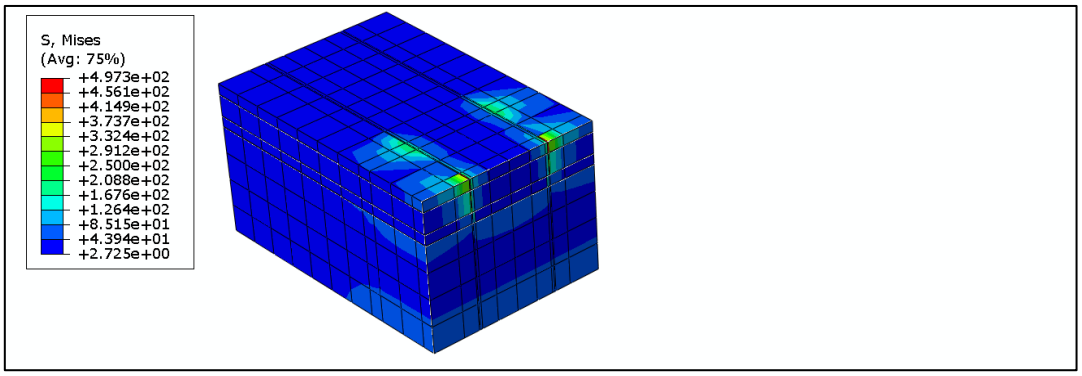

Fig. 8-12: Cross section for stresses under the middle trailer axle.

Fig. 8-12 above shows the cut section view of the stresses under the middle axle of the trailer, where the highest amounts of stresses are exerted along the pavement. For the calculation of vertical and horizontal strains, the functions E in the ABAQUS were used to determine fatigue and rut life of the pavement. Minimum amount of stresses on the pavement were exerted by the steering axle of the truck due to the least amount of axle load and tire pressure, as presented in **Fig. 8-13**.

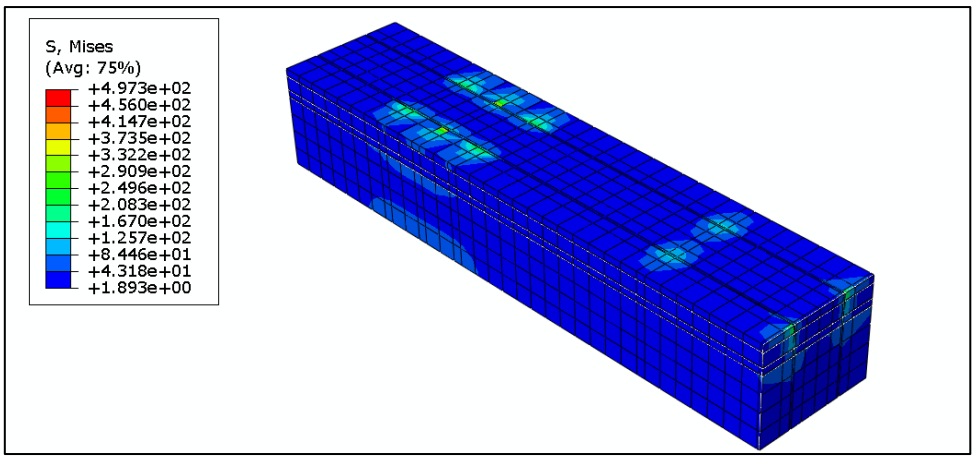

Fig. 8-13: Stresses under the steering axle.

Futhermore, the stresses were recorded under the tires at various lateral positions of axles. The following **Fig. 8-14** shows the screenshot taken when the lateral positioning of the truck was at extreme left of the lane during a uniform wander mode.

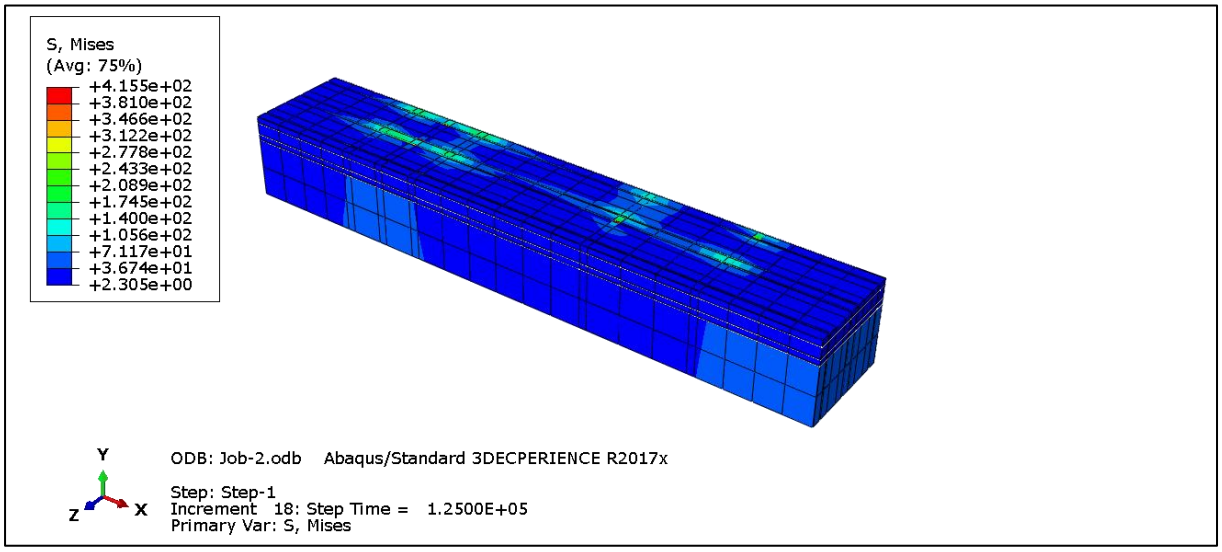

Fig. 8-14: Screenshot of truck tire stresses under a uniform wander mode.

Even during the selection of uniform wander mode, due to the geometric configuration of dual wheels on the driving axle of the tractor, the majority of load concentration is along the central part of the pavement lane as presented in **Fig. 8-15**. The effected area is overlapped by truck passes when a uniform wander mode is due to geometric configuration lateral dimensions of drive axles. The width of overlapping of truck passes under a uniform wander mode is around 1.5 m.

Even during the selection of uniform wander mode, due to the geometric configuration of dual wheels on the driving axle of the tractor, the majority of load concentration is along the central part of the pavement lane as shown in **Fig. 8-15**. The effected area is overlapped by truck passes when a uniform wander mode is due to geometric configuration lateral dimensions of drive axles.

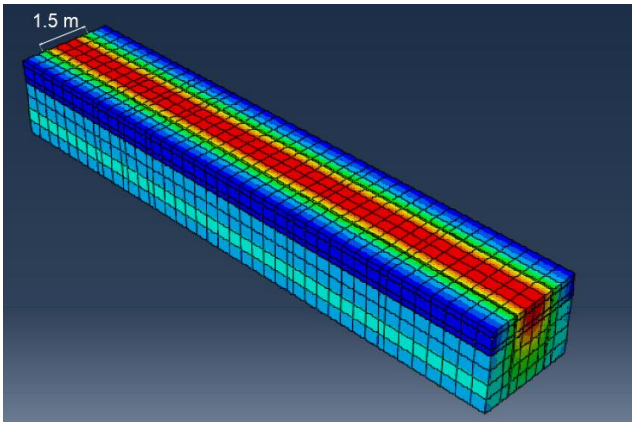

Fig. 8-15: Overlapping of wheel path width during uniform wander mode.

Since, validated material parameters along with the relevant boundary conditions, element size and element type are considered, therefore, simulation results were compared with the research mentioned in Section 8.3 and shown in **Table 8-4**. The progression of stress and strain follow the same distribution under loading due to the use of verified parameters. The same concept has been used for Thesis 4 and Thesis 5.

Table 8-4 Validated simulation results.

Layers	**Depth**	**Measured strains using simulations**	**Actual strains using reference research**	**Difference**	**Overall strain propagations towards depth**	
					Simulated	**Research**
Asphalt	50 mm	334 microns	317 microns	5.2 %	81.1 %	79.8%
	100 mm	316 microns	300 microns	5.2 %	72.6 %	72.4 %
	150 mm	281 microns	267 microns	5.1 %	64.3 %	64 %
	200 mm	274	261 microns	4.8 %	56.5 %	56.3 %
Base Course	350 mm	266 microns	253 microns	5.0 %	44.2 %	44.8 %
Subbase	410 mm	183 microns	175 microns	4.5 %	37.4 %	37.6 %
Subgrade	800 mm	141 microns	134 microns	5.1 %	19.5 %	19.1 %

Magnitude of strain values were observed along the longitudinal profile under each axle and tire with raw data obtained from ABAQUS and are shown in **Fig. 8-16**. As observed with the total length of the section being 20 m. The highest magnitude of strains are recorded along the middle axle of the trailer at 350 microns, followed by the front and back axles of the trailer at 286 microns. The minimum amount of strain occurs under the steering axle of the truck at 136 microns.

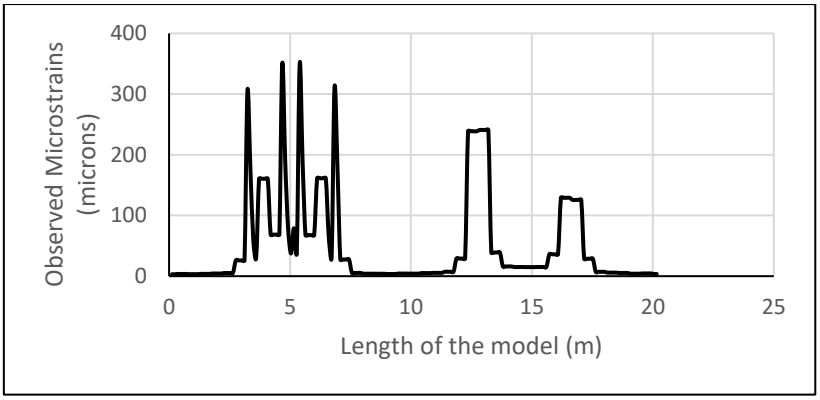

Fig. 8-16: Strain calculated along the longitudinal profile.

8.8 LEF and ESALs Calculation

The damage accumulated from each axle corresponding to design life of 15 years was then converted into equivalent damage to a standard 80 kN single axle load using load equivalency factor (LEF) [120] . A standard formula, in which a standard single axle load of 80 kN (18,000lbs) is divided to a designated axle load and the ratio is powered to four as shown below in 8-11.

$$LEF = \left(\frac{designated\ axle\ load(kN)}{standard\ axle\ load(kN)}\right)^4 \quad \text{8-11}$$

Correspoonding LEF values for each axle in the truck are shown in **Table 8-5**.

Table 8-5 Calculated LEF for each axle group.

Axle Type	**LEF**	**Damage effect compared to standard axle load**
Steering axle	0.48	Less than 2 times
Drive axle	3.03	More than 3 times
Front rear axle	0.79	Equivalent
Middle rear axle	0.79	Equivalent
Back rear axle	0.79	Equivalent

The LEF for a standard 80 kN single axle load is 1.00. A steering axle load of 66.75 kN would do less than two times the damage as that of an 80 kN standard axle load. A drive axle usually has a higher axle load of about 105.61 kN, hence the damage accumulated by this axle is three times that of damage accumulated by an 80 kN standard axle load. For the three single axles on the trailer, the damage from each axle was found to be equivalent to the standard axle load of 80 kN [121]. Hence, a total equivalent single axle to truck (ESAL/Truck) ratio of 1.55 was obtained and was calculated using the following Eq. 8-12 (AASHTO).

$$Truck\ Category\ Esals\ in\ Construction\ Year = load\ factor * Lane\ AADT * 3.65 \quad (8\text{-}12)$$

Table 8-6 shows the calculation of a construction year design ESALs.

Table 8-6 Construction year ESALs.

Truck Category	**Load Factor (ESALs/Truck)**	**Lane Average Annual Daily Traffic**	**ESALs in construction Year**
5 Axles	5.88	5000	29,400

Finally, total design ESALs calculated using the following Eq. 8-13.

$$Total\ design\ ESALs = total\ construction\ year\ ESALs * \frac{(1 + i_{B\ to\ D})^n - 1}{i_{B\ to\ D}} \quad (8\text{-}13)$$

Where n is base year of construction and $i_{B\ to\ D}$ is growth rate from base year to final year of design period. With a growth rate of 3.5%, a toal ESALs of 1,300,000 were obtained.

Using the E (Strain) values from the ABAQUS results, strains were calculated under each tire and each axle based on their orientations such as vertical strain on top of subgrade and horizontal strains on bottom of asphalt layer for calculation of rutting and fatigue cracking respectively. Using the equivalent damage calculation, all the measured strains from the axles for a specific number of passes were then combined into accumulated damage by a single axle 80 kN equivalency factor. Maximum magnitude of equivalent values of strains was calculated to be at 350 microns for a zero wander mode. Magnitudes of microstrain values observed under a zero wander mode for the remaining axles are presented in the **Table 8-7**.

Table 8-7 Observed vertical strain under each axle.

Axle type	**Strain (μ/μ)**
Steering Axle	136
Driving Axle	227
Front Trailer Axle	286
Middle Trailer Axle	350
Back Trailer Axle	286

Maximum magnitude of vertical strains under a zero wander ode have been recorded under the middle axle of the trailer tire, which is around 80% more than the remaining two axles of the trailer. The steering axle exerts the minim amount of vertical strain at 136 microns.

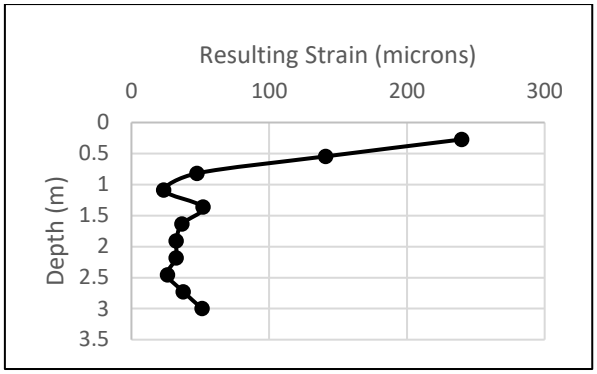

Fig. 8-17: Microstrains under equivalent axle load for a uniform wander mode.

During the moving load simulations along the 20 meter long crossection, when the uniform wander mode was used, with lateral acceleration of the truck kept around 1.84 m/s^2. The calculated vertical strain values under the top of subgrade were eventually reduced to a corresponding amount and shown in **Fig. 8-17**.

Furthermore, along the lateral section of the truck axle, strains were recorded at the bottom of the asphalt layer. Load equivalency factor was used to calculate the equivalent magnitude of strain observed under the tires, corresponding to the axle load of 80 kN. Accumulation of strains on the bottom of the asphalt layer for a lateral cross-section are shown in **Fig. 8-18** below.

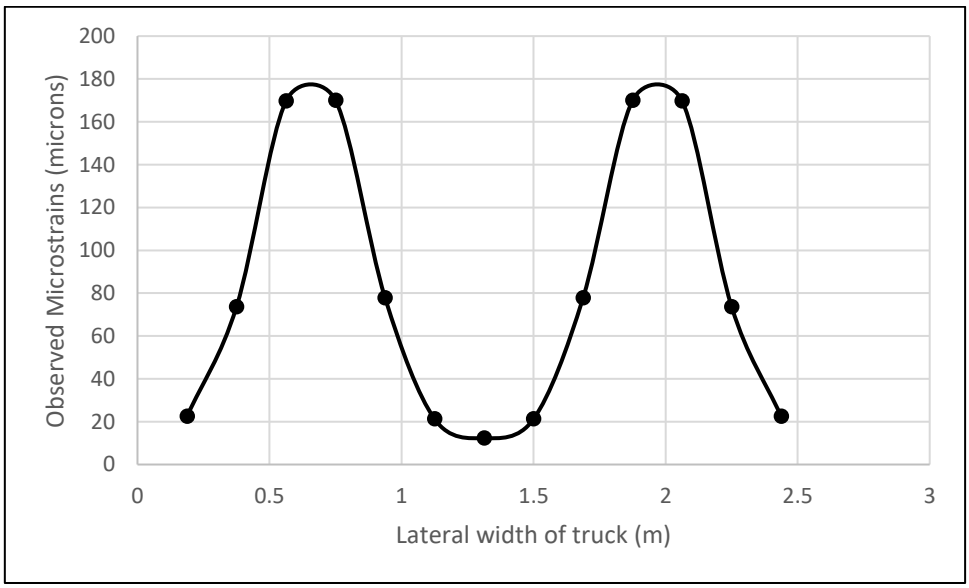

Fig. 8-18: Strains under equivalent loaded axle in a lateral cross section for a zero wander mode.

The effective with of the strains along the lateral cross-section under the bottom of asphalt layer is considered to be at 2.5 meters under the axles. Strain values were recorded under each axle of the truck and then converted into the equivalent truck axle using the load equivalent factor. Highest amount of strains were recorded under the driving axle and trailer axle tires. A maximum magnitude of 180 microns is obtained for an equivalent axle moving at 90 km/h under a zero wander mode.

The middle trailer axle exerts the maximum amount of strain with a magnitude of 80 microns, followed by the strains values of 60.4 microns under remaining trailer axles. The difference between the strain values observed along the lateral cross-section if high at higher magnitudes of strains in case of a middle trailer axle and driving axle of the truck. The difference observed for the zero wander and uniform wander mode under the middle trailer axle as shown in **Fig. 8-19**.

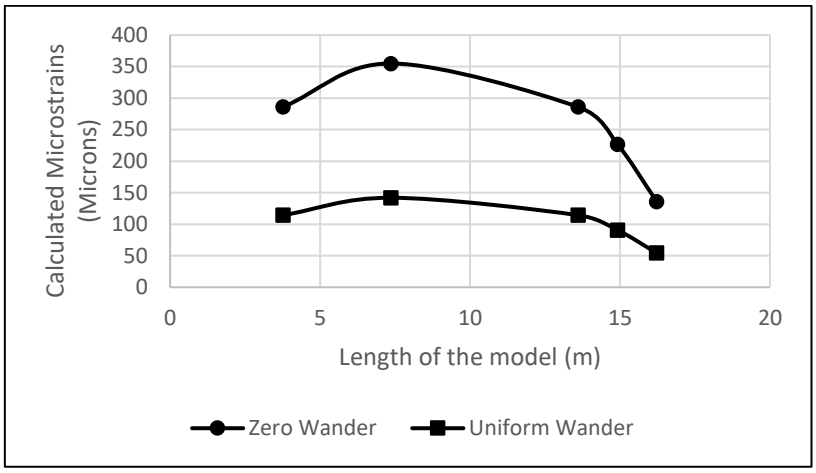

Fig. 8-19: Comparison of strains under the longitudinal profile for zero wander and uniform wander modes.

8.9 Rutting and Fatigue Cracking Evaluation

Using the equivalent values of microstrains observed with a projected traffic of 1.3 million ESALs for a design life of 15 years, number of loading cycles to rutting and fatigue cracking were calculated from the distress prediction models developed by Asphalt Institute. Two of the fatigue and rutting prediction models respectively given by Asphalt Institute are presented below in Eqs. 8-14 and 8-15 respectively [122].

$$N_f = 0.0796 * \varepsilon_c^{-3.291} * E^{-0.854} \quad 8\text{-}14$$

$$N_d = 1.365 * 10^{-9} * \varepsilon_t^{-4.477} \quad 8\text{-}15$$

Where, where N_f is the allowable number of load repetitions to prevent fatigue cracking and N_d is the allowable number of load repetitions to prevent permanent deformation (rutting), E is the elastic modulus of asphalt concrete layer, ε_t is horizontal tensile strain under HMA layer and ε_c is vertical compressive strain on top of the subgrade.

Microstrains obtained from FE modelling are used to calculate permanent plastic strain ε_p as per following Eq. 8-16,[123].

$$\varepsilon_p = \varepsilon_r * a_1 * N^{a_2} * T^{a_3} \quad 8\text{-}16$$

Where, ε_p is permanent strain ε_r is resilient strain N is number of load repetitions T is temperature, ℃ and a_1, a_2, a_3 are regression coefficients with values 1.69, 1.85, 0.275 respectively taken from (40). Finally, the rut depth occurring in asphalt layer can then be computed using the following Eq. 8-17, [114].

$$RD = \sum_{I=1}^{N} \varepsilon_P^I \, h^i \qquad 8\text{-}17$$

where RD is the total rut depth in the asphalt concrete layer (mm); N is the number of sublayers, ε_P^I is the plastic strain in the ith sublayer; and h^i is the thickness of the i-th sublayer (mm). However, in this research asphalt layer was not divided into subseueant sublayers, rather the accumulation of plastic strains at bottom of the asphalt layer and vertical strains on top of subgrade layer were used to calculate the rut depth.

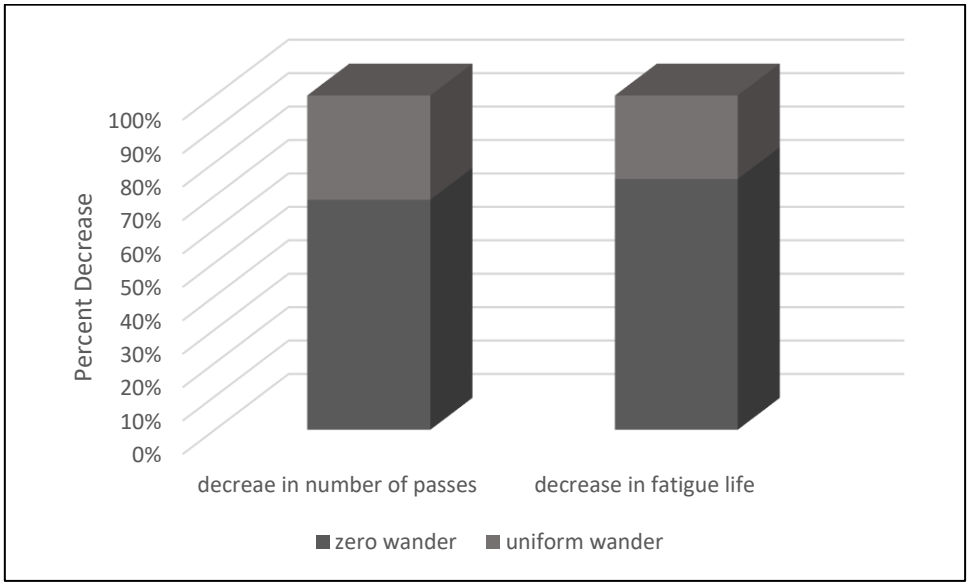

Fig. 8-20: Decrease in number of passes and fatigue life under zero wander and uniform wander mode.

Maximum amount of reduced number of passes occurs under a zero wander mode with 527,000 number of reduced passes by the end of lifetime of the pavement as shown in **Fig. 8-20**, and it translates to the decrease in fatigue life of around 1.2 years if the zero wander mode is used. On the other hand, the decrease in number of passes reduced by fatigue damage is only limited to 239,000 passes, corresponding the decrease in fatigue life of only 4 months when a uniform wander mode is used. However, the reduction in fatigue life can be furthered minimized if a larger amount of lateral width of the lane is available for the truck to wander.

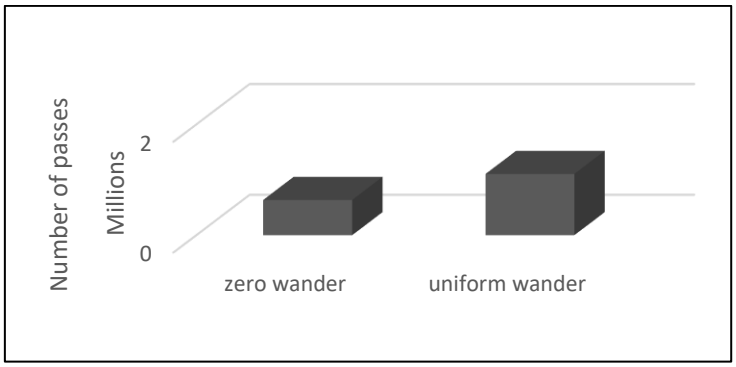

Fig. 8-21: Number of required passes to reach 6mm rut depth.

Asphalt pavement must be rehabilitated as it reached its terminal serviceability when the rut depth of 6 mm occurs on the pavement surface. **Fig. 8-21** compares the number of passes under each wander mode to reach a rut depth of 6 mm. Under a zero wander mode, the pavement only needs 735,286 number of passes to reach rut depth of 6 mm, however when uniform wander mode is used, the number of required passes to reach 6 mm increases to 1,205,380 which makes upto a 38% increase in number of passes. When an uniform wander mode is used, the pavement can sustain its serviceability until the end of its predicted lifetime for the same amount of traffic growth and number of passes.

Fig. 8-22: Measured rut depth at 1.3 million ESALs.

Rut depth was obtained using equation and also compared from the (U) deformation results in ABAQUS results section and presented in **Fig. 8-22**. With projected traffic of 1.3 million ESALs the pavement reaches a rut depth of 10.21 mm at the end of its service life. On the other hand, for the uniform wander mode, the rut depth remains at 6.2 mm at the end of the pavement's services life. The decrease in rut depth is around 1.5 times when a uniform wander mode is used. Magnitude of rut depth under a uniform wander mode provides the effectiveness of uniform wander mode in prolonging the service life of pavement as compared to the projected zero wander mode.

8.10 Conclusions and Findings

In this research, a fully loaded class A40 truck with maximum allowable weight of 40 kN has been used to analyze the effect of zero wander and uniform wander modes on resulting fatigue life and magnitude of rut depth in the flexible pavement. Moving load has been subjected to the pavement to simulate zero wander and uniform wander mode. After the simulations, stress, strains and deflections were recorded under each axle and tires along the longitudinal and lateral pavement profiles. Since the material property parameters and loading conditon parameters for simulations have been prevalidated as taken from Fahad et al. [27] and Ebrahimi et al. [111], experimental validation is not required for resutling fatigue and rutting values. Moreover, this research is focused on proposing a new method for evaluating the tire contact loading footprint and usage of different speed values with lateral wander modes for measuring rutting and fatigue cracking with numerical equations provided by Asphalt Institute.

A difference in magnitude of rut depth is 1.5 times lower and fatigue life can increase by a factor of 40% if a uniform wander mode is used, making the uniform wander mode an ideal selection for lateral wander of autonomous trucks. However, the lateral acceleration of the trucks must be adjusted and controlled to maximum the usage of allowable width inside the lane. Hence, an increase in the width of the lane would minimize the overlapping of wheel paths under a uniform wander mode. Following findings are obtainzed from this research.

1. Due to action of induced vertical strains, decrease in fatigue life is around 1.75 times more in case of a zero wander mode.
2. Fatigue life decreases by 14 months in case of a zero wander mode.
3. A rutting depth of 6 mm occurs under a uniform wander mode at about 1105,380 number of passes which roughly translates to 8 percent advancement of rutting progression near the end of service life of pavement.
4. In case of a zero wander mode, rutting life of pavement is reduced to half if the 6 mm rut depth scenario is considered.
5. Magnitude of lateral acceleration of the truck can influence the decrease in distresses in the pavement.
6. Overlap of wheel paths occurs in case of uniform wander mode, with the overlapping width of 1.5 m for an A40 type truck.
7. Acceleration for rut development in case of a zero wander is almost 2 times than that of a uniform wander mode.
8. After the end of service life of pavement, under zero wander mode, rut depth is around 10 mm.

9 Truck platoon optimization for autonomous trucks

Organization of truck platoon affect the pavement structure and can alter the service life of the pavement. Autonomous trucks can be programmed to adjust themselves in a truck platoon, thereby creating minimum pavement damage based on channelized loading and pavement recovery time. Therefore, selection of optimum platoon pattern based on types of trucks inside the platoon, the number of trucks in the platoon, headway distance, interplatoon distance as well as the use of different lateral wander modes for autonomous trucks has been analyzed. Four different headway distances from 2 m to 5 m are compared. The first platoon PT-1 only consists of semi trailers, the second platoon PT-2 only consists of rigid body trucks and the third platoon PT-3 consists of equally distributed random traffic mix. Analysis has been conducted for projecting zero wander and uniform wander movements for each truck in the platoon on a three layered pavement cross section at vehicle speeds of 90 km/h for a total of 15 years of pavement lifetime consisting of 1.4 million equivalent single axle loads in finite element software ABAQUS. Further details can be found in [124].

9.1 Thesis 4

I have performed the truck platoon optimization for autonomous trucks and came to the following results:

1. Decrease in headway distance of 1 m from the 5 m for the trucks in the platoon leads to 7% increase in rate of development of rutting and fatigue cracking.
2. For rigid trucks in the platoon, increase in wheelbase by 2 m can reduce the rutting damage by 30 %.
3. Increase in headway distance from 2 m to 5 m, leads in increased fatigue life and rutting performance of pavement to up to 1.6 years.
4. Fatigue life decreases by 40% in case of using a zero wander mode at headway distance of 5 m when compared to uniform wander mode.

9.2 Related publications

M. Fahad and R. Nagy, “Truck platoon analysis for autonomous trucks,”SN Appl. Sci., vol. 5, no. 5, 2023, doi: 10.1007/s42452-023-05352-5.

9.3 Methodology

The research methodology consists of setting out the headway distance ranging from 2 m to 5 m with an increment of 1 m in each scenario, coupled with selected platoon types ranging from PT-1 to PT-3 as presented in **Fig. 9-1**. A combination of these scenarios for each platoon type with various headway distance values of 2 m to 5 m is made, along with grouping of uniform wander mode and zero wander mode in the Finite Element model. Furthermore, analysis is done in the model, where optimum headway distance and optimum platoon types are identified based on micros trains evaluated. After selection of the optimum headway distance and platoon type, rutting and fatigue cracking analysis is done against uniform wander and zero wander modes for each scenario of headway distance values.

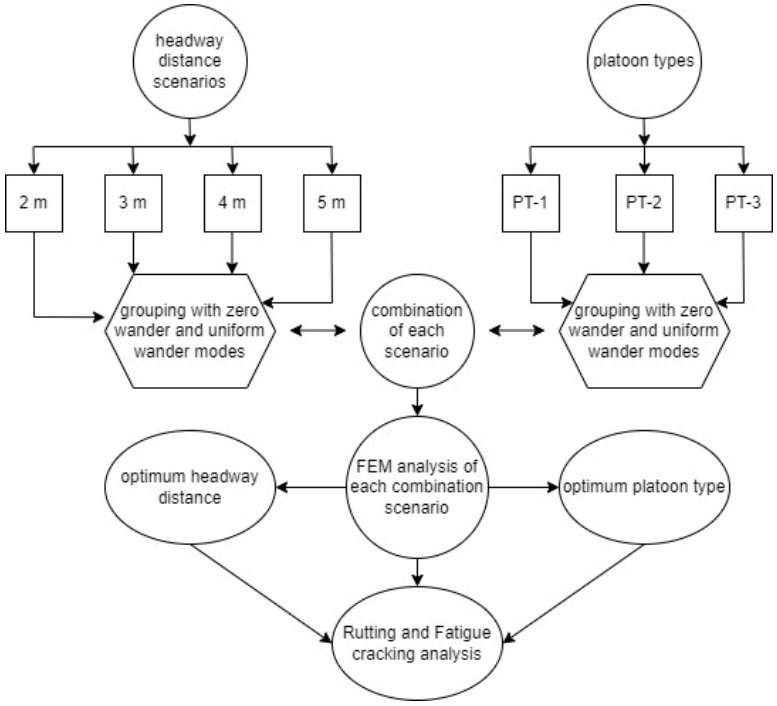

Fig. 9-1: Methodology flowchart.

9.4 Pavement Details

Conventional asphalt pavement consisting of asphalt layer, base course and subbase course resting on top of subgrade is considered for this analysis. Thickness of subgrade layer is kept at 2 m for modelling in ABAQUS. To accommodate a complete platoon in the model, length of the model is kept at 60 m and width of the model corresponds to a lane width of 3.5 m as shown in **Fig. 9-2**. The length of the model allows for analyzing various platoons and headway distances in this research.

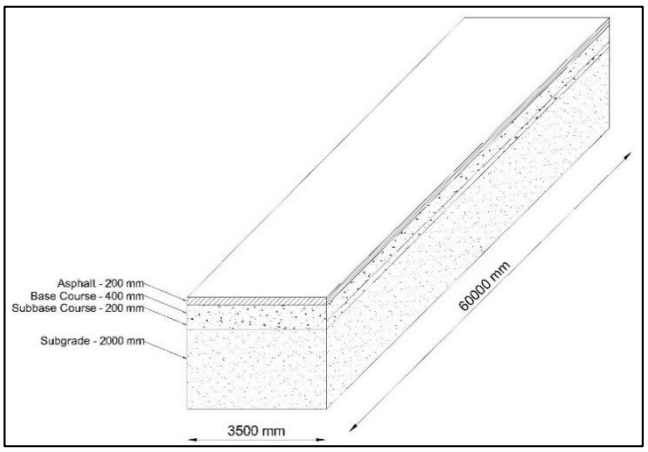

Fig. 9-2: Pavement details.

Validated pavement layer parameters in the form of elastic moduli and Poisson's ratio have been taken from Cheng et al. [25] as shown in **Table 9-1**. The Prony series parameters used in

Section 9 have been used in this section also for analyzing the viscoelastic properties of asphalt layer.

Table 9-1 Pavement layer properties.

Layer type	Thickness (cm)	Elastic modulus (kPa)	Possions ratio
Asphalt	20	950000	0.41
Base course	40	500000	0.35
Subbase course	20	350000	0.35
Subgrade	-	60000	0.4

9.5 Truck Loading Configurations

The class-1 truck as presented in **Fig. 9-3**, is a A40 European truck with maximum gross weight of 40 tonnes. It is a semitrailer with the attached trailer having tridem axles with single tires. For the tractor head, the steering axle has single axle with single tires and the drive axle has dual tires with single axle. The wheelbase if 7.555 m with center to center spacing of 1.31 m between each axle in the trailer. The steering and drive axle have wheel types of 295/80R22.5 and the trailer axles have tire types of 385/65R22.5.

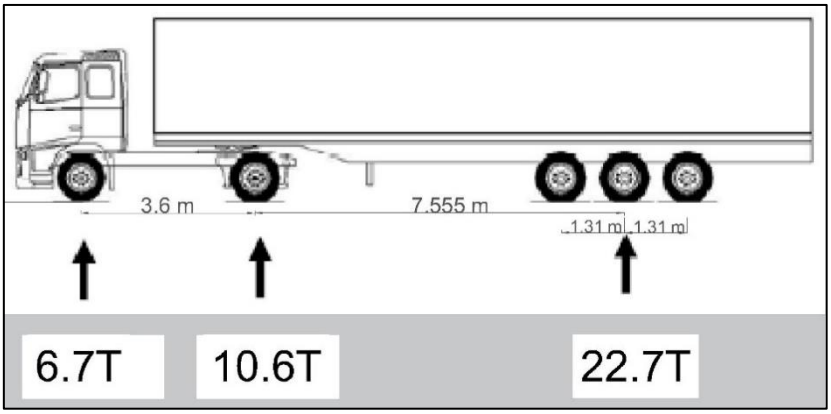

Fig. 9-3: Class-1 truck details.

Class-2 truck is a rigid body truck as shown in **Fig. 9-4**. It has a maximum gross weight of 26 tonnes. The wheelbase is limited to 5.5 m in this truck, with center to center spacing of dual tires of 1.31 m. The drive axle has 295/80R22.5 type wheel and dual tandem axles also have 295/80R22.5 type wheels.

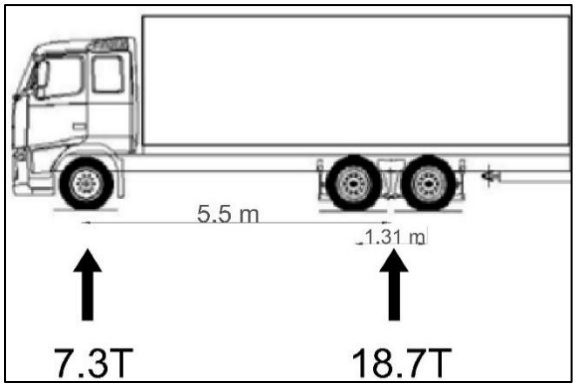

Fig. 9-4: Class-2 truck details.

Class-3 truck is also a rigid body truck included in the traffic mix as shown in **Fig. 9-5**, having two single axles working as drive axles and tandem axles with dual tires in the rear. Maximum gross weight is 34 tonnes having a slightly longer wheelbase of 5.6 m with center to center spacing of rear axle wheels of 1.37 m. the center to center spacing between the front drive axles is 2 m. Class-3 truck types are commonly used for transport of construction materials. The first two drive axles are single axles with 295/80R22.5 tires and rear axles are tandem axles with dual tires 295/80R22.5.

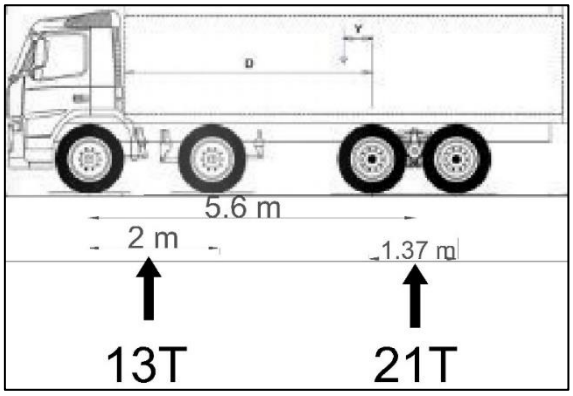

Fig. 9-5: Class-3 truck details.

With various combinations of axle loads and tires types, tire contact pressure has to be calculated under each tire, which depends on tire dimensions, loading on the tire and tire inflation pressure [125]. The size of tire contact are can also vary based on the tire inflation pressure [116]. Tire deflection, therefore, relates to tire contact area, and it has the highest effect on contact area size at lower inflation pressures. Methodology presented in section 9 has been used for tire pressure details calculation for all truck types. The tire type and its correposing load, tire inflation pressure, tire contact pressure and contact patch dimensions are shown in **Table 9-2**, **Table 9-3** and **Table 9-4**.

Table 9-2. Tire pressure and load details for the Class-1 truck.

Tire type	295/80R22.5	295/80R22.5	385/65R22.5	385/65R22.5	385/65R22.5
Twin vs Single	Single	Twin	Single	Single	Single
Axle load (Tons)	6.7	10.6	7.57	7.57	7.57
Load per wheel (kN)	32.85	25.98	37	37	37
Tire inflation pressure (kPa)	690	690	690	690	690
Tire contact pressure (kPa)	430	350	550	550	550
Contact patch Length/Width (mm)	250/330	250/310	275/310	275/310	275/310

Table 9-3 Tire pressure and load details for the Class-2 truck.

Tire type	295/80R22.5	295/80R22.5	295/80R22.5
Twin vs Single	Single	Twin	Twin
Axle load (Tons)	7.3	9.35	9.35
Load per wheel (kN)	35.79	45.84	45.84
Tire inflation pressure (kPa)	690	690	690
Tire contact pressure (kPa)	390	500	500
Contact patch Length/Width (mm)	250/330	250/310	250/310

Table 9-4 Tire pressure and load details for the Class-3 truck.

Tire type	295/80R22.5	295/80R22.5	295/80R22.5	295/80R22.5
Twin vs Single	Single	Single	Twin	Twin
Axle load (Tons)	6.5	6.5	10.5	10.5
Load per wheel (kN)	31.87	31.87	51.48	51.48

Tire type	295/80R22.5	295/80R22.5	295/80R22.5	295/80R22.5
Tire inflation pressure (kPa)	690	690	690	690
Tire contact pressure (kPa)	390	390	530	530
Contact patch Length/Width (mm)	250/330	250/330	250/310	250/310

9.6 Platoon Types

Number of trucks in a platoon can affect alter the pavement damage. With higher number of trucks in a platoon the time of continuous axle loads increases thereby resulting in earlier damage to the pavement. Song et al. [65] suggested using no more than 4 truck platoons, when compared with the fatigue damage from a 2 truck platoon, a damage of more than 30% occurs when using greater than 4 trucks. Melson et al. [83] studied the effect on transport costs and impact on pavement with various number of trucks in a platoon. Results showed that use of four trucks in a platoon generate the lowest transport related costs. However, the study didn't include the effect of number of trucks in a platoon ont he pavement damage. Three different platoon types based on different axle configurations are chosen as shown in the **Fig. 9-6**.

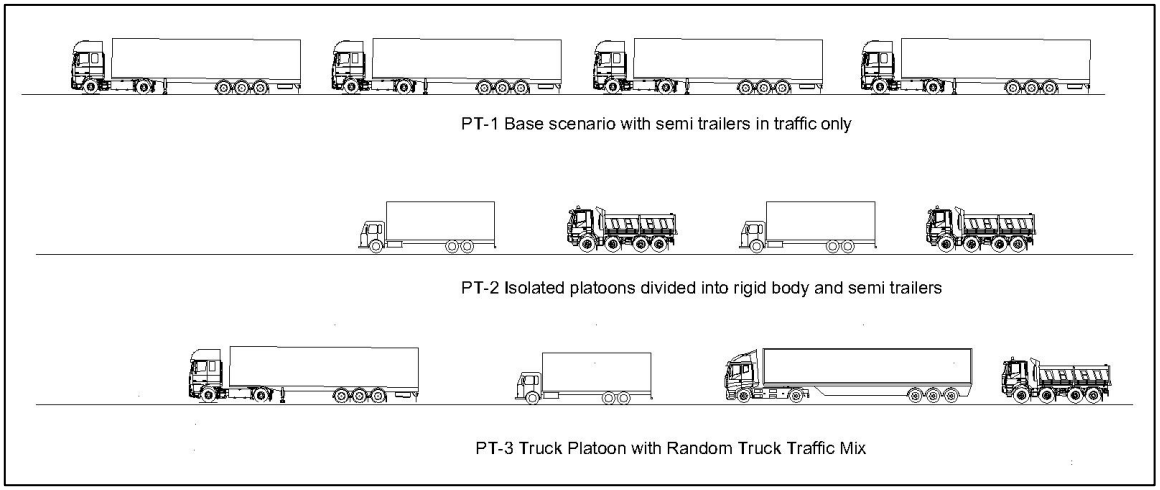

Fig. 9-6: Platoon types chosen.

For the traffic mix, in this research, three different types of trucks are considered. The first type of truck is a Class-1 truck, which is an European A40 type semitrailer as shown in figure. The other two trucks, Class-2 and Class-3 type trucks, are rigid body trucks. Class-2 truck is a conventional rigid body truck with only a single drive axle, while Class-3 type truck is a rigid body truck with dual drive axles, primarily used for construction material transport. It is assumed that the total traffic volume consists of 50% Class-1 trucks, 25% of Class-2 and 25% of Class-3 trucks. Dimensions, axles wight and configuration are taken from John Aurell et al. [8].

Traffic volume has been assumed to be 12 trucks using the tested highway section of 60 Meters. The rigid body trucks contribute to 50% of the traffic mix which leads to 25% of class 2 and 25% of class 3 trucks in the mixes. Three different truck platoons have been organized to study

the effect of different axle types in different platoons on pavement performance. First platoon type is a base scenario where only semitrailers are considered in the traffic mix; other scenarios are analyzed with reference to PT-1. Platoon configuration is presented in **Table 9-5**.

Table 9-5 Platoon configuration details.

Platoon type	Scenarios	Number of platoons
PT-1	Base scenario with semi trailer in traffic only	3
PT-2	Isolated traffic with rigid body trucks and semi trailers	3
PT-3	Random traffic mix platoon	3

In case of PT-2, the idea is to isolate the traffic based on rigid body and semi trailers. One passage of a 4 semitrailer truck platoon will do a different amount of damage than one passage of only the rigid body trucks, with the same amount of trucks in the platoon. Furthermore, the damage from all the platoons of PT-2 is accumulated and compared with the damage caused by PT-3, in which trucks are placed inside the platoon with the balance of maximum load of the platoon. An ideal PT-3 consists of two semi trailers and two rigid body trucks. The platoon size has been limited to 4 trucks of any configuration type.

Table 9-6 Truck types in platoons.

Truck type	Truck count	Number of platoons needed based on platoon type		
		PT-1	PT-2	PT-3
Class 1	4	1	1	2
Class 2	2	2	2	3
Class 3	2	2	2	3

Table 9-6 shows the truck volume assumed for each truck type and number of platoons needed for a specific truck for each truck type. Since in a PT-3 type platoon, a random traffic mix means more truck platoons are needed to cover the entire traffic with assumed traffic of 12 trucks.

9.7 Incorporation of Zero Wander and Uniform Wander Modes

For the use of zero wander mode, it is assumed that the trucks in thepro platoon would follow a straight path without any transverse movement with the lane. While performing analysis in FE mode, only the headway distance is changed among the trucks inside the platoon from 2 m to 5 m. A typical scenario in case of PT-3 platoon while using a zero wander mode is shown in **Fig. 9-7**.

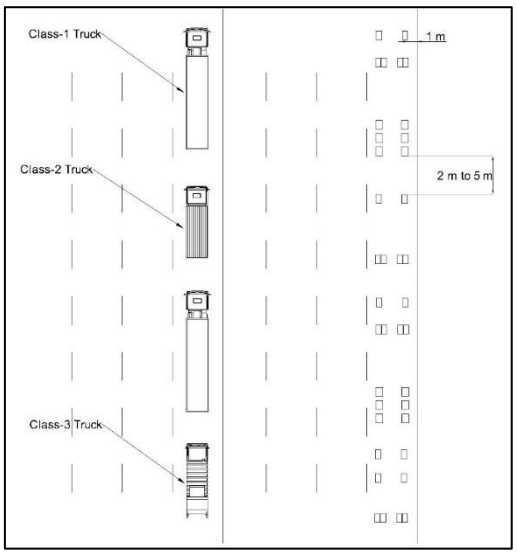

Fig. 9-7: Visualization of zero lateral wander

In this research, the uniform wander mode is selected based on the lateral wander of each truck in the platoon along a fixed path. Each truck in the platoon is given a fixed path to follow. Following this method, there is no overlapping of consecutive trucks in the platoon. Therefore, when each truck in the platoon passes through a fixed point on the pavement, repeated loading of trucks in the platoon on the specific point on the pavement are minimized.

In case of uniform wander mode, each truck in the platoon is given a predertmined base path and is allowed to laterally move with respect to that base path as presented in **Fig. 9-8**. In case of PT-3 platoon, the leading truck is positioned at exactly in the center of the lane with 1 m distance from the edge of the pavement to either edge of its outermost tires. For the second truck in the platoon which in this case is a class-2 truck, 0.5 m distance is provided from the left edge of the pavement and 20 cm for the third truck.

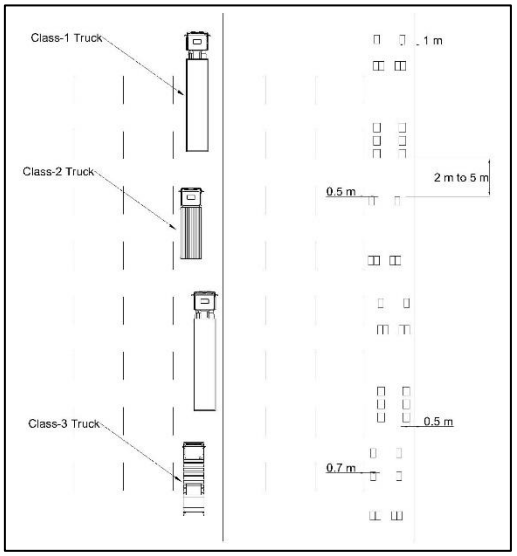

Fig. 9-8: Visualization of uniform lateral wander mode.

9.8 Finite Element Model Details

The 3D model has a length of 60 m to accommodate the platoons and trucks along the longitudinal direction, a width of 3.5 m and depth of 2.8 m with a greater thickness value given to the soil layer. The bottom of the model is simulated as elastic foundation in terms of friction characteristics to simulate higher thickness of natural soil layer underneath. Average pavement temperature and environmental conditions are used for modelling. Extreme temperature conditions are excluded to reduce the bias in pavement distress mechanisms. The model consists of 8 node linear brick elements with reduced integration and hourglass control CPE8R. The model consists of 33251 elements with element size of 220 for increased accuracy and reduced computation time as shown in **Fig. 9-9**.

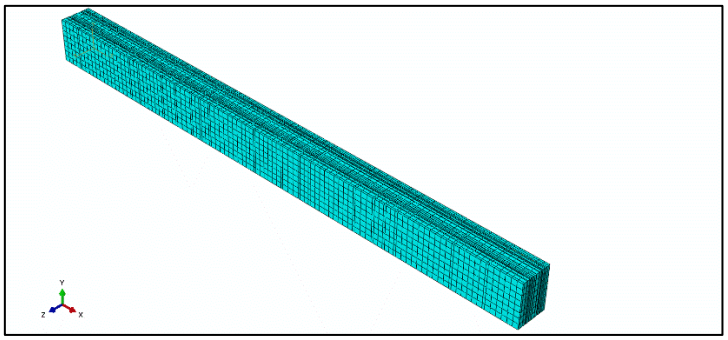

Fig. 9-9: 3D model mesh.

The interaction between the pavement layers is kept as normal surface-to-surface contact with hard and frictionless characteristics. For the boundary conditions, the bottom of the model is simulated as an elastic foundation, along the X axis, horizontal movements along X axis are not allowed and along Z axis, horizontal movement along Z are not allowed. Vertical movements are allowed in both planes of symmetry as shown in **Fig. 9-10**.

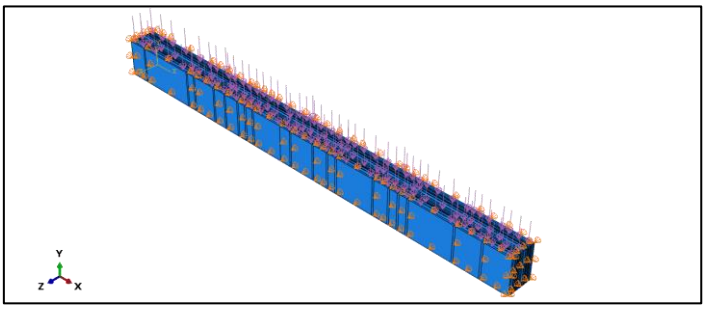

Fig. 9-10: Loading and boundary conditions for the model.

9.9 Results and Discussion

For a design life of 15 years with 1.4 million ESALs, simulations are conducted. The stress and train values at various components and intervals in them model are then gathered for analysis.

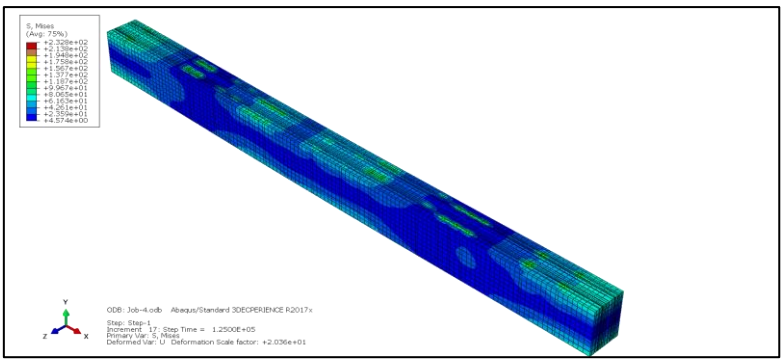

Fig. 9-11: S (mises) as observed form the simulations in uniform wander mode.

The distribution of strain values can be observed in **Fig. 9-11**. As observed, a higher concentration of stresses is occurring along the rear trailer axles of the Class-1 truck and later it occurs between the Class-1 trucks with its second pass and the Class-3 truck.

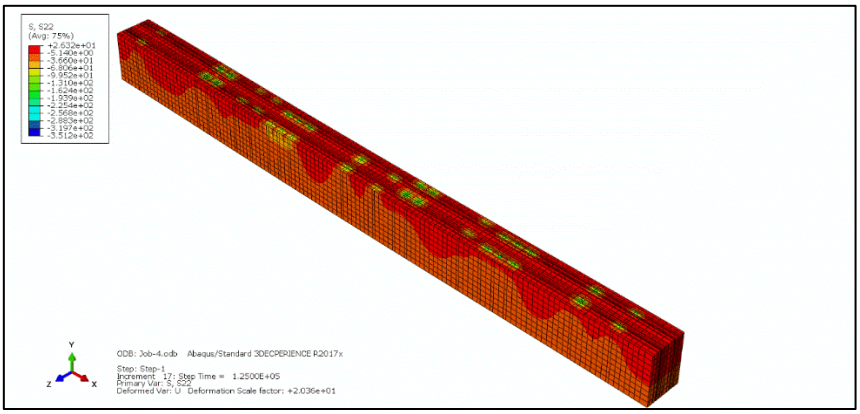

Fig. 9-12: Observed S(22) after the simulations in uniform.

Fig. 9-12 shows the stress profile generated under each passage of all the trucks in a PT-3 platoon. Usually, the higher concentration of stresses occur at rear axles of Class-1 truck and well as front axles of Class-2 trucks due to higher axle loading and shorter wheelbase. Furthermore, the steering axle of the second platoon's truck can be seen at the end of the model.

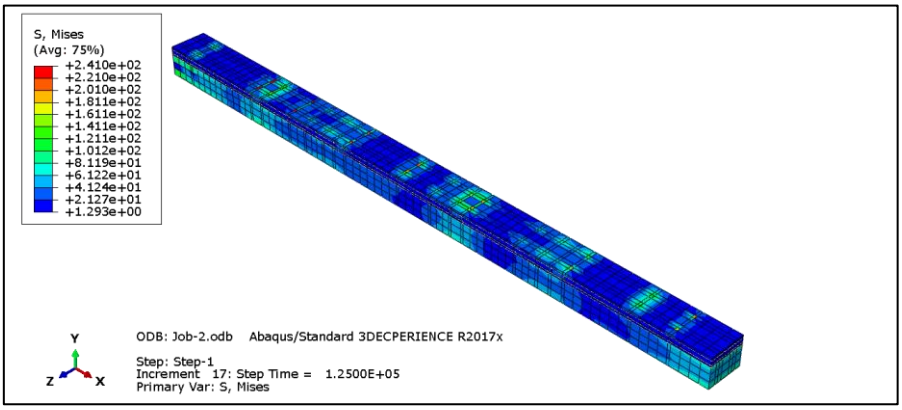

Fig. 9-13: S(mises) as observed in zero wander mode.

Fig. 9-13 shows the pattern of stresses induced in the pavement as a result of zero wander mode. In case of zero wander mode, channelized loading occurs and under axle loads of higher magnitudes in case of drive axle of class-2 truck and rear axles of class-3 truck, higher stress

concentration occurs. Moreover, the rear trailer axles of class-1 truck also exhibit higher stress concentration during its second passes. In this scenario, a headway distance of 2 m is provided which is not sufficient for the pavement to recover before the next truck passes through the same point, thereby inducing excessive stresses in the pavement.

9.10 Equivalent Single Axle Load Determination

Since the traffic mix contains variety of axle groups and axle loading, it is necessary to convert them into an equivalent single axle load (ESAL). An ESAL is a single standardized load application and causes an amount of damage to the pavement structure equivalent to one pass of a dual axle load of 80 kN at tire pressure of 758 kPa [126]. Different trucks are categorized based on the number of axle in each truck. Class-1 truck belongs to the axle semitrailer group of 5 Axles, Class-2 truck belongs to the 3 Axle group and Class-3 truck belongs to the 4 Axle group. Hence, each of this axle group have an equivalent ESAL amount termed as load factor. Following Eq. 9-1 is used to calculate the ESAL value, which is the load factor for each particular truck.

$$ESAL = \left(\frac{W_1}{W_2}\right)^4 \quad \text{9-1}$$

Where W_1 is the load on the designated axle or axle group and W_2 is the load on the standard axle or axle group. Load factors for each truck type in the traffic mix are shown in **Table 9-7**.

Table 9-7 Load Equivalency Factors for truck types.

	Axle Type	**Axle configuration**	**Load Equivalency Factor (LEF)**	**Total Load Factor (ESALs/Truck)**
Class-1 Truck	Steering axle	Single axle	1.23	3.5
	Drive axle	Dual axle	1.30	
	Trailer axles	Tridem axle	1.11	
Class-2 Truck	Steering axle	Single axle	1.39	2.6
	Drive axle	Dual axle	1.28	
Class-3 Truck	Steering axle group	Dual axle	1.59	4.1
	Drive axle	Dual axle	2.57	

As observed from the table above, the Class-3 truck yields the highest number of ESALs per truck due to higher axle load of 205.94 kN on its drive axle and load of 127.49 kN on its steering axle group. Least amount of ESALs per truck occur under the trailer axles of Class-1 truck having designated axle load of 222.61 kN which is divided by the equivalent single ESAL load of 200 kN for tridem axle group. The formula for calculating total ESALs in construction years is shown in Eq. 9-2.

$$\begin{aligned} &ESALs\ in\ construction\ year \\ &\quad = AADT\ (Lane) \\ &\quad * Load\ Factor * 3.65 \end{aligned} \quad \text{9-2}$$

Furthermore, the total ESALs for each truck category based on the percentage of shared traffic volume in terms of construction year annual average daily traffic (AADT) is presented in **Table 9-8.**

Table 9-8 ESALs for traffic mix.

	Truck Category	**Load Factor (ESALs/Truck)**	**Lane Average Annual Daily Traffic**	**ESALs in construction Year**
Class-1	5 Axles	3.5	3000	36750
Class-2	3 Axles	2.6	1500	13650
Class-3	4 Axles	4.1	1500	21525

Eq. 8-13 is used to calculate the total design ESALs for the pavement lifetime. For the total pavement design life of 15 years and annual growth rate of 3.5%, the total number of design ESALs calculated are 1.4 million ESALs. This traffic volume has been used for calculation of horizontal tensile strain and vertical compressive strain values.

9.11 Analysis of Microstrain Values

Observed strain component values from ABAQUS have been normalized to equivalent damage values of an 80 kN axle load for each truck type. The observed microstrains under the heaviest axle group for each truck type in case of zero wander mode are shown in **Fig. 9-14**.

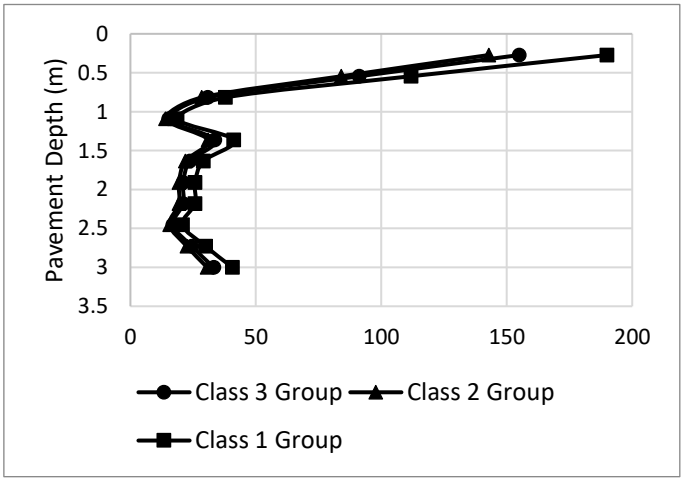

Fig. 9-14: Vertical Strains under all platoon.

As observed, the highest accumulation of vertical strain magnitudes occur under the Class-1 truck due to channelized loading when using the zero wander mode, in this case 186 microns of strain is accumulated under the Class-1 truck category type, for Class-2 trucks since the axle weight as well as percentage of annual truck traffic is lower than that of Class-1, therefore, the equivalent strain magnitude is only limited to 145 microns. Class-3 type truck however has a larger axle load resulting in larger load factor but due to less share with annual average daily traffic, the accumulation of vertical strains is only limited to 155 microns.

Fig. 9-15: Class-1 truck strain values with zero wander and uniform wander

Horizontal strain profiles for the class-2 truck resulting from uniform wander mode and zero wander mode are shown in **Fig. 9-15**. In case of zero wander mode maximum, strain magnitude reaches the value of 160 microns when cumulative equivalent single axle load is used for the class-2 truck. In case of a uniform wander mode, since a separate central path is provided to the second truck in PT-3, hence the peak is skewed towards the left part at 95 microns. The difference of about 65 microns exists between the two lateral wander modes.

However, when the uniform wander mode is used with a separate path provided to the 3rd truck in platoon with a distance of 0.5 m between the pavement edge and right most wheel as shown in **Fig. 9-16**, the resulting horizontal strain acting on the asphalt layer is much lower with magnitude of 130 microns. A slight increase is observed in the strain values for the truck with the uniform wander mode, it is due to the fact that a slight overlap of truck tires exists between different predetermined paths of trucks in the platoon due to limited pavement width available of 3.5 m. However, this increment is negligible when the pavement recovery time and the effect of headway distance are considered.

Fig. 9-16: Class-1 truck Second Pass strain values with zero wander and uniform wander mode.

For the PT-3, class-3 truck is the fourth truck in the platoon. Horizontal strain values are shown resulting from the cumulative equivalent single axle load calculated for this truck type. In case of the zero wander mode, horizontal strains reach the peak value of 206 microns during total

annual passes while using the equivalent single axle load from this truck type as presented in **Fig. 9-17**. The peak horizontal strain reaches 110 microns. Due to higher axle load on the front part of the truck and shorter wheelbase than the class-1 truck, the decrease in strains at uniform wander mode is only limited to 20 microns when compared to that of the class-1 truck.

Fig. 9-17: Class-4 truck strain values with zero wander and uniform wander mode.

Furthermore, the strains under different headway distances used for PT-3 platoons are compared in case of zero wander mode. **Fig. 9-18** compares the horizontal strains under the equivalent single axle load of class-1 truck and class-2 truck under various headway distances from the total annual truck passes. The headway distance of 2 m yields the horizontal tensile strains of 150 microns and the accumulated strain decreases to 138 microns with the headway distance of 5 m Hence, a reduction in 12 microns occur if more recovery time to pavement is given with headway increment of 3 m to the base headway distance of 2 m.

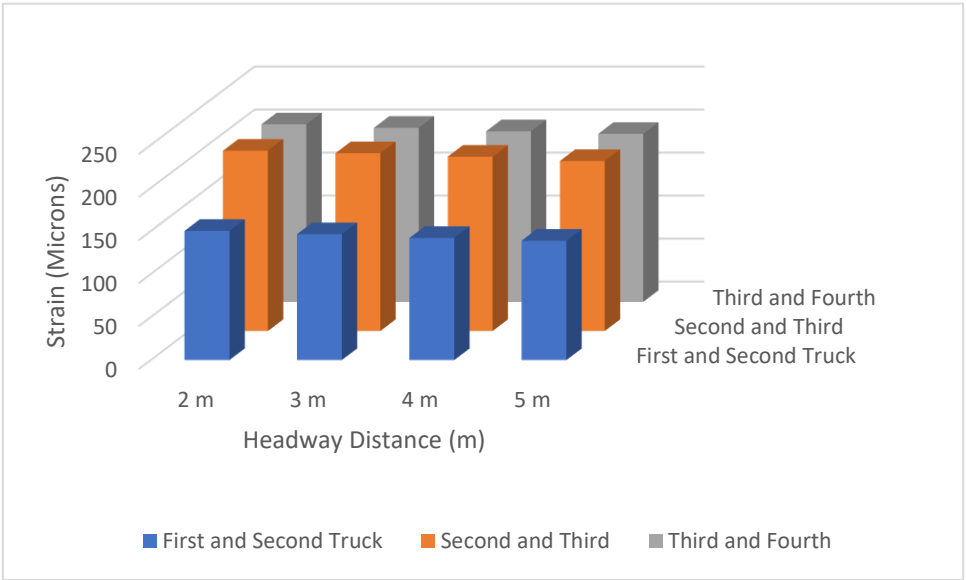

Fig. 9-18: Strains for various headway distance values between first and second truck.

Fig. 9-19 compares headway distances ranging from 2 m to 5 m with an increment of 1 m in three scenarios. From first and second truck the maximum Microstrains are observed at 150 microns, for the second and third truck, due to higher loading and axle weight magnitudes, the maximum strain values are at 209 microns at 2 m of heyday distance and values decrease by 12 microns at headway distance of 5 m to 197 microns.

In case of the third and fourth trucks' headway distance, the difference between strain values at headway distances of 2 m and 5 m is at 11 microns. It is observed that an average decrease in microstrains of 2.5 microns exists with 1 m increment in headway distance upto 5 m, however the increment is non-linear in nature, and it depends on elastic recovery, axle configurations and loading frequency of trucks in the platoon.

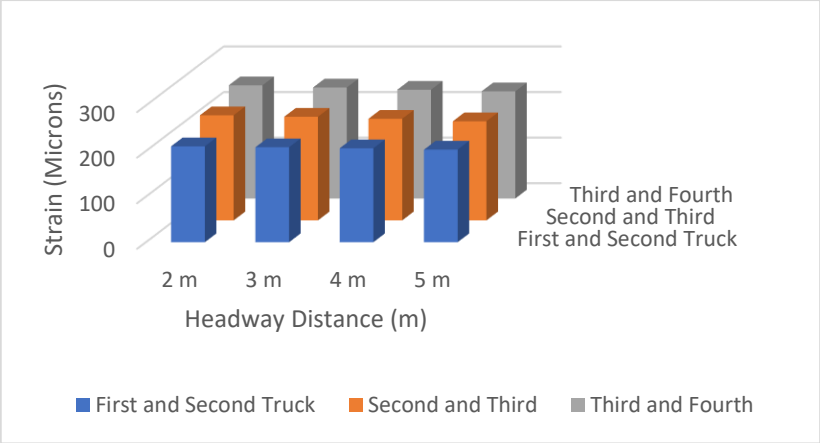

Fig. 9-19: Strains for various headway distance values between second and third truck.

Fig. 9-20 compares the resulting microstrains at various headway distance values between the four trucks in platoon pt-1. In case of the PT-1 scenario, higher accumulation of strains start under the second truck with headway distance of 2 m at 210 microns and the microstrains reduce to 203 microns at the headway distance of 5 m. the situation gets severe in terms of increased microstrains values for the third and fourth trucks in the platoon, where the headway distance of 2 m yields the strains of 248 microns and strain magnitude decreases to 235 microns with the headway distance of 5 m between third and fourth trucks.

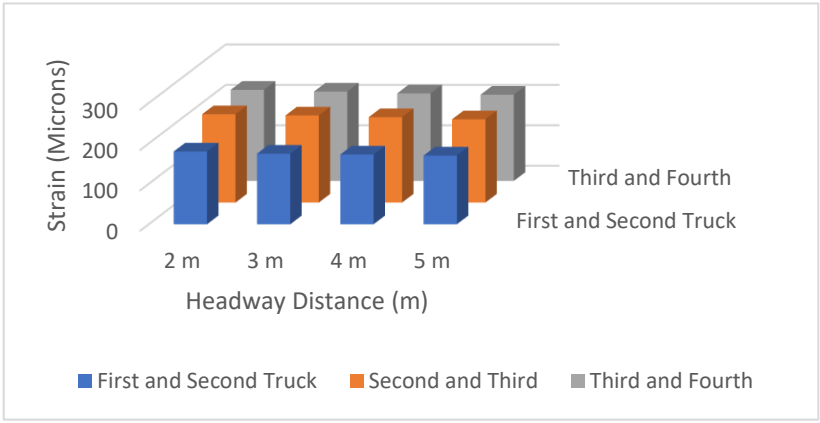

Fig. 9-20: Strains for various headway distance values between third and fourth truck.

Horizontal tensile strain values in case of PT-2 platoon are shown in **Fig. 9-21**. It can be observed that the highest magnitude of micorstrains exists under the front truck in the platoon when 2 m headway distance is used in case of a zero wander mode at 225 microns, which is 24 microns higher than that of PT-3. Furthermore, with as with increase in headway distance to 5 m, the decrease in microstrains under the fourth truck occurs at 213 microns, the magnitude at this point is still higher by 17 microns when compared to the PT-3 platoon.

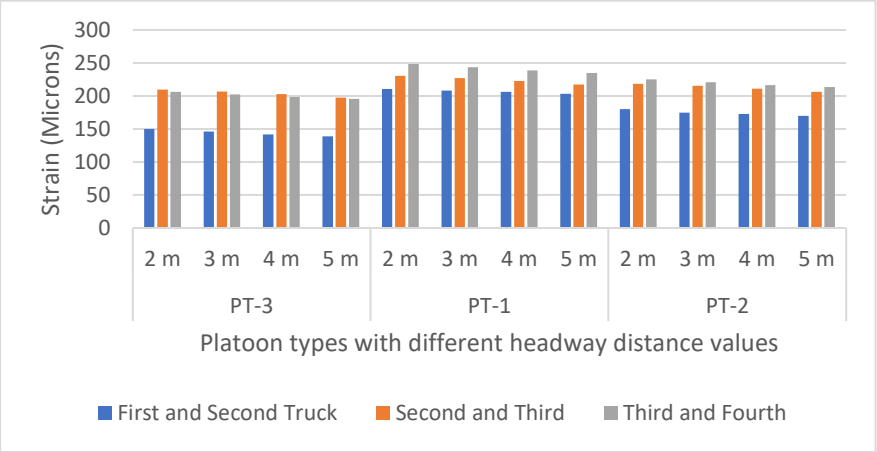

Fig. 9-21: Strains for various platoon types and headway distance values.

The PT-3 type platoon yields the lowest accumulation of strains when compared against PT-2 and PT-3 platoons at various headway distances ranging from 2 m to 5 m as shown in **Fig. 9-22**. Highest microstrains in each platoon type exists under the last truck in the platoon due to effect of channelized loading when a zero wander mode is used. The decrease in microstrains due to increase of headway distance of 5 m is limited in case of PT-1 platoon to 7 microns and in case of PT-2 to 10 microns, the decrease is much higher in case of PT-3 platoon by 12 microns.

The difference of 24 microns exists between PT-2 and PT-3 platoons under the fourth truck, and the difference of 33 microns exists between PT-3 and PT-1 under the fourth truck. Hence, the PT-3 type platoon exhibits the least accumulation of strains when the effect of channelized loading and elastic recovery of pavement is considered with increase in headway distance. It is recommended to use the random truck mix in an equally distributed loading frequency, thereby increasing the elastic recovery of the pavement.

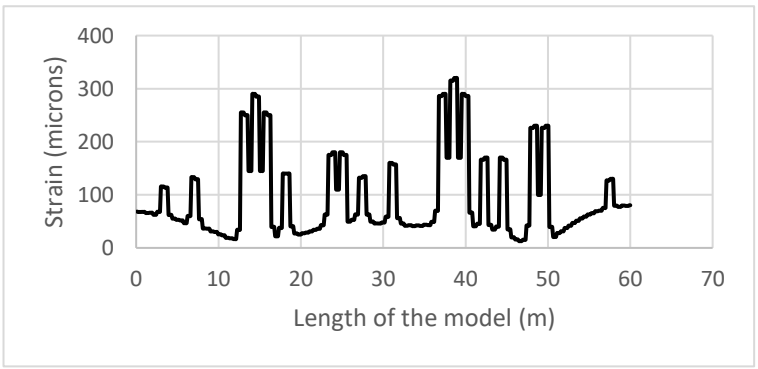

Fig. 9-22: Longitudinal strain profile for zero wander mode of PT-3 platoon.

It can be observed that the platoon starts with the class-1 trucks exhibiting a strain of 113 microns on its drive axle, and the strains gradually increase due to added tire pressure and axle load values for fifth wheel and trailer axles. In case of trailer axles, maximum load is exerted on the middle wheel of the trailer at strain value of 290 microns with remaining two axles showing the strain values of 255 microns each.

The next truck in the platoon is a class-2 truck with its drive axle coming in at 17 meters into the platoon. Due to higher axle load of this truck as compared to the class-1 truck for the steering axle, strain values of around 140 microns are shown at this point. The strain values increase as the higher load is exerted, resulting in strains 180 microns under each dual tire assembly. The third truck in this case is again a class-1 truck making is second pass with its drive axle making the pass at 26 m in the model. Since 2 m headway distance is given, a very little time is available for the pavement to fully recover, hence the accumulation of strains increase 1.2 times at the drive axle to 135 microns.

Furthermore, a gradual increase in microstrains is observed under the fifth wheel and trailer axles, with the middle trailer axle exhibiting the highest strain value of 320 microns. The last truck in this four truck platoon is a class-3 truck with a higher axle load on its front axles as compared to class-1 and class-2 type trucks, arriving at 41 m in the model. Therefore, an ideal recovery distance of 8 m is recommended between each platoon.

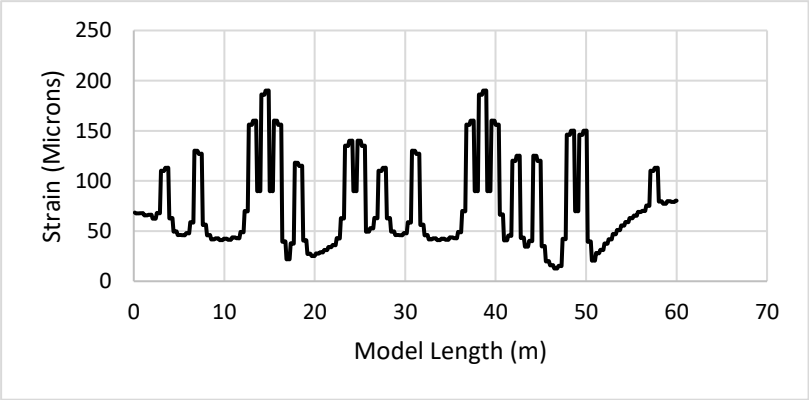

Fig. 9-23: Longitudinal Strain profile of PT-3 platoon under uniform wander mode.

In case of a uniform wander mode, with a specified dedicated path given to each truck in the platoon, the PT-3 is shown with the headway distance of 2 m in **Fig. 9-23**. Class-1 truck leads the platoon with microstrains of 113 microns under its steering axle. The strain values gradually increase to 130 microns under the drive axle of the truck, highest microstrains under Class-1 truck are observed under its middle trailer axles with peak value of 190 microns and 160 microns under remaining two trailer axles. Class-1 truck is then followed by the class-2 truck at 18 m in the model. Due to higher accumulation of axle load and small wheelbase, a higher amount of microstrains appear under the steering axle with value of 115 microns, exhibiting a 5% increase in strains compared to the steering axle of class-1 truck.

9.12 Pavement Distress Analysis

With the equivalent strain values obtained from simulations, the pavement failure modes such as rutting and fatigue cracking have been calculated based on the 15-year pavement lifetime consists of 1.4 million ESALs applications. Number of repetitions to failure for fatigue

cracking have been calculated using the Asphalt Institute model, as shown in Eqs. 9-3, 9-4 and 9-5 [127].

$$N_f = C * 0.0796 * \varepsilon_h^{-3.291} * E^{-0.854} \quad 9\text{-}3$$

$$C = 10^M \quad 9\text{-}4$$

$$M = 4.84 * \left(\frac{v_b}{v_v + v_b} - 0.69\right) \quad 9\text{-}5$$

Where N_f is the fatigue life (design repitions to failure), ε_h is the horizontal tensile strain at bottom of asphalt layer, E is the dynamic modulus of asphalt concrete in MPa, v_v is the percent air voids in total mix and v_b is the percent binder volume. The data for percent air voids and percent binder volume has been taken from Cheng et al. [57].

For evaluation of rutting, Per Ullidtz Eq. 9-6 is used.

$$N_f = \frac{1}{R} * 3.069 * 10^{10} * \left(\frac{E}{E_0}\right)^{3.26b} * {\varepsilon_v}^{-3.26} \quad 9\text{-}6$$

Where N_f is the number of load repititons to failure, R is the regional factor of value 1.75, E is the dymanic modulus of structural layer in MPa, E_0 is the adjusted reference elastic modulus of 158 MPa, b is 1.16 if $E < E_0$, otherwise value of b is 1, and ε_v is vertical compressive strain on the top of layer. Moreover, for evaluation of rut depth based on corresponding number of reptitions to failure, following Eq. 9-7 is used.

$$\mathrm{d_p} = 25\mathrm{mm} * \left[\frac{N}{10^6} * \left(\frac{\varepsilon_v}{1230\ microns}\right)^{7.14}\right]^{0.5} \quad 9\text{-}7$$

Where, $\mathrm{d_p}$ is the rut depth in mm, N is the number of reptitions to failure for rutting and ε_v is the vertical compressive strain on the top of layer. Rutting and fatigue cracking predictions based on number of loading repititons to failure and rut depth as a of functional failure of pavement are further calculated.

Decrease in fatigue life in number of years for uniform wander and zero wander modes along with various headway distance of 2 m to 5 m for the selected optimum PT-3 platoon are presented in **Fig. 9-24**, the decrease in fatigue life in number of years is only 6 months in case of a uniform wander mode at 2 m and at the same scenario for zero wander mode, decrease in fatigue life reaches to 2.4 years, thereby causing am accelerated decrease in pavement life as a result of channelized loading with very little elastic recovery time available to the pavement.

Moreover, it can be observed that a gradual decrease in reduction of fatigue life of pavement occurs as the headway distance in case of zero wander is increased to 5 m. a difference of almost 1 year of reduction in fatigue life exists between zero wander and uniform wander modes at headway distance of 5 m.

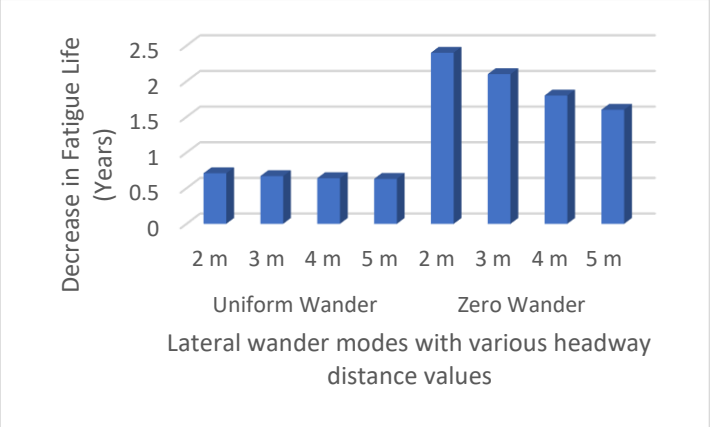

Fig. 9-24: Decrease in fatigue life under various headway distance values and lateral wander modes.

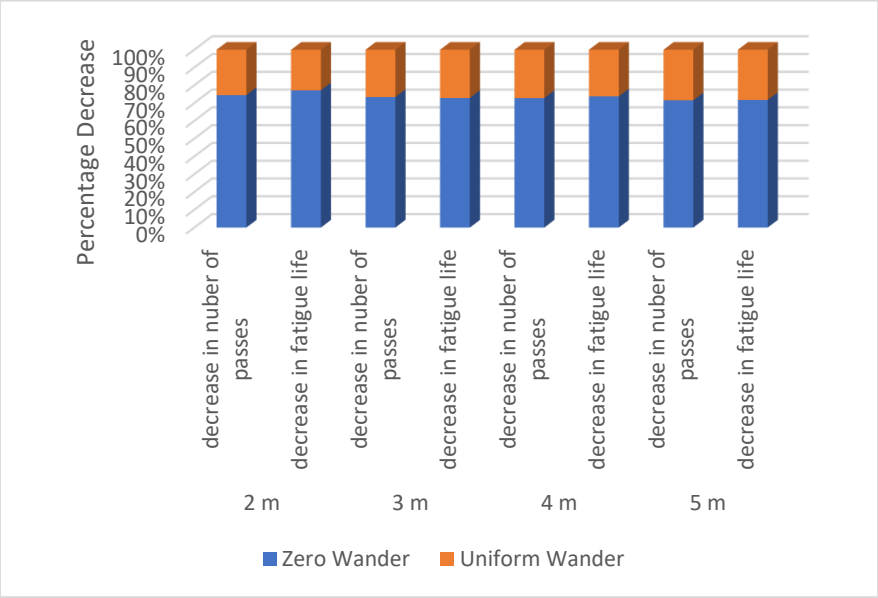

Fig. 9-25: Decrease in number of passes and fatigue life in percentage under various headway distance values and lateral wander modes.

Fig. 9-25 shows the percentage decrease in fatigue life under uniform and zero wander modes with various headway distances ranging from 2 m to 5 m. In case of a uniform wander mode., the difference in decrease in fatigue life is only 0.8 percent when owing from headway distance of 2 m to 5 m while in case of zero wander modes, the difference between headway distance of 2 m and 5 m is 20%, thereby exhibiting a significant reduction in decrease in fatigue life if headway distance is increased. Moreover, at headway distance of 5 m, in case of uniform wander mode, the decrease in fatigue life is 40% less than that of zero wander mode. Hence, when a uniform wander mode is used along with separate paths assigned to each truck in the platoon, the fatigue life of almost 1.2 years can be gained.

Fig. 9-26: Number of passes to reach rut depth value of 6 mm under various lateral wander modes and headway distance values.

Fig. 9-26 compares the number passes required to reach rut depth of 6 mm, against uniform wander and zero wander modes, along with headway distance ranging from 2 m to 5 m. The least number of passes are exhibited by the zero wander mode at only 239,875 passes, corresponding to acceleration in rutting by 2.6 years out of 15 years design life of the pavement.Thereby, the acceleration of rutting propagation is only limited to 6 months when 5 m headway distance is used. Hence, It is recommended to use the headway distance of 3 m with uniform wander mode to accommodate higher highway capacity.

Fig. 9-27: Rut depth at 1.4 million ESALs under various headway distance values and lateral wander modes.

Rut depth at the end of service life of pavement after 15 years at 1.4 million ESALs for trucks in a PT-3 platoon is shown in **Fig. 9-27**. In case of headway distance of 2 m while using a zero wander scenario, the rut depth reaches 13.3 mm which is 38% higher than the rut depth for a uniform wander mode while using 2 m headway distance. In case of a 5 m headway distance of zero wander mode, the magnitude of rut depth still stays at damaging magnitude of 12.2 mm, hence channelized loading in case of zero wander mode has a severe effect on rutting progression in the pavement. It is suggested to use the headway distance of 3 m when a uniform wander mode is used.

9.13 Conclusions and Recommendations

In this research, the effect of headway distance and grouping of trucks based on their axle configurations on platoon formation has been analyzed in combination with the use of zero

wander mode and uniform wander mode. Since, headway distance can influence the pavement elastic recovery when the loads pass through the specific point on the pavement, the resulting strain accumulations in terms of vertical compressive strains and longitudinal tensile strains have been obtained through finite element modeling.

A 3D FE model has been used to simulate the effect of three different types of platoons based on the category of trucks inside each platoon. The platoon truck size is limited to only 4 trucks and each platoon is simulated along with variable headway distances of 2 m to 5 m with 1 m increment. Furthermore, the effects of lateral wander modes beginning with the zero wander mode and uniform wander mode have been analyzed. In case of uniform wander mode, each truck in the platoon is given a predetermined path to follow along with the uniform wander mode applied in ABAQUS.

Effect of headway distance on accumulation of strains, is highly critical and headway distance of less than 3 m causes excessive damage to the pavement under repeated loading cycles in case of zero wander mode. In case of using the uniform wander mode, headway distance has a less significant effect on the development of damaging strains since there is only a slight overlap of wheel paths for all the trucks in the platoon. PT-3 platoon yields the least amount of accumulative strains among other platoons. The use of pavement failure prediction models for rutting and fatigue racking indicate that zero wander mode can cause premature failure of the pavement, however if the uniform wander mode is used in combination with the use of PT-3 platoon, pavement life can be increased.

1. Rigid body trucks also induce considerable amount of stresses in the pavement resulting in damaging strains with 75% damage as class-1 truck.
2. With the increase in the wheelbase to 2 m, the magnitude of stresses exerted by rigid body trucks in the pavement can be reduced by 30%.
3. With the use of rigid body trucks, the platoon length can however be optimized to allow for larger headway distance of upto 5 m, resulting in more recovery time for the pavement.
4. The use of PT-1 drastically increase the strains by 60% due to very minimal relaxation time and excessive repetitions of same loads type.
5. Spacing between truck platoons have a minimal effect on pavement damage when the spacing is 10 m or more for traffic speed of 90 km/h.
6. Interplatoon distance in case of a uniform wander mode has no significant impact on pavement elastic recovery since a minute section of pavement is loaded repeatedly by each truck in the platoon.
7. Accumulated microstrains in case of a uniform wander mode decrease by 45% under each axle of the following truck when compared against zero wander mode.
8. Interplatoon distance of 5 m is suggested while using the uniform wander mode. in this research , selection of random platoon type pt-3 is suitable for the use of uniform wander mode, due to less accumulation of strains and variable loading frequencies due to different axle configurations, it is recommended to use a random platoon PT-3 mixed with equally distributed trucks based on their axle orientations.
9. A class 1 truck has an advantage over the other types due to its longer wheelbase and higher number of axles, regardless of the highest maximum gross weight of 40 T.

10. The use of wide base tire for a drive axle of both class-2 and class-3 trucks is recommended since it can reduce the accumulation of permanent strains under drive axles by 35%.
11. With the use of pt-2 platoon, microstrains increase by 24 microns at headway distance of 2 m between the first two trucks in the platoon and micro strains increase by 17 microns in case of PT-2 platoon with heady distance of 5 m.
12. It is suggested to use the PT-3 type platoon with headway distance of 5 m while using a uniform wander mode.
13. Fatigue life decreases by 40% in case of using a zero wander mode at headway distance of 5 m when compared to uniform wander mode.
14. Zero wander mode, decrease the pavement life by 1.2 years.
15. In case of zero wander mode, the fatigue life increases by 13% when moving from headway distance of 2 m to 5 m.
16. Uniform wander mode delays the rutting progression by 2.6 years when compared against zero wander mode.
17. At the end of service life of the pavement, the rut depth in case of zero wander mode is 38% higher than that of uniform wander mode at headway distance of 2 m.

10 Lane width optimization and life cycle cost analysis of pavement in regards to autonomous trucks

Lateral wander of autonomous truck can be further improved by optimizing the uniform wander. Increase in available lane width for the autonomous trucks can increase the performance efficiency of this mode. This research is based on finding the optimum, combination of lane width increment and asphalt layer thickness reduction among different scenarios. Furtemroe, initial construction sots and costs for all major and minor maintenance interventions are analyzed for uniform wander and zero wander modes. Therefore, In this research with assumed maximum lane width of 4.35 m, difference combination of lane width and asphalt layer thickness scenarios have been analyzed using finite element modelling in ABAQUS. Considering the base pavement width of 3.75 m, increment for each scenario is 15 cm and reduction in asphalt layer thickness is at 2 cm. Performance efficiency of each scenario is conducted while considering the initial construction costs and damage assessment for each scenario. Moreover, life cycle cost analysis (LCCA) is conducted for the base scenario and selected optimum scenario. Maintenance interventions are introduced for both lateral wander modes based on the damage strain data obtained from ABAQUS and relevant salvage values are determined. Further details can be found in [128].

10.1 Thesis 5

I have performed the lane width optimization and life cycle cost analysis of pavement in regards to autonomous trucks and came to the following results:

1. Increase in the truck lane width to 4.2 m from the 3.75 m 20 cm scenario with an asphalt layer thickness of 16 cm leads to savings in construction costs by 20%.
2. An increase in the truck lane width for an uniform wander mode for 4.2 m increases the pavement's fatigue lifetime by 28 %.
3. Base scenario requires the first maintenance intervention by first 5 years, however the 4.2 m scenario requires the first intervention after 8 years.

10.2 Related publications

1. M. Fahad and R. Nagy, "Effective lane width analysis for autonomous trucks," SN Appl. Sci., vol. 5, no. 9, 2023, doi: 10.1007/s42452-023-05446-0
2. M. Fahad, C. Koren and R. Nagy, "Sustainability Implications of Lateral Wander Modes for Autonomous Trucks," SN Appl. Sci., (Accepted for publication: 12 Feb 2024)

10.3 Methodology

The use of uniform lateral wander mode has been analyzed in a conventional layered asphalt pavement. Since, only the change in cross section of asphalt pavement is being analyzed, therefore, the initial construction costs only include the amount of material being used in various scenarios. Reducing the structural width of asphalt layers can have high impacts on reduced construction costs in longer pavement cross sections. Moreover, the width of lane can be increased only be a certain extent, since increasing the width of lane beyond a certain point would increase the construction costs than the base scenario. Therefore, pavement width should be increased until the initial construction costs get equal to or higher than that of base scenario. Moreover, the base scenario in case of zero wander mode is also analyzed for comparison with that of uniform wander mode. Illustration of research methodology is shown in **Fig. 10-1**.

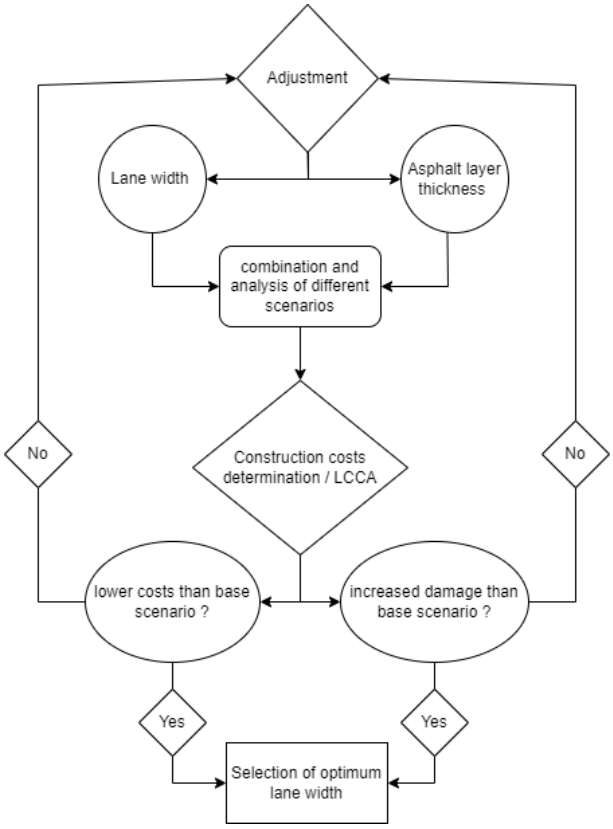

Fig. 10-1: Research methodology.

10.4 Pavement Details

The standard pavement width on a highway lane for trucks is 3.75 m as shown in **Fig. 10-2**. Increments of 15 cm are given with values of 3.9 m, 4.05 m and 4.2 m and 4.35 m. The design vehicle is an A40 European truck trailer with maximum gross weight of 40 Tonnes and a pavement section length of 50 m. Since the asphalt layer constitute the majority of construction costs in the pavement as compared to other pavement layers with a magnitude of 80% [129]–[131]. Therefore, the base scenario is selected the thickness of 20 cm and trial thickness values of 18 cm, 16 cm and 14 cm.

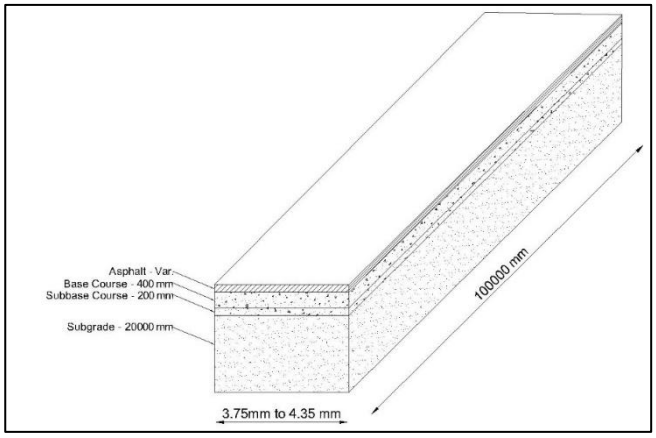

Fig. 10-2: Pavement details.

10.5 Material Model

Costs of initial pavement construction are taken from [132], [133] based on various thickness values of asphalt layer in the pavement. The software environment in terms of modelling has been considered to be average without any extreme climatic conditions for reducing the bias in pavement distress mechanisms. For the pavement design the use of elastic modulus, Poisson's ratio and layer thickness have significant effect and horizontal tensile strain on bottom of asphalt layer in microns and vertical compressive strain on top of subgrade are evaluated during the analysis part [134]. A conventional asphalt pavement is being used in this research, all associated costs related to layer construction are mentioned specifically for a standardized lane width starting with the base width of 3.75 m as shown in **Table 10-1**.

Table 10-1 Simulated scenarios.

Scenarios	**Lane width [m]**	**Asphalt layer thickness alternatives cm]**	**Percentage decrease in pavement structure thickness**
a	3,75	20	Base scenario
b	3,9	16, 18	10 %
c	4,05	14, 16, 18	15 %
d	4,2	14, 16, 18	20 %
e	4,35	14, 16, 18	25 %

Since only the thickness of asphalt layer has been changed, therefore, the $cost/m^3$ of asphalt layer that includes supply, construction and finishing costs has been used from [135] with an amount of 720 $Euros/m^3$. Various width and thickness values for asphalt layer are tested with a fixed assumed length of pavement at 100 km. All initial costs for each scenario are presented in **Table 10-2**.

Table 10-2 Initial pavement construction costs for all scenarios

Width [m]	**Thickness [cm]**	**Area** $[m^2]$	**Volume** $[m^3]$	**Amount for whole pavement structure [millions]**	**Increment from the base scenario [multiple]**
3.75	20	3	300.000	216	
3.9	18	3.042	304.200	219	+1,2
	16	2.964	296.400	213	+1,0
4.05	14	2.997	299.700	215	+1,7
	16	3.078	307.800	221	+1,9

Width [m]	**Thickness [cm]**	**Area** $[m^2]$	**Volume** $[m^3]$	**Amount for whole pavement structure [millions]**	**Increment from the base scenario [multiple]**
4.05	18	3.159	315.900	227	+2,1
4.2	14	3.108	310.800	223	+2,2
	16	3.192	319.200	229	+2,6
	18	3.276	327.600	235	+3,0
4.35	14	3.219	321.900	231	+2,4
	16	3.306	330.600	238	+2,7
	18	3.393	339.300	244	+3,2

As observed, the 3.75 m base scenario leads to the minimum amount of initial construction costs of 216 million. As the lane width is increased, the resulting costs also increases and three different asphalt layer thickness scenarios are selected with lane width of 3.9 m and above. The most costly option in terms of initial construction costs is the 4.35 m scenario, where the 18 cm asphalt thickness scenario can reach 244 millions. Although the higher lane width scenarios are costly in the beginning, the resulting maintenance costs will be reduced. The 3.75 m scenario favors initial construction costs however, resulting maintenance costs are projected to increase.

10.6 Finite Element Model Details

A typical four layered pavement structure has been modelled consisting of asphalt layer with variable thickness values for 14 cm to 20 cm with 2 cm increments. Environmental conditions are kept at average without any extreme pavement temperature conditions. Lower pavement layers consist of base and subbase course with fixed thickness values resting on the subgrade. Hence, the total model depth varies, depending on the thickness of asphalt layer. Variable lane width also exists for each model constructed, started with the width of 3.75 m going upto 4.35 m. Length of the model is kept constant at 100 m for the A40 truck to perform a complete pass under uniform wander mode. With Annual Average Daily Traffic of 11,000, the simulations are performed for the analysis period of 40 years.

Model consists of CPE8R elements with 8 node linear brick, reduced integration with hour glass control characteristics. Different trials with element sizes were conducted to check the accuracy of the model for all width and thickness scenarios, therefore the final model has 27542 elements with element size of 100 for increased accuracy and reduced computation time. Model mesh is shown in **Fig. 10-3**.

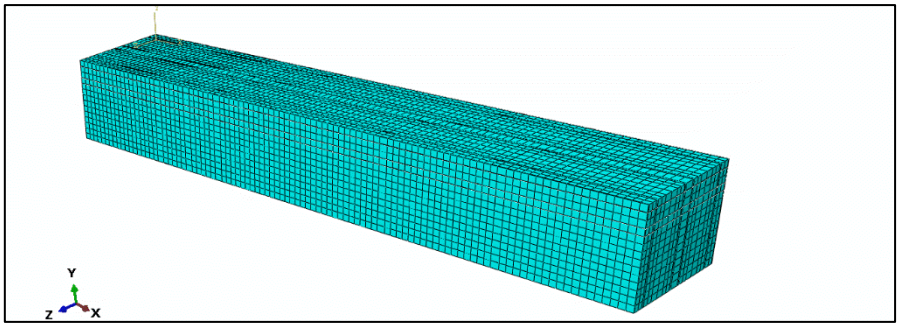

Fig. 10-3: Mesh details.

Boundary conditions and loading are kept the same for all different scenarios of variable thickness and width values. Layer to layer interaction has been kept normal and continuous, with frictionless characteristics. Nodes are free to move around vertical directions but are restricted in perpendicular horizontal directions. The bottom of the model is assumed elastic and a value of 0.03 is assigned. Boundary conditions and loading details are shown **Fig. 10-4**.

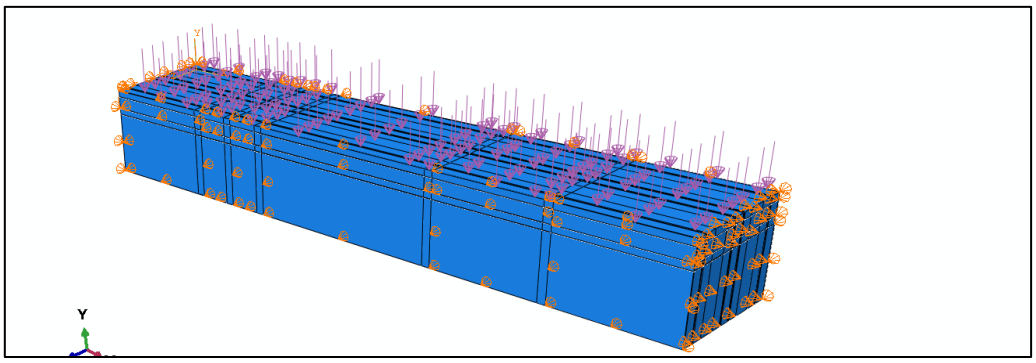

Fig. 10-4: Boundary conditions and loading.

10.7 Results and Discussion

Simulations have been conducted on ABAQUS by considering the AADT of 11,000 Trucks for a total analysis period of 40 years. An A40 truck has been simulated under a uniform wander mode where different predetermined paths for lateral wander have been selected [105]. Simulations have been run on different models created with varying thickness and width values.

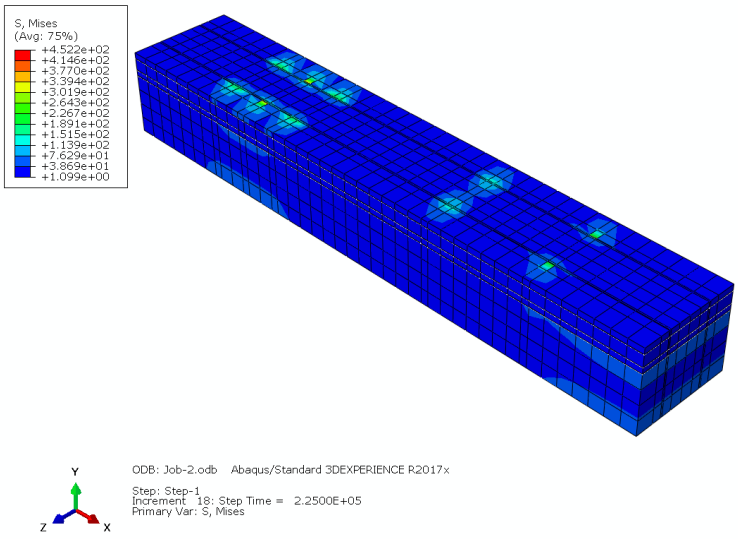

Fig. 10-5: S (mises) at base scenario

Fig. 10-5 shows the screenshot taken for the S(Mises) under the base scenario of 3.75 m width for the truck lane and 20 cm thickness assumed for the asphalt layer. Since this is a base scenario, all other suggested scenarios are compared with this scenario. S(Mises) reach a maximum accumulated magnitude of 390 microns under all passes of trucks.

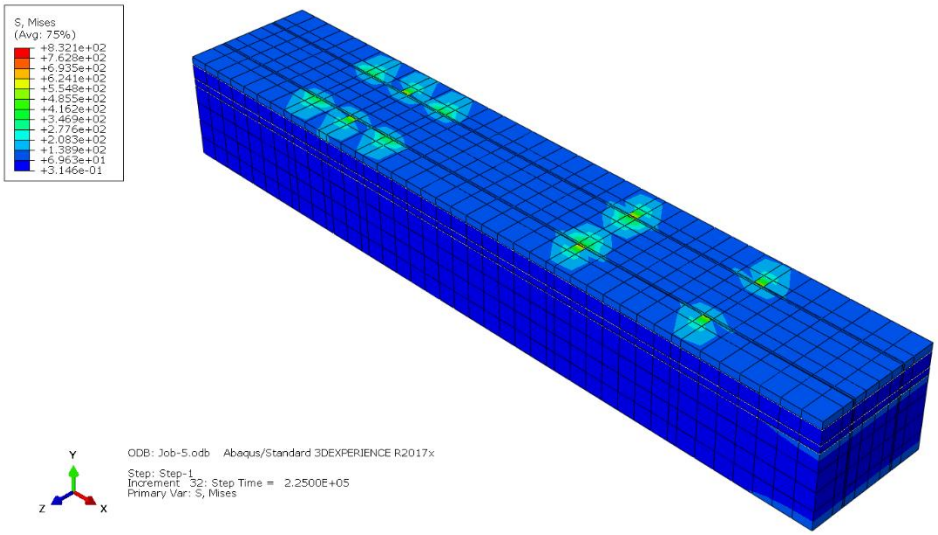

Fig. 10-6: S (Mises) at 3.9 m, 16 cm.

In the first alternative scenario as shown in **Fig. 10-6**, width of the truck lane is increased to 3.9 m and various thickness values of 16 cm and 20 cm are simulated. By decreasing the thickness in this scenario, total accumulated microstrains exponentially increase to 560 microns. The reason being the footprint width of the trailer tires of the truck is larger than the

width increment provided for adequate uniform wander. Therefore, an extra width of 15 cm from the base scenario wouldn't do any favor in terms of reducing the resulting strains.

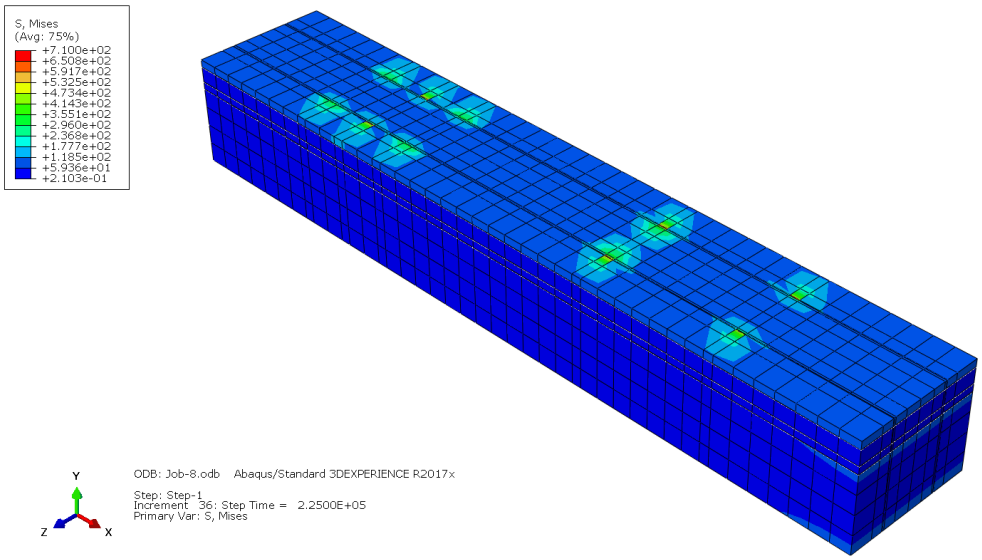

Fig. 10-7: S(Mises) at 4.05 m, 16 cm.

The second alternative scenario as shown in **Fig. 10-7** increases the lane width to 4.05 m and various reduced thickness values of 18 cm, 16 cm and 14 cm are analyzed. This scenario performs better in terms of reduced accumulated strains as compared to the first alternative scenario, however, the accumulated microstrains are still higher than the base scenario especially when less than 16 cm of width is analyzed. Total magnitude of microstrains remain at 440 microns and 415 microns when analyzed at thickness levels of 16 cm and 20 cm respectively. The 20 cm option, however, is not economically viable.

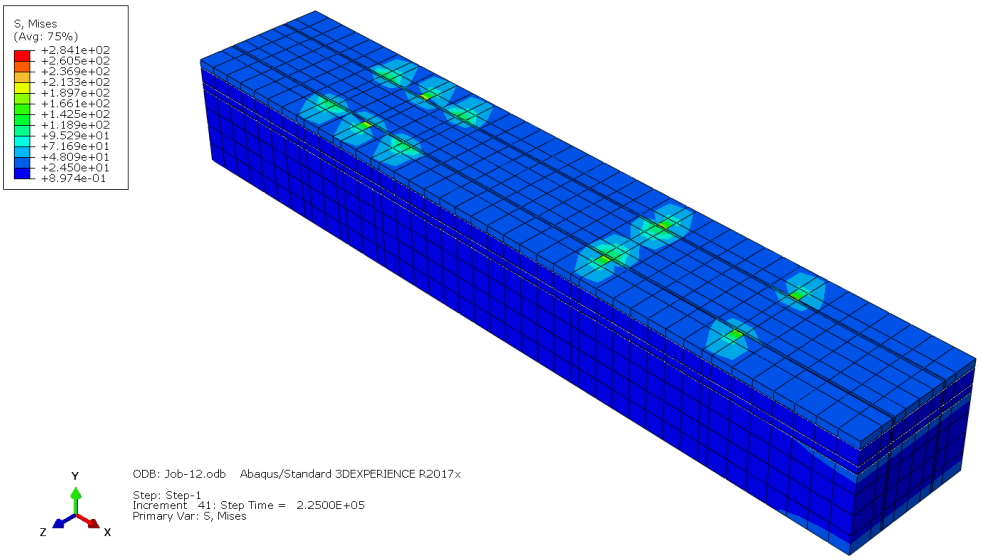

Fig. 10-8: S(Mises) at 4.20 m, 16 cm.

The third alternative scenario as shown in **Fig. 10-8** increases the lane width to 4.20 m and thickness values are tested at 18 cm, 16 cm and 14 cm. It can be observed from the figure above that considerable decrease in microstrains occur as compared to the previously mentioned scenarios. This is due to the fact that the rear trailer tires have no more overlaps on the same point of the lane, since enough lateral distance is available for the truck to perform uniform wander adequately. Resulting accumulated microstrains are at 250 microns and 315 microns at thickness values of 16 cm and 14 cm respectively. Thickness values greater than 16 cm would render this scenario uneconomical since a minute level of decrease in accumulated strains occur at higher thickness values, which also compromise the economical value of this scenario.

.

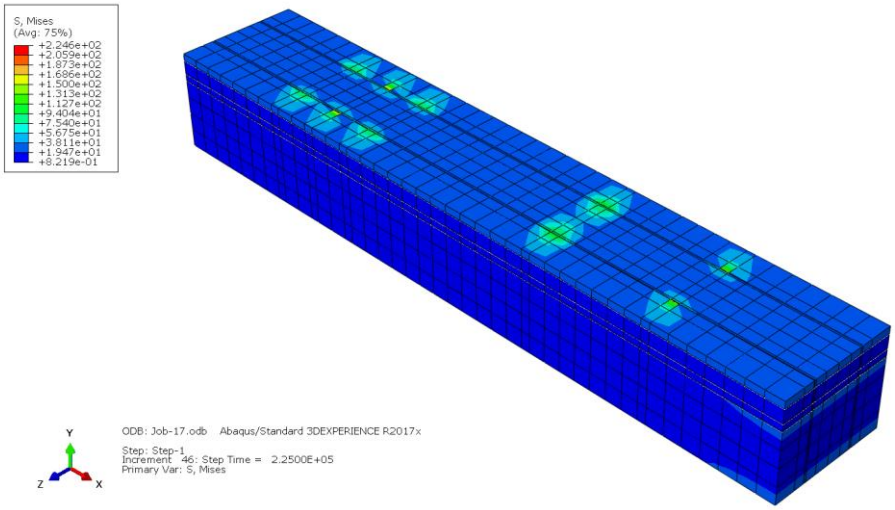

Fig. 10-9: S(Mises) at 4.35 m, 16 cm.

The Fourth scenario as shown in **Fig. 10-9** consists of pavement lane width of 4.35 m, which is tested at asphalt layer thickness levels of 16 cm and 18 cm. Increased lane width further decreases the accumulated the strains to 209 microns, however the decrease in this case is not significant as compared to the third alternative. Furthermore, an increased width beyond 4.05 m would render this scenario uneconomical even with the use of 14 cm asphalt layer thickness. In order to utilize this scenario properly, further increment of lane width of upto 30 cm is required. Therefore, the favorable scenario is to use 4.20 m of lane width with 16 cm of asphalt layer thickness.

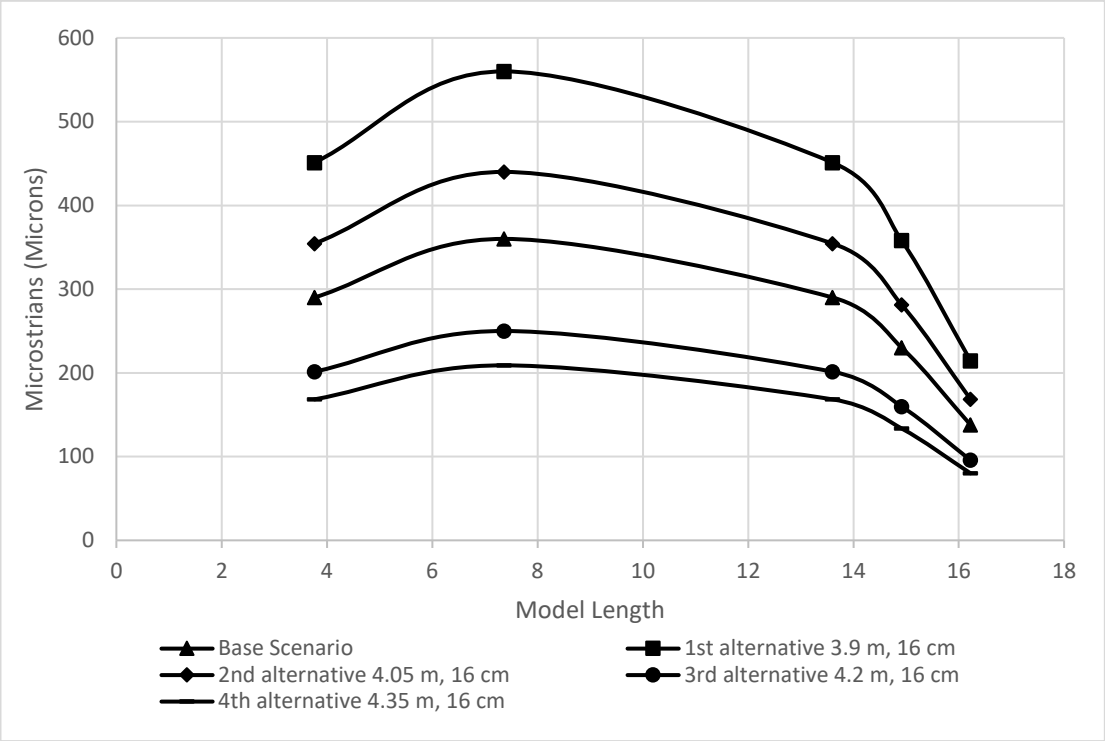

Fig. 10-10: Accumulative strain comparisons of different scenarios.

Fig. 10-10 compares the prominent scenarios with varying lane width and asphalt layer thickness values. It has been found that the use of 14 cm thickness levels for 3.9 m and 4.2 m don't make a significant difference, therefore they are not included in this comparison. Total accumulated strain values are gathered for these scenarios, with the base scenario lying along the middle of this chart at 390 microns. Furthermore, the second alternative peak strains are at 560 microns which is highest among all the scenarios. The third alternative, however, stays at 440 microns, which is better than the second scenario, however still exhibiting higher strains than the base scenario. The third scenario remains at 250 microns for 16 cm thickness value, which is the second last among all other options. Finally, fourth scenario exhibits minimum strain values among all the options, however, the efficiency analysis doesn't favor the use of 4.35 m scenario as mentioned in the next section.

Economical worth of the pavement structure at the end of its service life and initial construction costs for the pavement section of 100 km would determine the selection of best possible scenario. Therefore, it is important to calculate initial construction costs and conduct performance efficiency analysis for all the considered scenarios with varying thickness and width values. Initial construction costs have been calculated using [94], [96], [135]. Performance analysis compares the economic viability of each scenario with the accumulated microstrains throughout the analysis period. Initial construction costs would increase if the combination of lane width and asphalt thickness magnitudes exceed a certain value. Therefore, it is ideal to test all the scenarios in terms of initial construction costs and perform efficiency testing of each scenario based on accumulated pavement damage. Performance analysis is conducted by performing damage assessment under each scenario with rutting and fatigue cracking evaluation, and further details on damage assessment based on rutting and fatigue cracking can be found in [105].

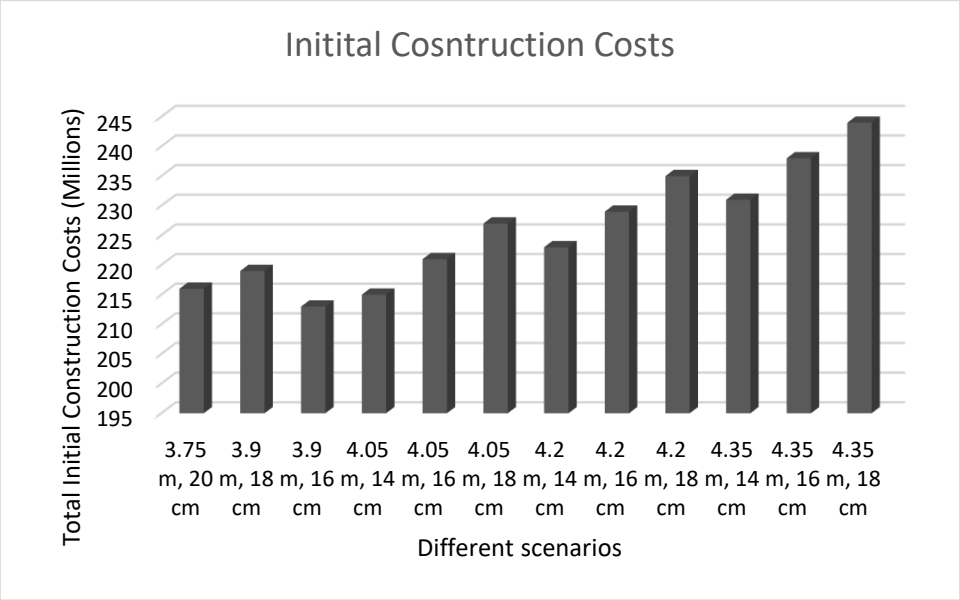

Fig. 10-11: Initial construction costs for all scenarios.

Fig. 10-11 compares the IC for different width and cross secton scenarios. An increasing trend is observed starting with 3.75 m, 20 cm scenario until the thickness reaches 18 cm for the same scenario. However, for the 3.9 m, 16 cm scenario, costs are reduced due to reduced thickness of the asphalt layer but as the width increase, the IC slightly increase proportionally. However, it can be observed that the increase in costs by lane width increment is less than the increase in cost by asphalt layer thickness increment. For the same amount of lane width, an increase in thickness with 2 cm changes the costs by 9 Millions. If the thickness is kept the same and width increases by proportions of 15 cm, the increase in costs are 5 Million. An average difference of 4 Millions exists when between lane width and asphalt layer thickness variation, so 15 cm and 2 cm respectively. The effect increases with longer highway sections.

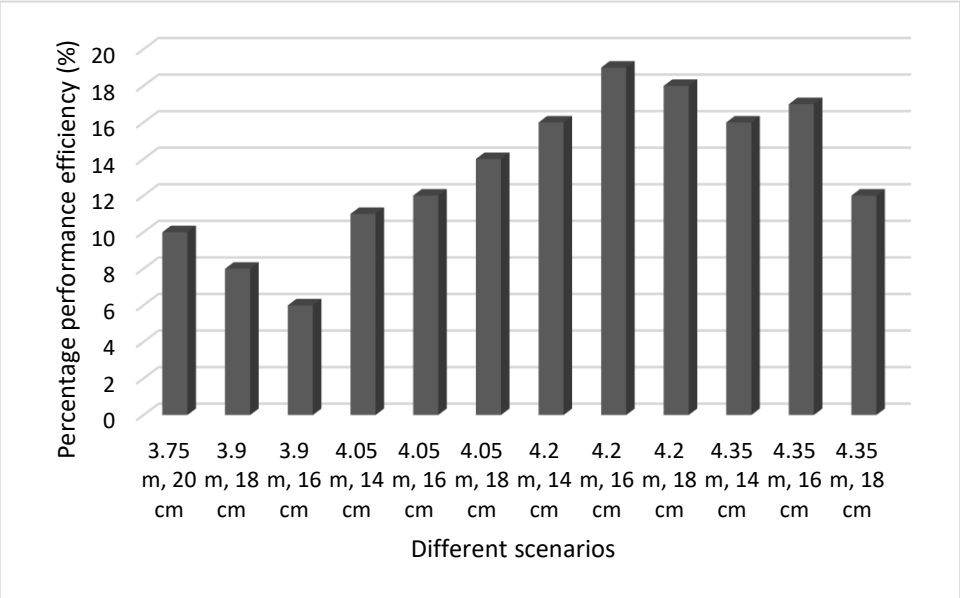

Fig. 10-12: Performance efficiency of different scenarios.

Performance efficiency for each scenario is shown in **Fig. 10-12**. A lane width with 3.9 m and 16-18 cm option, provides less performance efficiency in terms of increased lifetime and reduced costs. Since the lane width of 3.9 m is still not enough to increase the savings in lifecycle costs, therefore, this scenario is not favorable. Increase in width to 4.05 m improves the performance efficiency further. However, efficiency increase continues until the increased width of 4.2 m, since the width increase is now upto 45 cm from the base scenario, further increment in the with would render it uneconomical due to higher construction costs however, the pavement lifetime still continues to improve at 4.2 m width and 16 cm thickness, the highest performance efficiency of upto 20% is achieved. The scenario after this point favors in pavement performance but the construction costs also increase due to higher demand of materials, therefore increase in pavement performance is not in par with the rising construction costs making further increase in width uneconomical.

10.8 NPV and Salvage value

Since the traffic mix contains variety of axle groups and axle loading, it is necessary to convert them into an equivalent single axle Since the use of 4.2 m width for the truck lane exhibits the least amount of initial construction costs with respect to the most prolonged lifetime with cost effectiveness among other scenarios, showing the highest performance efficiency, therefore the intervention period will come later for this scenario than other aforementioned scenarios. Full depth reclamation is used as a pavement rehabilitation strategy. Since it has been indicated that high percentage recycled asphalt pavement (RAP) for full depth asphalt pavements provides superior performance by using accurate mix design practices thereby reducing the costs incurred during pavement's life cycle [136]. Therefore, two alternative benefits exist, either the pavement thickness for full depth reclamation can be reduced or the salvage value would increase if the full depth reclamation is not performed.

NPV discounts the future costs of the rehabilitation procedures to the present value. Since the prices used for pavement rehabilitation in the future would differ therefore, all the costs must be converted to the present state where the Net Present Value consists of initial pavement construction costs, the rehabilitation costs for full depth reclamation and salvage value after the analysis period. NPV calculation is showin in Eq 10-1.

$$NPV = Initial\ cost + \sum_{k=1}^{N} Rehab\ Cost_k \left[\frac{1}{(1+i)^{n_k}}\right] - Salvage\ Value \left[\frac{1}{(1+i)^{n_a}}\right] \quad \text{10-1}$$

Where NPV is net present value, i is discount rate, n is time period in years, n_k is number of years from initial construction and n_a is length of analysis period. Lower NPV corresponds to higher cost efficiency of rehabilitation strategies.

Salvage values indicates the residual value of the pavement after the analysis period as shown in Eq. 10-2. Salvage value is linked to the last rehabilitation conducted on the pavement, thus even after the analysis period, the pavement can still continue to perform functionally.

$$Salvage\ value = \frac{Remaining\ service\ life}{service\ life} \times CLR \quad (10\text{-}2)$$

Where CLR is the cost of last rehabilitation. Since, the maintenance performance strategy herein is only the full depth asphalt reclamation in the mid span of design life of 40 years therefore, the salvage value for the remaining life and actual service life of full depth reclamation alternative is used. The first option for increase in salvage values is shown below where using the scenario of 4.2 m lane width and using 16 cm with initial asphalt layer thickness, salvage value of the pavement is increased by 13 years.

Data used for LCCA is as follows:

- Road length. 100 Km
- Lane Width: 3.75m, 3.9m, 4.15m, 4.2m, 4.35m at different crosssections
- Traffic speed: 90 Km/h
- Analysis period: 40 Years
- Average Annual Daily Truck Traffic(AADTT): 11,000 trucks/day
- Traffic Growth rate: 0.75 %
- Discount rate: 4%

10.9 LCCA

It has been assumed that around 75% of pavement structure on its length of 100 km would require the maintenance interventions throughout its lifetime and each intervention being applied to a certain section of the highway since all the AADTT would not cover the entire 100 km of the highway in a single trip. Due to the increased performance period under the 4.2 m lane width scenario, two options are available to design maintenance and rehabilitation strategies. The first option is to remove the major component of maintenance costs for LCCA. The second option is to keep the same interventions options for the 4.2 m lane width scenario as that of the base scenario, which in turn would increase the salvage value of the pavement with increased pavement lifetime.

The first option as shown in **Table 10-3** which favours the the prolongation of pavement's service life greater than 40 years which is after the analysis period, the salvage value can be further increased as shown in Table above. Base scenario needs the first major rehabilitation intervention after 5 years, while the 4.2 m lane width scenario can stay upto 8 years. Moreover, the cost of general maintenance works is less for the 4.2 m scenario due to lower damage accumulated after first 8 years. Maintenance free period for the 4.2 m can last longer by 5 years than the base scenario. If all the maintenance and rehabilitation interventions are followed for 4.2 m, the same way as for the base scenario, the pavement can function after the analysis period of 40 years and functional life can reach upto 53 years. In this case, the salvage value for the 4.2 m scenario is enhanced by 14.8 M after 53 years, compared to 15.6 M for the base scenario after 40 years. Therefore, 4.2 m scenario makes a fundamental difference in life cycle

cost reduction of pavement by increasing the salvage value with a prolonged lifetime after analysis period.

Table 10-3 Comparison of alternative scenario and base scenario based on increase in performance period

Life Cycle of the Pavement	**Base scenario [Performance Period Timeline] [Years]**	**Value/Cost [Millions]**	**Alternative Scenario (4.2 m, 16 cm) [Performance Period Timeline] [Years]**	**Value/Cost [Millions]**
Initial Construction	0	216	0	229
Maintenance free period	1-5		1-8	
General maintenance	6-11	1.2	9-16	0.9
Removal of Wearing Course	11	6.5	16	6.5
Maintenance free period	11-13		17-25	
General maintenance	14-21	1.2	26-32	0.9
Removal of bituminous layers	21	8.3	32	8.3
Maintenance free period	21-23		32-37	
General maintenance	24-31	1.2	37-43	0.9
Full depth reclamation and using cement treated base course	31	24.6	43	24.6
Maintenance free period	31-33		44-49	
General maintenance	34-40	1.2	50-53	0.9
Salvage value		15.6 M	14.8 M	

In the second option as shown in **Table 10-4**, the reduction in rehabilitation interventions is performed by removing the first rehabilitation intervention, that includes the removal and paving of wearing course layer. Hence, all the general maintenance related activities can be removed along the first 16 to 25 years in the pavement lifetime while yielding the same salvage value as the base scenario with reduced maintenance and rehabilitation costs. Since the majority of costs are related to the rehabilitation interventions where milling and replacement is conducted, therefore such costs can be reduced and will have a high impact on the present value of pavement structure.

The rehabilitation maintenance program consists of general maintenance costing 1.2 million Euros followed by the first rehabilitation of removal, of wearing course. In the first maintenance free period, the base scenario maintenance free period last for 5 years, however for the 4.2 m option, maintenance free period lasts for 8 years. Moreover, the cost of general maintenance, which includes crack and chip sealing, varies for each scenario.

In case of a base scenario the cost is 1.2 million Euros while in case of 4.2 m, the cost stands at 0.9 million Euros. Other major rehabilitation phases that include removal of wearing course, removal of asphalt layers and full depth reclamation costs the same for both scenarios however, in case of 4.2 m option the major rehabilitation intervention that includes removal of asphalt layers can be removed. Since the pavement is performing better structurally along the lifetime of 18-28 years. In case of base scenario, the pavement would require an intervention in the 21st year while in case of 4.2 m scenario, the pavement needs the second major intervention only by 29th year. By removing a major portion of rehabilitation intervention, life cycle costs can be saved.

Table 10-4 Comparison of base scenario and alternative scenario based on increase in salvage value

Life Cycle of the Pavement	**Base scenario [Performance Period Timeline] [Years]**	**Value/Cost [Millions]**	**Alternative Scenario (4.2 m, 16 cm) [Performance Period Timeline] [Years]**	**Value/Cost [Millions]**	**Life Cycle of the Pavement**
Initial Construction	0	216	Initial Construction	0	229
Maintenance free period	1-5		Maintenance free period	1-8	
General maintenance	6-11	1.2	General maintenance	9-16	0.9
Removal of Wearing Course	11	6.5	Removal of asphalt layers	17	6.5

Life Cycle of the Pavement	Base scenario [Performance Period Timeline] [Years]	Value/Cost [Millions]	Alternative Scenario (4.2 m, 16 cm) [Performance Period Timeline] [Years]	Value/Cost [Millions]	Life Cycle of the Pavement
Maintenance free period	11-13		Maintenance free period	18-24	
General maintenance	14-21	1.2	General maintenance	25-28	0.9
Removal of bituminous layers	21	8.3	Full depth reclamation and using cement treated base course	29	24.6
Maintenance free period	21-23		Maintenance free period	30-36	
General maintenance	24-31	1.2	General maintenance	37-40	0.9
Full depth reclamation and using cement treated base course	31	24.6			
Maintenance free period	31-33				
General maintenance	34-40	1.2			
Salvage value		15.6 M	Salvage value		58.3 M

10.10 Conclusions

Since the use of autonomous trucks require an appropriate form of uniform wander mode, additional lane width available to perform lateral wander can further improve the performance of the pavement. Autonomous trucks can be programmed to later their traversing path based on the safe lateral distance available within the lane. Due to strict right of way requirements and budget constraints, only a limited amount of increment in lateral width is allowed. Moreover, due to increase in pavement lane width, the thickness of asphalt layer can be further reduced as bigger lane width would lead to fewer instances of channelized loading under uniform wander mode by autonomous trucks. Therefore, an ideal scenario for increase in

pavement lane width and decrease in pavement layer thickness is established to allow for further reduction in initial construction costs and life cycle costs.

It has been assumed in this research that maximum allowable width for the truck lane is limited at 4.35 m. It has been found that the initial 16 cm increment in width from the base sbeario width of 3.75 m doesn't do significant change in decreased pavement damage, since each trailer tire needs a width grater than 30 cm to avoid overlapping along the same longitudinal path. Since, the uniform wander will work in conjunction with optimum platoon, therefore, it is ideal to avoid any chance of overlapping by the passing trucks. Moreover, further decrease in asphalt layer thickness leads to sudden premature permanent deformation and cracking, resulting in higher life cycle costs. Therefore, by performing simulations with varying asphalt thickness and lane width scenarios, an optimum combination is created with lane width of 4.2 m and asphalt layer thickness of 16 cm for this aforementioned pavement section. Moreover, two different LCCA scenarios have been proposed where either the pavement leaves a salvage value of 58.3 millions USD at the end of analysis period of 40 years or pavement continues to function for the next 13 years with an optimum performance efficiency.Followng are the finidgs of this research:

1. Selection of the 4.2 m scenario requires higher initial costs than the base scenario of 3.75 m width, but the pavement structure performs better with lower maintenance costs
2. Initial construction costs are increased by using the 4.2 m scenario by 13 Million euros.
3. LCCA analysis shows high performance of 4.2 m scenario requiring less rehabilitation interventions, saving upto 26 million Euros.
4. General maintenance works require less budget since the pavement performs considerably better under the 4.2 m scenario, thus reducing the general maintenance costs by 300,000 Euros for each intervention.
5. Base scenario requires the first maintenance intervention by first 5 years, however the e 4.2 m scenario requires the first intervention after8 years.
6. Length of maintenance free period for 4.2 m scenario is higher by 5 years when compared to the base scenario.
7. Use of 4.2 m scenario leads to increased salvage value and prolonged lifetime of the pavement structure, even after the analysis period of 40 years.
8. After the 40 years analysis period, salvage value of 58.3 million Euros exists, making a difference of 45 million Euros in increased salvage value.
9. Full depth reclamation helps in reduced overall pavement's life cycle costs for all pavement width scenarios.
10. Optimum combination of asphalt layer thickness and lane width affects the economic worth and longevity of the pavement structure.

11. A lane width of 4.2 m, along with 16 cm of asphalt layer thickness, can increase the performance efficiency of the pavement structure in terms of its economic worth and lifetime by 20%.
12. Pavement thickness variation of upto 8 cm doesn't make any considerable change in the costs of pavement removal and full depth reclamation, since removal and replacement can be accomplished in a single stage.

11 Utilization, General Conclusions, Limitations and Summary

This research will be highly beneficial for autonomous vehicle manufacturers, government agencies and transport authorities in order to develop an accurate framework based on the findings of this research. The developed framework will be beneficial for its integration with the current transport infrastructure system and it would enable some technical modifications in parameters in this existing framework to integrate the foregoing of autonomous trucks smoothly without obstructions. The framework includes the development protocols for the geometric design of the highways especially catered for autonomous trucks.

The presentation of optimum lane width for the autonomous truck traffic would bring changes in geometric alignment and right of way practice protocols in highway engineering. Essentially the optimum lane width would prolong the service life of the pavement by utilizing the concept of uniform lateral wander. The development of optimum platoon pattern would enable the highway management agencies to enforce and enable the occurrences of best possible truck load mixes in terms of axles and the number of axles in a given platoon mix. The criteria in the findings of this research can be followed and it can be practiced by transport management agencies in the EU. The summary of utilization of the findings of this research is shown in the table below:

Table 11-1 Research Utilization Summary

Findings/Methodologies	Details	Utilized By	Benefits of Outcome	Applicability for further research
Impact of autonomous trucks on pavement performance	Assessment of three lateral wandering modes and their impacts on pavement response	Transport authorities, vehicles manufacturers, researchers and Students	Development of framework for integration of autonomous trucks in current transport infrastructure	Yes
Optimum Platoon Pattern	Development of optimum platoon pattern consisting of a dedicated number of trucks and maximum cumulative axle loading pattern	Highway agencies, transport authorities, vehicles manufacturers, researchers and Students	Increased pavement life and reduction in pavement rehabilitation costs	Partial
Optimum Lane Width	Development of optimum lane width for the autonomous traffic lane by decreasing the design thickness and increment in lane width in uniform lateral wander mode	Highway agencies, vehicles manufacturers, researchers and Students	Aiding the development of framework for revised criteria in geometric design of pavements for autonomous trucks, decreased construction costs,	Yes

Integration of autonomous trucks is bringing fundamental changes in the current infrastructure system. In terms of their impacts on pavement structure, the use of lateral wander options becomes significant. Since it has been observed that in order to provide added safety, fuel efficiency and lane utilization, autonomous trucks will be programmed to follow a zero lateral wander mode. However, employment of zero wander mode leads to premature damage to the pavement structure in terms of rutting and fatigue cracking. The use of uniform wander mode

is the solution to this issue; therefore, the autonomous trucks can utilize the uniform wander mode to distribute themselves uniformly along the lateral path while travelling in the lane, thereby increasing the pavement's life in terms of rutting and fatigue cracking when compared to human driven trucks.

Moreover, the two lateral wander modes, namely a zero wander mode and uniform wander mode have been analyzed by incorporating significant parameters consisting of lane width variations, asphalt layer thickness variations, platoon size, headway distance, speed, tire footprint variations, tire pressure variations, axle configurations and various maintenance variations during life cycle analysis.

Detailed platoon analysis along with the platoon size, number of platoon and lateral wander modes has been performed using finite element modelling. Significant impacts in terms of induced strains and pavements relief time are observed. Magnitude of induced strains and amount of relief time available after the passage of each load generate significant impacts on decisions related to platoon design where headway distance, axle configurations and loading types are combined in an appropriate form to minimize the occurrence of rutting and fatigue induced damage.

Tire footprint details have been further analyzed to utilize their usage in modelling of loading on the pavement structure. Methods involving the calculation of tire contact length patch and corresponding load based on the tire configuration have been introduced. Therefore, this method can be adopted for any truck tire type configuration to analyze its impact on the pavement. A comparative study on two different tire types combined with the use of two different lateral wander modes provides significant in depth information in terms of tire pressure and tire type loading impact on the pavement.

Furthermore, novel approach in terms of finite element modelling has been introduced in terms of material behavior analysis using various material models, adjustment of boundary and loading conditions for the models, introduction of tire pressure and tire footprint input analysis for the models, analysis of horizontal and vertical strain as a result of loading and projection of modelling data on longitudinal and transverse profiles of the pavement.

Life cycle cost analysis has been performed to analyze the economical worthiness of both lateral wander modes along with variable lane width and asphalt layer thickness scenarios. Optimized maintenance interventions have been introduced for maximum utilization of the uniform wander mode for increased salvage value and service life of the pavement. With the proper budget management of a highway project, considerable savings during initial construction can be allocated to maintenance interventions later during the service life of the pavement with the use of uniform wander mode.

In terms of limitations of this research, the effect of climate and temperature variations have not been included in order to keep the scope of this research strictly to effects of aforementioned parameters including tire types, lateral wander modes, speed variations, different axle configurations, and different platoon variations on rutting and fatigue cracking. Furthermore, only average temperature and environmental conditions have been used without extremes to reduce the bias in rutting and fatigue cracking determination. Validation of simulations has been performed with simulations conducted by parallel research.

Future research deals with the use of machine learning algorithms for prediction of rutting and fatigue cracking based on variations in tire types, axle configurations, lateral wander modes, platoon orientations and lane width scenarios. Furthermore, the future research consists of using different mixture types for pavement cross-sections and evaluation of pavement response including variations in platoon speeds in terms of the extent of rutting and fatigue cracking based on these parameters.

Effects of speed, tire footprint, axle configurations, headway distance, platoon orientation, maintenance interventions and different lateral wander modes considered as fundamental findings of this research are mentioned below.

1. Rut depth increases by a factor of 2 from wide tire to dual tire, the factor slightly increases as the speed gets down to 50 km/h.
2. Effects of uniform wander and zero wander are highly significant when dual tire assembly is used;
3. In case of super single tire, the rut depth decreases by an average of 2 mm if uniform wander is used instead of zero wander mode.
4. Dual tires at zero wander only require 3.23 million passes to reach a rut depth of 6 mm, on the other hand, super single tire require 30 million passes to reach a rut depth of 6 mm using zero wander mode.
5. Increase in micro-strains is more prominent at lower speeds, since, micro-strains decrease by a factor of 0.5 while moving from 5 km/h to 50 km/h, furthermore, micro-strains increase by factor of 0.3 while going from 50 km/h to 80 km/h;
6. At super slow speeds, dual wheel moving at zero wander mode, decrease in fatigue life of the pavement is 3.5 years which is 1.45 times more than the dual wheel moving at uniform wander and 3.4 times more than wide tire moving at uniform wander mode;
7. When dual wheel uniform wander and wide tire zero wander is compared, the increase in fatigue damage for a wide tire zero wander is just 1.2 times more than that of dual wheel at uniform wander mode, hence even if high concentration of tire pressure is exerted, the uniform wander saves the pavement from increased fatigue damage.
8. Fatigue life decreases by 14 months in case of a zero wander mode.
9. Overlap of wheel paths occurs in case of uniform wander mode, with the overlapping width of 1.5 m for an A40 type truck.
10. Acceleration for rut development in case of a zero wander is almost 2 times than that of a uniform wander mode.
11. With the increase in the wheelbase to 2 m, the magnitude of stresses exerted by rigid body trucks in the pavement can be reduced by 30%.
12. With the use of rigid body trucks, the platoon length can however be optimized to allow for larger headway distance of upto 5 m, resulting in more recovery time for the pavement.
13. The use of PT-1 drastically increase the strains by 60% due to very minimal relaxation time and excessive repetitions of same loads type.

14. In case of the use of PT-1, it is recommended to increase the headway distance of 2 m to 5 m, that results in increase fatigue life and rutting performance of pavement to up to 1.6 years.
15. Spacing between truck platoons have a minimal effect on pavement damage when the spacing is 10 m or more for traffic speed of 90 km/h.
16. Interplatoon distance in case of a uniform wander mode has no significant impact on pavement elastic recovery since a minute section of pavement is loaded repeatedly buy each truck in the platoon.
17. Accumulated microstrains in case of a uniform wander mode decrease by 45% under each axle of the following truck when compared against zero wander mode.
18. A class 1 truck has an advantage over the other types due to its longer wheelbase and higher number of axles, regardless of the highest maximum gross weight of 40 T.
19. The use of wide base tire for a drive axle of both class-2 and class-3 trucks is recommended since it can reduce the accumulation of permanent strains under drive axles by 35%.
20. Fatigue life decreases by 40% in case of using a zero wander mode at headway distance of 5 m when compared to uniform wander mode.
21. Acceleration of propagation of rutting reaches 2.6 years to reach rut depth of 6 mm when the zero wander mode is used.
22. Due to excessive channelized loading, a higher headway distance of grater than 5 m is required for the uniform wander mode.
23. Selection of the 4.2 m scenario requires higher initial costs than the base scenario of 3.75 m width, but the pavement structure performs better with lower maintenance costs
24. Initial construction costs are increased by using the 4.2 m scenario by 13 Million euros.
25. LCCA analysis shows high performance of 4.2 m scenario requiring less rehabilitation interventions, saving upto 26 million Euros.
26. General maintenance works require less budget since the pavement performs considerably better under the 4.2 m scenario, thus reducing the general maintenance costs by 300,000 Euros for each intervention.
27. After the 40 years analysis period, salvage value of 58.3 million Euros exists, making a difference of 45 million Euros in increased salvage value.
28. A lane width of 4.2 m, along with 16 cm of asphalt layer thickness, can increase the performance efficiency of the pavement structure in terms of its economic worth and lifetime by 20%.

12 Publications list

M. Fahad, R. Nagy, and P. Fuleki, “Creep model to determine rut development by autonomous truck axles on pavement,” Pollack Period.,pp. 1–6, 2021, doi: 10.1556/606.2021.00328.

R. Nagy, and M. Fahad, “A comparison between rut depth values obtained from 2D and 3D Finite Element modelling”, In: IEEE International Conference on Cognitive Infocommunications (eds.) 12th IEEE International Conference on Cognitive Infocommunications (CogInfoCom 2021) : Proceedings Online kiadás, International : IEEE (2021) 1,098 pp.735-746. , 12 p.

A. Borsos, C. Koren, E. Mako, D. Miletics, R. Nagy, M. Fahad, and Z. Magyari, “Road environment for autonomous vehicles In: Horváth, Balázs; Horváth, Gábor (eds.) XI. Nemzetközi Közlekedéstudományi Konferencia: „Közlekedés a Járvány után: folytatás vagy újrakezdés” Győr, Hungary :Szechenyi Istvan University (2021) 567 p. pp. 140-147.

M. Fahad and R. Nagy, “Fatigue damage analysis of pavements under autonomous truck tire passes,” Pollack Period., vol. 17, no. 3, pp. 59–64, 2022, doi: 10.1556/606.2022.00588.

M. Fahad and R. Nagy, “A burkolatok fáradásos károsodásának elemzése autonóm tehergépkocsik esetén” AZ ASZFALT: A MAGYAR ASZFALTIPARI EGYESÜLÉS (HAPA) HIVATALOS SZAKMAI LAPJA 29 : 2 pp. 53-57. , 5 p. (2022).

R. Nagy, and M. Fahad, “Autonóm járművek sávtartásának hatása a pályaszerkezet méretezésre – irodalomkutatás”: Effect of lane keeping of autonomous vehicles on road pavement design – literature review In: XXIV. Nemzetközi Építéstudományi Online Konferencia – ÉPKO Hungarian Technical Scientific Society from Transilvania (2020) pp. 117-121. , 5 p.

M. Fahad and R. Nagy, “Influence of class A40 autonomous truck on rutting and fatigue cracking,” Pollack Period., pp. 3–8, 2023, doi: 10.1556/606.2023.00760.

M. Fahad and R. Nagy, “Truck platoon analysis for autonomous trucks,” SN Appl. Sci., vol. 5, no. 5, 2023, doi: 10.1007/s42452-023-05352-5

M. Fahad and R. Nagy, “Effective lane width analysis for autonomous trucks,” SN Appl. Sci., vol. 5, no. 9, 2023, doi: 10.1007/s42452-023-05446-0

M. Fahad, C. Koren and R. Nagy, “Sustainability Implications of Lateral Wander Modes for Autonomous Trucks,” SN Appl. Sci., (Accepted for publication: 12 Feb 2024)

References

[1] B. S. Jahromi, T. Tulabandhula, and S. Cetin, “Real-time hybrid multi-sensor fusion framework for perception in autonomous vehicles,” *Sensors (Switzerland)*, vol. 19, no. 20, pp. 1–23, 2019, doi: 10.3390/s19204357.

[2] S. A. El-Hamrawy and A. I. Abu El-Maaty, “Effect of Excess Axle Loads and High Tire Pressures on Flexible Pavement Performance,” *ERJ. Eng. Res. J.*, vol. 35, no. 4, pp. 383–389, 2012, doi: 10.21608/erjm.2012.67197.

[3] D. B. Casey, G. D. Airey, and J. R. Grenfell, “A Comparison of Uniform and 3-D Tyre Contact Pressure Representations Using a Finite Element Method,” *Transp. Res. Procedia*, vol. 14, pp. 2402–2410, 2016, doi: 10.1016/j.trpro.2016.05.280.

[4] H. Noorvand, G. Karnati, and B. S. Underwood, “Autonomous vehicles: Assessment of the implications of truck positioning on flexible pavement performance and design,” *Transp. Res. Rec.*, vol. 2640, no. April 2018, pp. 21–28, 2017, doi: 10.3141/2640-03.

[5] M. Alinizzi, J. Y. Qiao, A. Kandil, H. Cai, and S. Labi, *Integration and Evaluation of Automated Pavement Distress Data in INDOT’s Pavement Management System*. 2017. doi: 10.5703/1288284316507.

[6] Y. Chen, H. Zhang, X. Q. Zhu, and D. W. Liu, “The Response of Pavement to The Multi-Axle Vehicle Dynamic Load,” *Proc. 2015 Int. Conf. Electr. Autom. Mech. Eng.*, vol. 13, no. Eame, pp. 238–241, 2015, doi: 10.2991/eame-15.2015.65.

[7] T. Jones and R. Bishop, “The Future of Autonomous Vehicles: Global Insights gained from Multiple Expert Discussions,” *Futur. Agenda*, vol. 2020, no. May, pp. 1–164, 2020, [Online]. Available: www.futureagenda.org

[8] J. Aurell, T. Wadman, and V. Trucks, “Vehicle combinations based on the modular concept,” *Nord. Va gteknisk Fo rbundet (Nordic Road Assoc.*, vol. 1, no. 1, p. 2007, 2007.

[9] D. T. Group, “Daimler Truck ’ s independent subsidiary Torc Robotics collaborates with leading logistics companies on autonomous trucking,” 2022.

[10] J. M. Lutin, A. L. Kornhauser, and E. Lerner-Lam, “The revolutionary development of self-driving vehicles and implications for the transportation engineering profession,” *ITE J. (Institute Transp. Eng.*, vol. 83, no. 7, pp. 28–32, 2013.

[11] M. H. R. Consulting, “Automated Vehicle Symposium 2016,” 2016.

[12] NHTSA, “Connected Vehicles, About V2V,” 2020.

[13] R. Bishop *et al.*, “White Paper: Automated Driving & Platooning - Issues and Opportunities,” *ATA Technol. Maint. Counc. Futur. Truck Program, Autom. Driv. Platooning Task Force*, no. 2015, pp. 1–48, 2015, [Online]. Available: http://orfe.princeton.edu/~alaink/SmartDrivingCars/ITFVHA15/ITFVHA15_USA_FutureTruck_ADP_TF_WhitePaper_Draft_Final_TF_Approved_Sept_2015.pdf

[14] S. M. Kouchak and A. Gaffar, “Determinism in future cars: Why autonomous trucks are easier to design,” *2017 IEEE SmartWorld Ubiquitous Intell. Comput. Adv. Trust. Comput. Scalable Comput. Commun. Cloud Big Data Comput. Internet People Smart City Innov. SmartWorld/SCALCOM/UIC/ATC/CBDCom/IOP/SCI 2017* - , no. February, pp. 1–6, 2018, doi: 10.1109/UIC-ATC.2017.8397598.

[15] “Autonomous trucks disrupt US logistics | McKinsey.” https://www.mckinsey.com/industries/travel-logistics-and-infrastructure/our-insights/distraction-or-disruption-autonomous-trucks-gain-ground-in-us-logistics (accessed Apr. 11, 2022).

[16] J. Anderson, N. Kalra, K. Stanley, P. Sorensen, C. Samaras, and O. Oluwatola, *Autonomous Vehicle Technology: A Guide for Policymakers*. 2016. doi: 10.7249/rr443-2.

[17] D. Hang, D. McFadden, K. Train, and K. Wise, “Is vehicle depreciation a component of marginal travel cost?: A literature review and empirical analysis,” *J. Transp. Econ. Policy*, vol. 50, no. 2, pp. 132–150, 2016.

[18] D. J. Fagnant and K. Kockelman, “Preparing a nation for autonomous vehicles: Opportunities, barriers and policy recommendations,” *Transp. Res. Part A Policy Pract.*, vol. 77, pp. 167–181, 2015, doi: 10.1016/j.tra.2015.04.003.

[19] L. T., “Autonomous Vehicle Implementation Predictions: Implications for Transport Planning,” *Transp. Res. Board Annu. Meet.*, vol. 42, no. 5 June 2020, pp. 1–39, 2020, [Online]. Available: https://www.vtpi.org/avip.pdf

[20] D. Milakis, B. Van Arem, and B. Van Wee, “Policy and society related implications of automated driving: A review of literature and directions for future research,” *J. Intell. Transp. Syst. Technol. Planning, Oper.*, vol. 21, no. 4, pp. 324–348, 2017, doi: 10.1080/15472450.2017.1291351.

[21] W. Gruel and J. M. Stanford, “Assessing the Long-term Effects of Autonomous Vehicles: A Speculative Approach,” *Transp. Res. Procedia*, vol. 13, pp. 18–29, 2016, doi: 10.1016/j.trpro.2016.05.003.

[22] Z. Wadud, “Fully automated vehicles: A cost of ownership analysis to inform early adoption,” *Transp. Res. Part A Policy Pract.*, vol. 101, pp. 163–176, 2017, doi: 10.1016/j.tra.2017.05.005.

[23] F. Report, “Emerging Freight Truck Technologies : Effects on Relative Freight Costs,” no. May, 2018.

[24] Y. Huang and K. M. Kockelman, “What will autonomous trucking do to U.S. trade flows? Application of the random-utility-based multi-regional input–output model,” *Transportation (Amst).*, vol. 47, no. 5, pp. 2529–2556, 2020, doi: 10.1007/s11116-019-10027-5.

[25] H. Cheng, J. Liu, L. Sun, and L. Liu, “Critical position of fatigue damage within asphalt pavement considering temperature and strain distribution,” *Int. J. Pavement Eng.*, vol. 0, no. 0, pp. 1–12, 2020, doi: 10.1080/10298436.2020.1724288.

[26] R. Wu and J. T. Harvey, “Evaluation of the Effect of Wander on Rutting Performance in HVS Tests,” *Proc. 3rd Int. Conf. Accel. pavement testing.*, no. January 2008, 2008.

[27] M. Fahad, R. Nagy, and P. Fuleki, “Creep model to determine rut development by autonomous truck axles on pavement,” *Pollack Period.*, pp. 1–6, 2021, doi: 10.1556/606.2021.00328.

[28] J. Pais, P. Pereira, and L. Thives, “Wander Effect on Pavement Performance for Application in Connected and Autonomous Vehicles †,” pp. 2–10, 2023.

[29] P. Andersson and P. Ivehammar, “Benefits and Costs of Autonomous Trucks and Cars,” *J. Transp. Technol.*, vol. 09, no. 02, pp. 121–145, 2019, doi: 10.4236/jtts.2019.92008.

[30] A. Engholm, A. Björkman, Y. Joelsson, I. Kristoffersson, and A. Pernestål, “The emerging technological innovation system of driverless trucks,” *Transp. Res. Procedia*, vol. 49, no. 2019, pp. 145–149, 2020, doi: 10.1016/j.trpro.2020.09.013.

[31] “S T U D Y C Onnected C a Rs Racing Ahead With Autonomous Cars and Digital Innovation,” pp. 18–23, 2015.

[32] G. Hagemann *et al.*, “Delay and Environmental Costs of Truck Crashes,” no. March, p. 132, 2013.

[33] S. A. Bagloee, M. Tavana, M. Asadi, and T. Oliver, “Autonomous vehicles: challenges, opportunities, and future implications for transportation policies,” *J. Mod. Transp.*, vol. 24, no. 4, pp. 284–303, 2016, doi: 10.1007/s40534-016-0117-3.

[34] D. Paddeu and J. Denby, “Decarbonising road freight: Is truck automation and platooning an opportunity?,” *Clean Technol. Environ. Policy*, vol. 24, no. 4, pp. 1021–1035, 2022, doi: 10.1007/s10098-020-02020-9.

[35] Z. B. Biramo and A. A. Mekonnen, “Modeling the potential impacts of automated vehicles on pollutant emissions under different scenarios of a test track,” *Environ. Syst. Res.*, vol. 11, no. 1, 2022, doi: 10.1186/s40068-022-00276-2.

[36] Roland Berger Strategy Consultants GmbH, “On the Road Toward the Autonomous Truck: Opportunities for OEMs and Suppliers,” no. January, p. 11, 2015, [Online]. Available: https://www.rolandberger.com/en/Publications/pub_autonomous_truck.html

[37] E. Kim, Y. Kim, and J. Park, “The Necessity of Introducing Autonomous Trucks in Logistics 4.0,” *Sustainability*, vol. 14, no. 7, p. 3978, 2022, doi: 10.3390/su14073978.

[38] F. Chen, M. Song, X. Ma, and X. Zhu, “Assess the impacts of different autonomous trucks’ lateral control modes on asphalt pavement performance,” *Transp. Res. Part C Emerg. Technol.*, vol. 103, no. March, pp. 17–29, 2019, doi: 10.1016/j.trc.2019.04.001.

[39] K. Georgouli, C. Plati, and A. Loizos, “Autonomous vehicles wheel wander: Structural impact on flexible pavements,” *J. Traffic Transp. Eng. (English Ed.*, vol. 8, no. 3, pp. 388–398, 2021, doi: 10.1016/j.jtte.2021.04.002.

[40] Alaa H. Abed and A. A. Al-Azzawi, “Evaluation of Rutting Depth in Flexible Pavements By Using Finite Element Analysis and Local Empirical Model,” *Am. J. Eng. Appl. Sci.*, vol. 5, no. 2, pp. 163–169, 2012, doi: 10.3844/ajeassp.2012.163.169.

[41] M. Sadeghnejad, M. Arabani, and M. Taghipoor, “Predicting the impact of temperature and stress on the glasphalt mixtures’ rutting behavior,” *Int. J. Pavement Res. Technol.*, vol. 11, no. 3, pp. 300–310, 2018, doi: 10.1016/j.ijprt.2017.10.006.

[42] L. Mo, D. Shu, X. Li, M. Huurman, and S. Wu, “Experimental investigation of bituminous plug expansion joint materials containing high content of crumb rubber powder and granules,” *Mater. Des.*, vol. 37, pp. 137–143, 2012, doi: 10.1016/j.matdes.2012.01.003.

[43] A. D. Tibljaš, T. Giuffrè, S. Surdonja, S. Trubia, J. Arbib, and T. Seba, “Introduction of Autonomous Vehicles: Roundabouts design and safety performance evaluation,”

RethinkX, vol. 10, no. 4, pp. 1–14, 2018, doi: 10.3390/su10041060.

[44] J. Hua, "Finite Element Modeling and Analysis of Accelerated Pavement Testing Devices and Rutting Phenomenon," *Ph.D. Diss.*, vol. Purdue Uni, 2000.

[45] G. ping He and W. gun Wong, "Laboratory study on permanent deformation of foamed asphalt mix incorporating reclaimed asphalt pavement materials," *Constr. Build. Mater.*, vol. 21, no. 8, pp. 1809–1819, 2007, doi: 10.1016/j.conbuildmat.2006.05.024.

[46] I. L. Al-Qadi, P. J. Yoo, M. A. Elseifi, I. Janajreh, G. Chehab, and A. Collop, "Effects of tire configurations on pavement damage," *Asph. Paving Technol. Assoc. Asph. Paving Technol. Tech. Sess.*, vol. 74, no. January, pp. 921–961, 2005.

[47] I. L. Al-Qadi, P. J. Yoo, M. A. Elseifi, and S. Nelson, "Creep Behavior of Hot-Mix Asphalt due to Heavy Vehicular Tire Loading," *J. Eng. Mech.*, vol. 135, no. 11, pp. 1265–1273, 2009, doi: 10.1061/(asce)0733-9399(2009)135:11(1265).

[48] R. Imaninasab, B. Bakhshi, and B. Shirini, "Rutting performance of rubberized porous asphalt using Finite Element Method (FEM)," *Constr. Build. Mater.*, vol. 106, pp. 382–391, 2016, doi: 10.1016/j.conbuildmat.2015.12.134.

[49] W. Huang, X. Zhang, H. Rong, and B. Chen, "Finite Element Method for predicting rutting depth of steel deck asphalt pavement based on Accelerated Pavement Test," no. Icmeis, pp. 935–942, 2015, doi: 10.2991/icmeis-15.2015.177.

[50] F. H. White T, Haddock J, Hang A, "Contributions of pavement structural layers to rutting of hot mix asphalt pavements. Transportation research board." Washington, D.C, 2002.

[51] Y. Zhefu, "Research on the fatigue damage of the asphalt pavement," *Appl. Mech. Mater.*, vol. 256–259, no. PART 1, pp. 1776–1779, 2013, doi: 10.4028/www.scientific.net/AMM.256-259.1776.

[52] H. Di Benedetto, C. De La Roche, H. Baaj, A. Pronk, and R. Lundström, "Fatigue of bituminous mixtures," *Mater. Struct. Constr.*, vol. 37, no. 267, pp. 202–216, 2004, doi: 10.1007/bf02481620.

[53] I. L. Al-Qadi and W. N. Nassar, "Fatigue Shift Factors to Predict HMA Performance," *Int. J. Pavement Eng.*, vol. 4, no. 2, pp. 69–76, 2003, doi: 10.1080/1029843031000159325 4.

[54] F. M. Nejad, E. Aflaki, and M. A. Mohammadi, "Fatigue behavior of SMA and HMA mixtures," *Constr. Build. Mater.*, vol. 24, no. 7, pp. 1158–1165, 2010, doi: 10.1016/j.conbuildmat.2009.12.025.

[55] K. Chatti, H. B. Kim, K. K. Yun, J. P. Mahoney, and C. L. Monismith, "Field investigation into effects of vehicle speed and tire pressure on asphalt concrete pavement strains," *Transp. Res. Rec.*, no. 1539, pp. 66–71, 1996, doi: 10.3141/1539-09.

[56] A. Loulizi, I. L. Al-Qadi, S. Lahouar, and T. E. Freeman, "Measurement of vertical compressive stress pulse in flexible pavements: Representation for dynamic loading tests," *Transp. Res. Rec.*, no. 1816, pp. 125–136, Jan. 2002, doi: 10.3141/1816-14.

[57] H. Cheng, L. Liu, and L. Sun, "Determination of Layer Modulus Master Curve for

Steel Deck Pavement using Field-Measured Strain Data," *Transp. Res. Rec.*, vol. 2673, no. 2, pp. 617–627, 2019, doi: 10.1177/0361198119828685.

[58] L. G. R. de Mello, M. M. de Farias, and K. E. Kaloush, "Effect of temperature on fatigue tests parameters for conventional and asphalt rubber mixes," *Road Mater. Pavement Des.*, vol. 19, no. 2, pp. 417–430, 2018, doi: 10.1080/14680629.2016.1261728.

[59] E. D. Sotelino, "Damage Analysis of Jointed Plain Concrete Pavements in Indiana Part I Finite Element Modeling and Damage Analyis," no. August 2005, 2004.

[60] M. R. S. Mshali and W. J. M. Steyn, "Effect of truck speed on the response of flexible pavement systems to traffic loading," *Int. J. Pavement Eng.*, vol. 0, no. 0, pp. 1–13, 2020, doi: 10.1080/10298436.2020.1797733.

[61] O. E. Gungor and I. L. Al-Qadi, "Wander 2D: a flexible pavement design framework for autonomous and connected trucks," *Int. J. Pavement Eng.*, vol. 0, no. 0, pp. 1–16, 2020, doi: 10.1080/10298436.2020.1735636.

[62] F. Zhou, S. Hu, W. Xue, and G. Flintsch, "Optimizing the Lateral Wandering of Automated Vehicles to Improve Roadway Safety and Pavement Life," *Transp. Res. Rec. J. Transp. Res. Board.*, vol. Vol 2673, no. Issue 11, p. 37, 2019, [Online]. Available: https://trid.trb.org/view/1674281%0Ahttps://doi.org/10.15787/VTT1/1QXWSN%0Ahttps://www.vtti.vt.edu/utc/safe-d/wp-content/uploads/2019/12/02-008_Final-Research-Report_Final.pdf%0Ahttps://trid.trb.org/view/1674281

[63] H. Wang, J. Zhao, X. Hu, and X. Zhang, "Flexible Pavement Response Analysis under Dynamic Loading at Different Vehicle Speeds and Pavement Surface Roughness Conditions," *J. Transp. Eng. Part B Pavements*, vol. 146, no. 3, p. 04020040, 2020, doi: 10.1061/jpeodx.0000198.

[64] S. M. Hadian*, "Investigation and analysis of fracture failure and fatigue cracking in High-rise pavement using simulation software of ABAQUS," *Ann. Civ. Environ. Eng.*, vol. 3, no. 1, pp. 032–039, 2019, doi: 10.29328/journal.acee.1001015.

[65] M. Song, F. Chen, and X. Ma, "Organization of autonomous truck platoon considering energy saving and pavement fatigue," *Transp. Res. Part D Transp. Environ.*, vol. 90, no. December 2020, p. 102667, 2021, doi: 10.1016/j.trd.2020.102667.

[66] C. Tóth, É. Lakatos, L. Pethő, and S. Cho, "Temperature Profile Modelling in Flexible Pavement Design," vol. 15, no. 2, pp. 84–89, 2021.

[67] I. L. Al-Qadi and H. Wang, "Pavement Damage Due to Different Tire and Loading Configurations on Secondary Roads," p. 57, 2009.

[68] A. H. Alavi, H. Hasni, N. Lajnef, and K. Chatti, "Continuous health monitoring of pavement systems using smart sensing technology," *Constr. Build. Mater.*, vol. 114, no. August, pp. 719–736, 2016, doi: 10.1016/j.conbuildmat.2016.03.128.

[69] H. Wang, "Analysis of Tire-Pavement Interaction and Pavement Responses Using a Decoupled Modeling Approach," *Transp. Res. Board*, no. 1215, pp. 1–159, 2011.

[70] N. Lajnef, K. Chatti, H. Hasni, and A. H. Alavi, "Feasibility of Early Damage Detection Using Surface Mounted Sensors on Existing Pavements," no. August, 2016.

[71] Y. Cho, C. Liu, T. Dossey, and B. F. Mccullough, “a Sphalt O Verlay D Esign M Ethods for R Igid P Avements C Onsidering R Utting , R Eflection C Racking , and F Atigue C Racking Bureau of Engineering Research the University of Texas At Austin,” *Reproduction*, no. October, pp. 313–319, 1998.

[72] M. O. Pi *et al.*, “FINAL REPORT IMPROVING RIGID PAVEMENT SMOOTHNESS USING POLYLEVEL ® Project #: RES2016-18 UTC Report Submitted to TDOT By :,” no. May, 2018.

[73] G. Sun, J. Ling, Z. Tao, J. Qian, and Y. Cai, “Effect of geotextile on reduction of reflective cracking induced by traffic load in asphalt concrete,” *HKIE Trans. Hong Kong Inst. Eng.*, vol. 27, no. 2, pp. 77–84, 2020, doi: 10.33430/V27N2THIE-2017-0023.

[74] C. Si, X. Su, E. Chen, and Z. Yan, “Comparative study on dynamic response of deck pavement of two kinds of box girder bridges under moving loads,” *Shock Vib.*, vol. 2019, 2019, doi: 10.1155/2019/6052745.

[75] Z. Dong, Y. Tan, L. Cao, and H. Liu, “Combining strain measurement and FEM simulation to obtain dynamic response of asphalt pavement,” *International Journal of Pavement Research and Technology*, vol. 2, no. 5. pp. 231–235, 2009. doi: 10.6135/ijprt.org.tw/2009.2(5).231.

[76] P. Cao, D. C. Feng, and R. X. Jing, “Based on FE method to research resistant rutting ability of pavement structure in Heilongjiang province,” *Appl. Mech. Mater.*, vol. 128–129, pp. 1349–1354, 2012, doi: 10.4028/www.scientific.net/AMM.128-129.1349.

[77] P. J. Yoo and I. L. Al-Qadi, “Effect of transient dynamic loading on flexible pavements,” *Transp. Res. Rec.*, no. 1990, pp. 129–140, 2007, doi: 10.3141/1990-15.

[78] A. Setyawan, I. Kusdiantoro, and Syafi’i, “The effect of pavement condition on vehicle speeds and motor vehicles emissions,” *Procedia Eng.*, vol. 125, pp. 424–430, 2015, doi: 10.1016/j.proeng.2015.11.111.

[79] D. Li and J. S. Smith, “Proceedings of the 2019 Winter Simulation Conference Y. Shi, J. Du; C. Szabo, P. Haas, and Y-J. Son, eds.,” *Proc. 2019 Winter Simul. Conf.*, no. 2018, pp. 2049–2060, 2019.

[80] “IET Intelligent Trans Sys - 2018 - Zhai - Cooperative look-ahead control of vehicle platoon travelling on a road with.pdf.”

[81] J. Chen, H. Chen, J. Gao, J. A. Pattinson, and R. Quaranta, “A business model and cost analysis of automated platoon vehicles assisted by the Internet of things,” *Proc. Inst. Mech. Eng. Part D J. Automob. Eng.*, vol. 235, no. 2–3, pp. 721–731, 2021, doi: 10.1177/0954407020949726.

[82] I. Al-Qadi, E. Okte, A. Ramakrishnan, Q. Zhou, and W. Sayeh, *Truck Platooning on Flexible Pavements in Illinois*, no. 21. 2021. [Online]. Available: https://apps.ict.illinois.edu/projects/getfile.asp?id=9659

[83] C. Melson, “Investigating the Impacts of Truck Platooning on Transportation Infrastructure in the South Central Region,” *Publications*, no. 19, pp. 1–2, 2021, [Online]. Available: https://digitalcommons.lsu.edu/transet_pubs/84

[84] M. E. Bouchihati, “The impact of Truck Platooning on the pavement structure of Dutch Motorways The impact of Truck Platooning on the pavement structure of Dutch

Motorways The link between truck platooning and road surface wear," *Delft Univ. Technol.*, 2020.

[85] P. Marsac *et al.*, *Optimization of truck platoon wander patterns based on thermo-viscoelastic simulations to mitigate the damage effects on road structures*, vol. 96 LNCE. Springer International Publishing, 2020. doi: 10.1007/978-3-030-55236-7_11.

[86] F. M. Nejad, H. Sorkhabi, and M. M. Karimi, "Experimental Investigation of Rest Time Effect on Permanent Deformation of Asphalt Concrete," *J. Mater. Civ. Eng.*, vol. 28, no. 5, p. 06015016, 2016, doi: 10.1061/(asce)mt.1943-5533.0001498.

[87] D. Kim and Y. R. Kim, "Development of Stress Sweep Rutting (SSR) test for permanent deformation characterization of asphalt mixture," *Constr. Build. Mater.*, vol. 154, pp. 373–383, 2017, doi: 10.1016/j.conbuildmat.2017.07.172.

[88] F. E. Pérez-Jiménez, R. Miró, R. Botella, T. López-Montero, and A. H. Martínez, "The Effect of Temperature, Rest Periods and Ageing on the Response of Bituminous Materials in Fatigue Tests: Considerations and Proposals on Analytical Dimensioning Models," *Materials (Basel).*, vol. 15, no. 3, 2022, doi: 10.3390/ma15030790.

[89] T. Al-Mansoori, A. Al-Adhadh, and J. Hussein, "Influence of temperature and rest period on damage repair of aged asphalt," *Key Eng. Mater.*, vol. 857 KEM, no. August, pp. 138–144, 2020, doi: 10.4028/www.scientific.net/KEM.857.138.

[90] W. A. Zeiada, P. P. Gudipudi, B. S. Underwood, and M. I. Souliman, "Effect of loading waveform pattern and rest period on fatigue life of asphalt concrete using viscoelastic continuum damage model," *Transp. Res. Rec.*, vol. 2672, no. 28, pp. 451–461, 2018, doi: 10.1177/0361198118773892.

[91] U. Hasan, A. Whyte, H. Al Jassmi, and A. Hasan, "Lifecycle Cost Analysis of Recycled Asphalt Pavements: Determining Cost of Recycled Materials for an Urban Highway Section," *CivilEng*, vol. 3, no. 2, pp. 316–331, 2022, doi: 10.3390/civileng3020019.

[92] P. Babashamsi, N. I. Md Yusoff, H. Ceylan, N. G. Md Nor, and H. Salarzadeh Jenatabadi, *Evaluation of pavement life cycle cost analysis: Review and analysis*, vol. 9, no. 4. Chinese Society of Pavement Engineering, 2016. doi: 10.1016/j.ijprt.2016.08.004.

[93] J. T. Harvey, J. Meijer, H. Ozer, I. Al-Qadi, A. Saboori, and A. Kendall, "Pavement Life Cycle Assessment Framework," *Fhwa-Hif-16-014*, p. 244, 2016.

[94] A. Braham, "Comparing life-cycle cost analysis of full-depth reclamation versus traditional pavement maintenance and rehabilitation strategies," *Transp. Res. Rec.*, vol. 2573, pp. 49–59, 2016, doi: 10.3141/2573-07.

[95] A. Riekstins, V. Haritonovs, and V. Straupe, "Life cycle cost analysis and life cycle assessment for road pavement materials and reconstruction technologies," *Balt. J. Road Bridg. Eng.*, vol. 15, no. 5, pp. 118–135, 2020, doi: 10.7250/bjrbe.2020-15.510.

[96] J. Santos and A. Ferreira, "Life-cycle cost analysis system for pavement management at project level," *Int. J. Pavement Eng.*, vol. 14, no. 1, pp. 71–84, 2013, doi: 10.1080/10298436.2011.618535.

[97] M. Akbarian *et al.*, "Overview of pavement life cycle assessment use phase research at the MIT concrete sustainability hub," *Airf. Highw. Pavements 2019 Innov. Sustain.*

Highw. Airf. Pavement Technol. - Sel. Pap. from Int. Airf. Highw. Pavements Conf. 2019, no. February 2020, pp. 193–206, 2019, doi: 10.1061/9780784482476.021.

[98] Y. Zhang, R. Luo, and R. L. Lytton, "Characterizing Permanent Deformation and Fracture of Asphalt Mixtures by Using Compressive Dynamic Modulus Tests," *J. Mater. Civ. Eng.*, vol. 24, no. 7, pp. 898–906, 2012, doi: 10.1061/(asce)mt.1943-5533.0000471.

[99] L. Uzarowski, "The Development of Asphalt Mix Creep Parameters And Finite Element Modelling Of Asphalt Rutting," 2006.

[100] R. K. Abu Al-Rub, M. K. Darabi, C. W. Huang, E. A. Masad, and D. N. Little, "Comparing finite element and constitutive modelling techniques for predicting rutting of asphalt pavements," *Int. J. Pavement Eng.*, vol. 13, no. 4, pp. 322–338, 2012, doi: 10.1080/10298436.2011.566613.

[101] J. Harvey, J. Roesler, N. Coetzee, and C. Monismith, "CALTRANS Accelerated Pavement Test (CAL/APT) Program: Summary Report: Six Year Period: 1994-2000," no. June 2000, pp. 1994–2000, 2000.

[102] R. V. Siddharthan, M. Nasimifar, X. Tan, and E. Y. Hajj, "Investigation of impact of wheel wander on pavement performance," *Road Mater. Pavement Des.*, vol. 18, no. 2, pp. 390–407, 2017, doi: 10.1080/14680629.2016.1162730.

[103] F. Wang and R. B. Machemehl, "Mechanistic-empirical study of effects of truck tire pressure on pavement: Measured tire-pavement contact stress data," *Transp. Res. Rec.*, no. 1947, pp. 136–145, 2006, doi: 10.3141/1947-13.

[104] S. Mecheri, F. Rosey, and R. Lobjois, "The effects of lane width, shoulder width, and road cross-sectional reallocation on drivers' behavioral adaptations," *Accid. Anal. Prev.*, vol. 104, no. December 2016, pp. 65–73, 2017, doi: 10.1016/j.aap.2017.04.019.

[105] M. Fahad and R. Nagy, "Fatigue damage analysis of pavements under autonomous truck tire passes," *Pollack Period.*, vol. 17, no. 3, pp. 59–64, 2022, doi: 10.1556/606.2022.00588.

[106] I. L. Al-Qadi, P. J. Yoo, M. A. Elseifi, I. Janajreh, G. Chehab, and A. Collop, "Effects of tire configurations on pavement damage," *Asph. Paving Technol. Assoc. Asph. Paving Technol. Tech. Sess.*, vol. 74, no. June 2015, pp. 921–961, 2005.

[107] T. John, "Reflectibve Cracking Study" HVS Report 597 2008.

[108] L. Petho, "Influence of Temperature distribution on the design of pavement structures," *Period. Polytech. Civ. Eng.*, vol. 52, no. 1, pp. 45–53, 2008, doi: 10.3311/pp.ci.2008-1.07.

[109] T. Olexa and J. Mandula, "Comparison of complex modulus and elasticity modulus of bitumen bonded materials," *Pollack Period.*, vol. 11, no. 3, pp. 131–140, 2016, doi: 10.1556/606.2016.11.3.12.

[110] M. Fahad and R. Nagy, "Influence of class A40 autonomous truck on rutting and fatigue cracking," *Pollack Period.*, pp. 3–8, 2023, doi: 10.1556/606.2023.00760.

[111] M. Ghorban Ebrahimi, M. Saleh, and M. A. M. Gonzalez, "Interconversion between viscoelastic functions using the Tikhonov regularisation method and its comparison with approximate techniques," *Road Mater. Pavement Des.*, vol. 15, no. 4, pp. 820–

840, 2014, doi: 10.1080/14680629.2014.924428.

[112] H. Alimohammadi, J. Zheng, A. Buss, V. R. Schaefer, C. Williams, and G. Zheng, "Finite element viscoelastic simulations of rutting behavior of hot mix and warm mix asphalt overlay on flexible pavements," *Int. J. Pavement Res. Technol.*, vol. 14, no. 6, pp. 708–719, 2021, doi: 10.1007/s42947-020-0057-5.

[113] P. Primusz and C. Tóth, "Use of the Modified Ramberg-Osgood Material Model to Predict Dynamic Modulus Master Curves of Asphalt Mixtures," *Materials (Basel).*, vol. 16, no. 2, 2023, doi: 10.3390/ma16020531.

[114] Y. Deng, X. Shi, Y. Zhang, and J. Chen, "Numerical modelling of rutting performance of asphalt concrete pavement containing phase change material," *Eng. Comput.*, no. 0123456789, 2021, doi: 10.1007/s00366-021-01507-3.

[115] M. Šušnjar, D. Horvat, M. Zorić, Z. Pandur, and D. Vusić, "Comparison of real axle loads and wheel pressure of truck units for wood transportation with legal restrictions," *Int. Symp. For. Mech.*, pp. 1–11, 2011.

[116] M. Saarilahti, "Modelling of the Wheel and Tyre," *Univ. Helsinki, Dep. For. Resour. Manag.*, vol. APPENDIX 5, no. 2002, p. 87, 2002.

[117] R. A. Douglas, *Tyre/road contact stresses measured and modelled in three coordinate directions*, no. September. 2009.

[118] S. L. Weissman, "Influence of tire-pavement contact stress distribution on development of distress mechanisms in pavements," *Transp. Res. Rec.*, no. 1655, pp. 161–167, 1998, doi: 10.3141/1655-21.

[119] ASHTO, "Libro En Ingles - Paviment Design Manual," vol. 1, p. 146, 1997.

[120] G. Leonardi, "Finite element analysis for airfield asphalt pavements rutting prediction," *Bull. Polish Acad. Sci. Tech. Sci.*, vol. 63, no. 2, pp. 397–403, 2015, doi: 10.1515/bpasts-2015-0045.

[121] O. F. New, R. P. Structures, C. Of, P. Deformation, and F. O. R. F. Pavements, "Guide for Mechanistic-Empirical Design," no. February, 2004.

[122] B. Huang, L. N. Mohammad, and M. Rasoulian, "Three-dimensional numerical simulation of asphalt pavement at Louisiana accelerated loading facility," *Transp. Res. Rec.*, no. 1764, pp. 44–58, 2001, doi: 10.3141/1764-06.

[123] P. W. Mayne, *COOPERATIVE HIGHWAY PROGRAM A Synthesis of Highway Practice - Cone Penetration Testing*. 2007.

[124] M. Fahad and R. Nagy, "Truck platoon analysis for autonomous trucks," *SN Appl. Sci.*, vol. 5, no. 5, 2023, doi: 10.1007/s42452-023-05352-5.

[125] H. K. Shanbara, F. Ruddock, and W. Atherton, "Rutting Prediction of a Reinforced Cold Bituminous Emulsion Mixture Using Finite Element Modelling," *Procedia Eng.*, vol. 164, no. June, pp. 222–229, 2016, doi: 10.1016/j.proeng.2016.11.613.

[126] Alaska Department of Transportation and Public Facilities, "Alaska Flexible Pavement Design Manual Alaska Department of Transportation," 2020, [Online]. Available: http://dot.alaska.gov/stwddes/desmaterials/mat_pav_engineer.shtml#

[127] R. Model, "Deterioration Models for Managing," no. 99, pp. 31–34.

[128] M. Fahad and R. Nagy, “Effective lane width analysis for autonomous trucks,” *SN Appl. Sci.*, no. April, 2023, doi: 10.1007/s42452-023-05446-0.

[129] J. Cirilovic, N. Vajdic, G. Mladenovic, and C. Queiroz, “Developing Cost Estimation Models for Road Rehabilitation and Reconstruction: Case Study of Projects in Europe and Central Asia,” *J. Constr. Eng. Manag.*, vol. 140, no. 3, 2014, doi: 10.1061/(asce)co.1943-7862.0000817.

[130] I. Mahamid, “Early cost estimating for road construction projects using multiple regression techniques,” *Australas. J. Constr. Econ. Build.*, vol. 11, no. 4, pp. 87–101, 2011, doi: 10.5130/ajceb.v11i4.2195.

[131] R. E. Turochy, L. A. Hoel, and R. S. Doty, “Highway project cost estimating methods used in the planning stage of project development,” *Virginia Transp. Res. Counc.*, p. 40, 2001.

[132] A. Ferreira and J. Santos, “LCCA System for Pavement Management: Sensitivity Analysis to the Discount Rate,” *Procedia - Soc. Behav. Sci.*, vol. 53, pp. 1172–1181, 2012, doi: 10.1016/j.sbspro.2012.09.966.

[133] L. D. Bueno, L. P. Specht, D. da Silva Pereira, and J. Ribas, “Análise custo/benefício de implantação de diferentes estruturas de pavimentos flexíveis considerando a carga por eixo e o tipo de ligante,” *Acta Sci. - Technol.*, vol. 38, no. 4, pp. 445–453, 2016, doi: 10.4025/actascitechnol.v38i4.28497.

[134] C. Tóth and P. Primusz, “New Hungarian mechanistic-empirical design procedure for asphalt pavements,” *Balt. J. Road Bridg. Eng.*, vol. 15, no. 1, pp. 161–186, 2020, doi: 10.7250/bjrbe.2020-15.466.

[135] G. White, “Comparing the cost of rigid and flexible aircraft pavements using a parametric whole of life cost analysis,” *Infrastructures*, vol. 6, no. 8, 2021, doi: 10.3390/infrastructures6080117.

[136] C. Toth, L. Petho, S. Rosta, and P. Primusz, “Performance assessment of full depth asphalt pavements manufactured with high recycled asphalt pavement content,” *Acta Tech. Jaurinensis*, vol. 16, no. 1, pp. 18–26, 2023, doi: 10.14513/actatechjaur.00688.